Universidad de Huelva

Departamento de Ciencias Integradas

Study of an Ion Beam Accelerator for the LINAC Research Center in Spain

Memoria para optar al grado de doctora presentada por:

Angie Karina Ordúz

Fecha de lectura: 29 de marzo de 2019

Bajo la dirección de los doctores:

Ismael Martel Bravo

Antonio C.C. Villari

Huelva, 2019

Study of an Ion Beam Accelerator for the LINAC Research Center in Spain

Thesis for the Degree of Doctor

Angie Karina Ordúz

Industrial and Environmental Science and Technology Program

Academic advisors:
Ismael Martel Bravo[1], Antonio C.C. Villari[2]

[1]Department of Integrated Sciences
Faculty of Experimental Sciences
University of Huelva
Spain

[2]ReAccelerator Department
Facility for Rare Isotope Beams
Michigan State University
USA

Universidad de Huelva

2019

Study of an Ion Beam Accelerator for the LINAC Research Center in Spain

Abstract:

This thesis focuses on the study of an ion beam accelerator for the LINAC Research Center (LINCE) in Spain. The proposed superconducting LINAC operates at 72.75 MHz and is designed to accelerate, in a first phase, light and heavy ions with mass-to-charge ratio in the range $^{A}/_{Q} = 1$ to 7 and beam energies from 500 keV/n to about 8 MeV/n for heavy ions, and 40 MeV for protons.

LINCE developed from a previous project, the Linac Research Facility (LRF), an initiative to install a high-intensity, light- and heavy-Ion accelerator in the University of Huelva (Spain). The facility would be dedicated to basic nuclear research and multidisciplinary applications, notably using a high-intensity proton beam for radioisotope production of medical interest. Therefore, the main challenge of this thesis has been to devise a multi-ion LINAC accelerator capable of producing both high-intensity protons and heavy-ions with large A/Q. LINCE and LRF gathered a wide community of nuclear physicists and industrial shareholders from Spain and abroad, which contributed to different R&D activities coordinated by the local team at the University of Huelva.

This thesis details the beam dynamics of the LINAC and the design of selected accelerator elements, with special emphasis in a key element of the facility: the radiofrequency quadrupole (RFQ). The codes TRACK, DESRFQ and MAD-X have been used for particle tracking simulations, COMSOL MULTIPHYSICS for radio-frequency (RF), thermal and structural analysis, and AUTOCAD INVENTOR for the mechanical design. This document is presented in seven chapters that cover beam dynamics studies, the design of accelerator elements, geometry models, RF simulations, and engineering studies of the structure including heating, cooling and mechanical displacements.

Keywords: LINAC, LRF, LINCE, resonator cavities, beam dynamics, RFQ, University of Huelva.

Contents

Dedicada a Rosita, Elias, Mary y Orlando.

Introduction

Knowledge of subatomic degrees of freedom and nuclear structure has increased exponentially in the last decades through the use of heavy-ion accelerators. A number of facilities are currently operating in the European Union, delivering ion beams with intensities of up to 10^{12} particles/sec, which led them to be recognized as leading European research infrastructures. As the understanding of the atomic nucleus has improved, new physics domains have emerged that require the construction of a dedicated European facility to provide stable heavy-ion beams of higher intensity.

The European Collaboration on Stable-Ion Beams (ECOS)[1] was a working group of the Nuclear Physics European Collaboration Committee (NuPECC),[2] an expert committee of the European Science Foundation (ESF). In the latest report of ECOSECOS-LINCE, the construction of a high-intensity accelerator for stable beams of energies at and above the Coulomb barrier was considered as one of the most important goals in the next long-term plan of the nuclear physics community in Europe. This is the LINCE (ECOS) facility, where the acronym LINCE stands for European "LINac research CEnter".[3]

This accelerator should be dedicated to fundamental research requiring long beam times and high intensities, which will not be feasible at existing or newly planned facilities in the European Union. The ECOS report, which summarizes the interests of the nuclear-physics community in Europe, identifies several areas in which investigations can be only addressed with, or could strongly benefit from, the use of high-intensity stable beams:

- Synthesis and spectroscopy of super-heavy nuclei.
- Nuclear-structure studies at low, medium and high spin.
- Ground-state properties.
- Near-barrier transfer and fusion reactions.
- Nuclear astrophysics.
- Ion-ion collisions in plasma.

LINCE carries on a previous initiative entitled "The Linac Research Facility (LRF)" at the University of Huelva, which was initially founded by the Government of Spain. The new proposal emerges with the aim of developing in Europe a world-class facility producing high-intensity light- and heavy-ion beams in the milliamps range on target, and with energies around 8 MeV/u, using a dedicated superconducting continuum-wave (CW)linac.

A post accelerator system is also foreseen (not studied in this work) to increase the energies of light ions up to 200 MeV/u and of heavy ions up to around 50 MeV/u, thus enabling the possibility to fully address a unique class of

fundamental physics cases, e.g., Gamow-Teller studies and related fundamental interactions, isospin dynamics and nucleon-nucleon correlations in high-energy heavy-ion collisions. This worldwide unique facility should be able to perform high-precision long-run measurements of rare phenomena with having cross sections down to the picobarn regime. In addition to basic nuclear physics, it is also foreseen research in societal applications of nuclear physics is also foreseen, in particularly for medical physics investigations. The construction of the facility should be based on a reliable design using well-established technologies, aiming to provide an effective beam-time allocation of about 5000 h/y for fundamental physics and 2000 h/y for applications, also considering parallel operation.

In the present work a superconducting LINAC accelerator using state-of-the-art technology is proposed in order to produce high-intensity heavy-ion beams up to around 8 MeV/n and protons of about 40 MeV. The beam dynamics of such an accelerator is studied and, particularly, special care has been taken in developing a new design for a room-temperature radio frequency quadrupole (RFQ) injector for the proposed LINAC. RFQs are essential components of modern high-intensity accelerators; they are used to bunch, pre-accelerate and optimize the beam characteristics before being injected into accelerating RF cavities. This thesis presents the theoretical studies and modelling of a four vane RFQ operating at 72.75 MHz, designed to accelerate ions in the range of mass-to-charge ratio $A/Q = 1 - 1/7$, from 40 keV/u to 500 keV/u.

The first part of this study deals with the design of the RFQ begins with an overall beam dynamics study of the accelerator facility, from the ion source to the superconducting cavities, using a selection of ions, and energies, and beam parameters (intensity, transversal and longitudinal emittance, time structure, etc.) required by the scientific program were developed. This defines the layout of the facility, and the main characteristics of the beam transport lines and acceleration elements, like the RFQ and the superconducting RF cavities. Along the study, the characteristics of the beam at the ion source were been obtained from the model Supernanogam electron-cyclotron resonance (ECR) model Supernanogam of distributed by the company Pantechnik (France), a high -intensity multi-ion source widely used at heavy-ion accelerators.

After establishing the main characteristics and parameter ranges of input/output beams of the RFQ, the thesis continues with a dedicated electromagnetic and structural study, including thermal deformations and machining error analysis. The design was carried out using the codes codes TRACK,[4] DESRFQ[5] and MAD-X[6] for ion tracking and transport simulations, COMSOL MULTIPHYSICS[7] for Radio Frequency, thermal and structural analyses, and AUTOCAD INVENTOR[8] for the mechanical design.

Although a four-vanes RFQ structure with two independent buncher systems (for protons and heavy-ions) has been the initial choice for the ECOS-LINCE facility, there is an alternative study of a four-rod RFQ based on a four-rods system that could also suit the specifications and be significantly less expensive. This technical option is reviewed and discussed at the end of chapter 5, including a preliminary design study.

The work on the accelerator design was combined with the participation on selected nuclear physics measurements at the main EU accelerator facilities (LNL, HIE-ISOLDE and GSI). This offered the opportunity to learn relevant aspects of LINAC operation and commissioning, as well as becoming familiar with main detector parameters and beam characteristics requested by nuclear physicists. This information was extremely useful to define the design parameters of ECOS-LINCE and, in particular, the RFQ system.

This thesis is presented in seven chapters; a brief description of their contents is presented below.

Chapter 1 contains an introduction to the LINCE project and its applications, where special attention is paid to medical research.

The principal parameters and design requirements for LINCE are presented in Chapter 2.

In Chapter 3 the Radio-frequency accelerators and RFQ theories are described, as well the methodology and tools used for whole study.

The beam transport study for the whole facility is presented in Chapter 4. It includes the relevant parameters and a detailed study of the acceleration of protons and heavy ion beams through LINCE.

Chapter 5 is dedicated to the design of the RFQ. The first three sections contains the specific study of the beam dynamics for the 72.75 MHz four-vane model, the electromagnetic modelling, and the thermal and structural analysis. This study includes the design of cooling channels, heat transfer, mechanical stress, deformation and frequency shift. Additionally, in Appendix B a section dedicated to the design of a 200 MHz four-rods RFQ for proton and light-ion ($A/Q = 3$) acceleration is presented.

In chapter 6 the process followed for the construction of prototypes is presented. This chapter includes the building process of the aluminum and copper models and the results for frequency measurements.

Finally, the summary of the thesis is presented together with the most important conclusions in chapter 7.

Introducción

El conocimiento sobre los grados de libertad subatómicos y la estructura nuclear ha aumentado exponencialmente en las últimas décadas a través del uso de aceleradores de iones pesados. Actualmente existen una serie de instalaciones en funcionamiento en la Unión Europea, que emiten haces de iones con intensidades de hasta 10^{12} partículas/s, lo que las lleva a ser reconocidas como las principales infraestructuras de investigación europeas. A medida que aumenta la comprensión del núcleo atómico, han surgido nuevos campos en la física que requieren la construcción de una instalación europea dedicada para proporcionar haces de iones pesados estables de mayor intensidad.

La Colaboración europea en haces de iones estables (ECOS)[1] fue un grupo de trabajo del Comité Europeo de Colaboración en Física Nuclear (NuPECC),[2] un comité de expertos de la European Science Foundation (ESF). En el último informe de ECOS,[9] la construcción de un acelerador de alta intensidad para haces de energía estables en y por encima de la barrera de Coulomb, fue considerada como una de las metas más importantes en el próximo plan a largo plazo de la comunidad de física nuclear en Europa. Esta es la instalación de ECOS-LINCE, donde el acrónimo LINCE significa “CEnter de investigación de LINac” europeo.[3]

Este acelerador debe estar dedicado a la investigación fundamental, la cual requiere tiempos de haz más largos e intensidades altas, lo que no es factible en las instalaciones existentes o recientemente planificadas en la UE. El informe de ECOS, el cual resume los intereses de la comunidad de física nuclear en Europa, identifica varias áreas en las que las investigaciones solo pueden abordarse con el uso de rayos estables de alta intensidad o podrían beneficiarse de ellos:

- Síntesis y espectroscopia de núcleos superpesados.
- Estudios de estructura nuclear a baja, media y alta rotación.
- Propiedades del estado del suelo.
- Reacciones de fusión y transferencia cerca de la barrera.
- Astrofísica nuclear.
- Colisiones ion-ion en plasma.

LINCE sigue adelante con una iniciativa previa titulada "El Centro de Investigación Linac (LRF)" en la Universidad de Huelva (España), que fue inicialmente fundada por el Gobierno de España. La nueva propuesta surge con el objetivo de desarrollar en Europa una instalación de clase mundial que produzca haces de iones pesados de alta intensidad en el rango de miliamperios en el blanco con energías alrededor de 8 MeV/u, utilizando un acelerador lineal superconductor (CW).

También se plantea un sistema acelerador posterior(no estudiado en este trabajo) para aumentar las energías de los iones ligeros hasta 200 MeV/u y de los iones pesados hasta alrededor de 50 MeV/u, permitiendo así la posibilidad de abordar completamente una clase única de casos de física fundamental, por ejemplo, estudios de Gamow-Teller e interacciones fundamentales relacionadas, dinámica de isoespin y correlaciones nucleón-nucleón en colisiones de alta energía de iones pesados. Esta instalación única en todo el mundo debería poder realizar mediciones de alta precisión a largo plazo de fenómenos raros con secciones transversales hasta el régimen de picobarn. Además de la física nuclear básica, también se prevé la investigación en aplicaciones sociales de la física nuclear, en particular para las investigaciones de física médica. La construcción de la instalación debe basarse en un diseño confiable que use tecnologías bien conocidas y probadas, con el objetivo de proporcionar una asignación efectiva de tiempo de haz de aproximadamente 5000 h/y para física fundamental y 2000 h/ypara aplicaciones, considerando operación paralela.

En el presente trabajo, se propone un acelerador superconductor LINAC que utilice tecnología punta para producir haces de iones pesados de alta intensidad de hasta alrededor de 8 MeV/n y de protones de aproximadamente 40 MeV. Se estudia la dinámica del haz de dicho acelerador y, en particular, se ha prestado especial atención al desarrollo de un nuevo diseño para un inyector cuadrupolo de radiofrecuencia (RFQ) a temperatura ambiente para el LINAC propuesto. Los cuadrupolos de radiofrecuencia (RFQ) son componentes esenciales de los aceleradores modernos de alta intensidad; se utilizan para agrupar, pre-acelerar y optimizar las características del haz antes de ser inyectadas en cavidades aceleradoras de radio frecuencia. Esta tesis presenta los estudios teóricos y el modelado de una RFQ de cuatro vanos que opera en 72.75 MHz, diseñada para acelerar iones en el rango de relación masa/carga $A/Q = 1 - 1/7$, de 40 keV/u a 500 keV/u.

La primera parte de este estudio se enfocó en el estudio de la dinámica de haz para el acelerador en general, desde la fuente de iones hasta las cavidades superconductoras, utilizando una selección de iones y energías, y los parámetros del haz (intensidad, emitancia transversal y longitudinal, longitud, etc.) requeridos por el programa científico. Esto define el diseño de la instalación y las características principales de las líneas de transporte de haz y los elementos de aceleración, como por ejemplo la RFQ y las cavidades superconductoras de radio frecuencia. Las características del haz en la fuente de iones se obtuvieron del modelo Supernanogam de Pantechnik, una fuente de iones múltiples de alta intensidad ampliamente utilizada en aceleradores de iones pesados.

Después de haber establecido las características principales y los rangos de los parámetros para los haces a la entrada/salida de la RFQ, la tesis continúa con un estudio eletromagnético y técnico detallado, que incluye deformaciones térmicas

y análisis de errores de mecanizado. El diseño se llevó a cabo utilizando los códigos TRACK[4] y DESRFQ[5] y MAD-X[6] para las simulaciones de seguimiento y transporte de iones, COMSOL MULTIPHYSICS[7] para los análisis térmicos, estructurales y de radiofrecuencia e INVENTOR[8]para el diseño mecánico.

Si bien la estructura de la RFQ de cuatro vanos con dos sistemas de buncher independientes (para protones e iones pesados) fue la elección inicial para la instalación ECOS-LINCE, existe un estudio alternativo para una RFQ de cuatro barras que también podría ajustarse a las especificaciones y ser significativamente menos costosa. Esta opción técnica se revisa y discute al final del capítulo 5, incluido un estudio de diseño preliminar.

El estudio para el diseño del acelerador se compaginó con la contribución de determinadas mediciones de física nuclear en las principales instalaciones de aceleradores de la UE(LNL, HIE-ISOLDE y GSI). Esto brindó la oportunidad de aprender aspectos relevantes de la operación y puesta en marcha de un LINAC, así como la posibilidad de familiarizarse con los principales parámetros de los detectores y las características de haz solicitadas por los físicos nucleares. Esta información fue extremadamente útil para definir los parámetros de diseño de ECOS-LINCE y, en particular, para el sistema de RFQ.

La tesis se presenta en siete capítulos; una breve descripción de su contenido es presentado a continuación.

El Capítulo 1 contiene una introducción del proyecto LINCE y sus aplicaciones, donde se presta especial atención a la investigación en medicina.

Los principales parámetros y requisitos de diseño para LINCE se presentan en el Capítulo 2.

En el Capítulo 3 se describen los fundamentos de los aceleradores de radiofrecuencia y de la RFQ, así como la metodología y las herramientas utilizadas para realizar el estudio.

El estudio de dinámica de haz para todo el acelerador se presenta en el Capítulo 4. Se incluyen los parámetros relevantes del mismo y un estudio detallado de aceleración de protones e iones pesados a través de LINCE.

El capítulo 5 está dedicado al diseño de la RFQ. Las primeras tres secciones contienen el estudio específico de dinámica de haz, el modelado electromagnético, y los análisis térmicos y estructurales para el modelo de cuatro vanos de 72.75 MHz. Este estudio incluye el diseño de los canales de refrigeración, y los resultados para la transmisión de calor, stress mecánico, deformaciones y cambios de frecuencia. Adicionalmete, en el apéndice B se presenta una sección dedicada al diseño de una RFQ de cuatro barras de 200 MHz para la aceleración de protones e iones ligeros ($A/Q = 3$).

En el capítulo 6 se presenta el proceso seguido para la construcción de los prototipos. Este capítulo describe el proceso de fabricación de los modelos de aluminio y cobre, y los resultados de las pruebas de radiofrecuencia.

Finalmente, se presenta un resumen de la tesis junto con las conclusiones más importantes en el capítulo 7.

1

The ECOS-LINCE LINAC

This chapter presents the most relevant information regarding LINCE: the European "LINac research CEnter for stable high-intensity beams. Section 1.1 contains an introduction to the original project ECOS-LINCE initiative. In section 1.2 the basic research of the LINCE project is presented. The applications in nuclear physics and industrial fields are comprised in section 1.3.

1.1 The LRF and the ECOS-LINCE initiatives

Present knowledge of subatomic degrees of freedom and nuclear structure has increased exponentially in the last decades through the use of heavy-ion facilities. A number of facilities are presently operating at the European Union delivering ion beams with intensities of up to a few particle-nanoamps, which led them to be recognized as leading European research infrastructures. As the understanding of the atomic nucleus has increased, new physics domains have emerged that require the construction of a dedicated European facility to provide stable heavy-ion beams of higher intensity.

The recent report of the Committee for European collaboration in Nuclear Sciences (NuPECC) published in 2012 states that "the field of high-intensity accelerators intensely benefits from synergies between the production of radioactive beams, studies of subcritical reactor systems controlled by accelerators, the International Fusion Material Irradiation Facility (IFMIF[10]), the production of radio-pharmaceuticals, and the project for the creation of the European spallation source (ESS)". In addition, it emphasizes the important role they play in both large-scale facilities (FAIR,[11] SPIRAL2,[12] SPES[13]) and small-scale facilities, and claim that these should receive funds from governments to provide sufficient beam time availability.

In the last years, the ECOS working group strongly supported the construction of a dedicated high-intensity stable-ion-beam facility in Europe, with energies at and above the Coulomb barrier as part of the Long-Range Plan of the Nuclear-Physics community. LINCE will be a multi-user facility dedicated to ECOS science: fundamental physics, astrophysics, nuclear structure and reaction dynamics. Applied research is foreseen in the fields of medical physics, aerospace and material sciences with energetic heavy ions. The facility will produce a wide range of ions, from protons (45 MeV) up to Uranium (8.5 MeV/u) with 1 mA maximum beam intensity. A very compact linac has been designed using a HV platform with a double-frequency ECR ion source,[14] two-multi-harmonic bunchers,[15] an innovative CW RFQ design ($1< A/Q < 7$) and 26 accelerating cavities made of bulk niobium ($\beta = 0.045, 0.077$ and 0.15) working at 72.75 and 109.125 MHz.[16]

The ECOS report identifies several nuclear physics areas where investigations can only be addressed with high-intensity stable beams: super-heavy nuclei; nuclear structure and ground-state properties; near barrier transfer and fusion reactions; nuclear astrophysics and ion-ion collisions in plasmas. Applied research is foreseen in the fields of medical physics, energy, aerospace and material sciences.

In order to comply with such ambitious research program, it has been proposed the construction of a high-intensity CW superconducting linac for light- and heavy-Ion beams: the ECOS-LINCE facility. The design should be based on a reliable design using well-established technologies, aiming to provide smooth uninterrupted beam delivery during long-term experiments ($\sim$ months), and parallel operation for combining fundamental physics and applications.

General design characteristics:

1. Reliability and beam stability.
2. Easy, automatic, beam to tuning systeme.: including automatic tuning of the beam
3. High beam intensity: 1 mA for protons and light ions an $>10\,\mathrm{p}\mu\mathrm{A}$ for heavy ions.
4. The projected combined number of working hours to be considered are:
   - 5000 hours per year for Fundamental Physics
   - 2000 hours per year for Applications

1.2 Basic research

Superheavy Nuclei

Among the most important challenges in nuclear physics nowadays is the determination of the limits of stability, from the proton to the neutron rich side, up to extremely heavy masses and charges, e.g., the so-called region of super heavy elements (SHE). Therefore, investigating the existence of an island of stability beyond Uranium is a central topic in nuclear physics.

In the last years, a very important theoretical effort has been dedicated to obtaining the best descriptions and extrapolations of the mean field, far from the well-known $Z = 92$, toward higher masses. Among the diversity of models and results, the relativistic mean-field models show a region of stability cantered at $Z = 120$, $N = 172$.[17]

Regarding the experimental studies within this field, one of the biggest challenges is the increasing difficulty of producing SHE as the mass increases. A significant experimental effort has been dedicated to studying different fusion-evaporation reactions, where two main methods have been found to be successful. Firstly, reactions are induced by an intermediate-mass projectile impinging on either Pb or Bi stable targets. These reactions have been able

to produce elements up to $Z = 112$ at GSI (Germany), RIKEN[18] (Japan) and LBNL[19](USA). Using this method, RIKEN has reported the synthesis of element $Z = 113$ A second method is based on reactions between light ions and radioactive targets, usually from the region of actinides. Using a ^{48}Ca beam, neutron-rich isotopes of elements $Z = 112$, 116and 118 have been produced at the FLNR[20](Russia).

Together with the discovery of these new elements, there are also two important experimental results. Firstly, the expected increase in the half-lives of the new isotopes with the increasing neutron number as we approach the island of stability. Secondly, the measured cross sections for the relevant fission processes seem to be correlated with the variation of shell-correction energies and fission barriers. On the other hand, separators and detection systems of higher sensitivity and precision need to be further developed. This covers both in-beam nuclear studies of SHE and nuclear chemistry equipment and methods. Several neutron-rich elements present relatively long half-lives, from minutes up to days for isotopes near $N = 162$, which allows the application of new techniques, such as the use of Penning traps and measure masses and of other atomic and nuclear properties.

A very efficient tool for SHE production is provided by in-beam spectroscopy. The nuclei of interest are produced and separated from un-reacted beams and other reaction products. The relevant recoiling nuclei are identified at the focal plane of the separator using a correlated time-of-flight measurement between the prompt radiation at the target position and the recoils. The greatest challenge in this technique is to pick the extremely rare SHE events out of a background typically a factor 10^6 – 10^9 larger than the signal and special methods and strategies, allowing for a high counting rate, whereas keeping the required sensitivity needs to be developed. For cross sections below 1 nano−barn, in-beam studies are no longer possible, and the most efficient method consists in performing alpha decay spectroscopy at the focal plane of a separator. In this method, high currents of several particle-microamps are used with rotating target wheels. In order to make the most of the rare decays, all possible types of radiation (alpha, conversion-electron, gamma, X-ray, beta) need to be detected with high efficiency using focal plane arrays with high Si pixellation and excellent efficiency for the detection of conversion-electrons, X-rays and gamma rays.

Nuclear chemistry methods were among the first used in experiments performed at the UNILAC accelerator at GSI[21] (Germany) already in 1975, starting with a variety of heavy-ion reactions using mainly ^{238}U and ^{248}Cm targets and projectiles ranging from ^{238}U to ^{48}Ca. This has been, since then, an extremely successful and ongoing research program. The most recent and exciting experimental program is the gas-adsorption study of element 112, in

comparison with Hg and Rn – presumably the two extremes in the range of possible element 112 properties.[22] These experiments also have the potential to independently confirm results obtained with recoil separators.[23] The near future of research on SHE is in the search for stable and radioactive ion beams, of the highest possible intensity, together with the development of spectrometers and high-sensitivity instrumentation to detect charged particles.

The main priority of SHE research is to satisfy the demand for stable and radioactive ion beams of higher intensity.[24] The compound nuclei that can be reached with beams of stable ions are two representative targets: ^{208}Pb and ^{248}Cm. With the currently available stable beam intensities of about 1 particle pico − amps, and typical cross sections of 1 pico−barn, the production rate is only one atom per week. Therefore, improvements up to a factor of 100 would be required, which are also technically possible.

Nuclear Structure

Gamma-ray emission is one of the most important methods used to determine the structure of the nucleus, as it provides spin energy levels and parities. Great efforts have been made in the last decade to build highly efficient gamma arrays, such as the Advanced Gamma Tracking Array[25] (AGATA). The combination of such detector systems with a dedicated high-intensity stable beam facility will provide a unique tool to investigate, across the nuclear landscape, the evolution of shapes and dynamical motion, shell effects and residual interactions, and how they correlate with isospin, angular momentum and temperature.[26] Of particular interest are the fusion-evaporation reactions induced by the collision of heavy ions at energies around the Coulomb barrier, which are able to produce compound nuclei at high excitation and angular momentum. These reactions allow exploring super-deformation phenomena in medium-mass regions, where collective octupole and triaxial shapes have been observed, and other phenomena such as hyper-deformation,[27] shape transition and rotational damping, addressing new challenges to nuclear structure theory.[28] Intense experimental efforts are still needed for the detailed determination of spins and energies of super-deformed bands and their population mechanisms. Far from stability, the isospin quantum number plays a critical role in the dynamics of such asymmetric multibody nuclear systems. Experimental studies of single particle levels reflect a drastic change in shell gaps and standard magic numbers, which could eventually completely disappear. Theoretical analyses using microscopic models and mean-field theories should accommodate the extreme changes in nuclear size and diffusivity, including coupling to the continuum states, which will certainly lead to the discovery of new exciting and interesting phenomena.

High-intensity beams of heavy ions can also be used to reach both proton and

neutron rich systems, which can be studied by in-beam gamma-ray spectroscopy. Compound nucleus reactions at energies around the Coulomb barrier are an effective mechanism to produce proton rich nuclei, as the neutron emission process is usually the most effective de-excitation mode. A large number of nuclear systems can be reached by using accelerated heavy-ion beams, such as Xe, Pb or U. At energies below the Coulomb barrier, the one/two neutron evaporation channel is usually favored, which also gives it particular spectroscopic interest. The production of neutron-rich nuclei will become more efficient in "cold" nuclear reaction processes involving relatively low excitation energy, as in the case of multinucleon transfer reactions and deep inelastic processes at energies above the Coulomb barrier.[29]

Due to the large variety of reaction products and the fact that the production cross-sections of the interesting species decreases rapidly when approaching the drip-line, special devices and methods are needed to resolve the weak events from the background.[30] The required experimental sensitivity is achieved by using highly segmented gamma arrays in combination with ancillary particle detectors and/or large acceptance magnetic spectrometers, providing an efficient mass, charge and reaction channel selectivity. These techniques, in combination with the use of high-intensity stable beams of few tens particle-microamps ($\sim 1\,\mathrm{e}-\mathrm{mA}$), can be very competitive, allowing the development of a physics program complementary to the traditional radioactive beam facilities.

At the proton rich side, special effort should be dedicated to N=Z nuclei to study proton neutron pairing correlations, exotic deformations, coupling to the continuum and isospin symmetry in mirror nuclei.[31] These nuclei are also of astrophysical interest for studying the rp–process, which is relevant for stellar burning. Studies of mirror nuclei, currently limited to low spins and masses around $A = 50$, must also be extended to higher masses and/or angular momentum,[32].[33] Closer to the proton drip lines, detailed spectroscopic studies will provide better understanding of nuclear shape coexistence and exotic excitations; for example, the recent discoveries of triple-shape-coexistence in the region of Pb and Po isotopes demonstrate that more detailed spectroscopic studies are needed to understand these phenomena.[34]

In-flight gamma spectroscopy studies are complemented by particle decay studies like proton or alpha decay using the recoil Tagging Detection technique.[35] This technique allows extending these studies to the region of weakly bound systems, even beyond the proton drip line and well below the microsecond lifetime. The use of high-intensity beams in the range of several particle- microamps can be fully effective only if it is accompanied by a parallel investment in high efficient detection systems capable of sustaining high counting rates up to 100 kHz and robust high-power target systems.

Nuclear Molecules and Clustering Phenomena

The tendency of nuclear systems to exhibit molecular-like structures has been already known for many decades, with the alpha chain states in carbon isotopes being the paradigm of such nuclear structure phenomena.[36] It appears to originate as a consequence of the saturation properties of the residual nuclear interaction, which favors the formation of N=Z aggregations of protons and neutrons in nuclear states with low binding energies close to the cluster emission threshold.[37]

Clustering phenomena are found to be extremely abundant within stable nuclei, and a common effect characteristic of lighter drip-line nuclei. It is strongly related to extreme deformations, giving rise to shell model super and hyper-deformation. Of particular interest are, again, the N=Z nuclei and the exploration of clustering structures, which are presumably dominant in the region of super-heavy nuclei. Although cluster structures in nuclei have been reported since the early 1970's, theoretical approaches are still unable to provide a complete description of the experimental results and much experimental and theoretical work still needs to be done.[38]

On the experimental side, cluster spectroscopy has been traditionally under the domain of charged particle detectors due to the extraordinary challenge of detecting the extremely small expected gamma width. However, the new generation of gamma-particle detector arrays, which include high-efficiency gamma detection systems, should give new insights into exotic shapes in nuclei related to clustering. For these studies to become a reality, the availability of a high-intensity stable beam facility, where sufficiently long experiments can be carried out, is decisive.

Near-barrier Transfer and Fusion Reactions

Transfer reactions involving stripping and pick-up of neutrons and protons are particularly useful as a spectroscopic tool due to their selectivity, which can favor the population of specific single particle/hole states.[39] Thus, relevant spectroscopic information concerning the single-particle nature of the observed levels can be experimentally obtained, and then be compared with theoretical calculations. With the proper selection of the reaction and kinematical conditions, these reactions can be valuable a spectroscopic tool, as they provide single particle strength, spin and parity. Through one-nucleon transfer reactions, one can study shell structures close to the Fermi surface, whereas multi-nucleon transfer allows tackling nuclear correlations in the nuclear medium.[40] Using intense stable ion beams, shell evolution and nucleon-nucleon correlations can be studied along different mass chains up to the proton and neutron drip lines.

One of the important topics to be addressed is the understanding of the mechanism of correlated pair transfer of protons and neutrons and the effect of nucleon-nucleon correlation, particularly the role of multi pair-phonon states.[41] Experiments with medium-mass projectiles (e.g., ^{40}Ca) on heavy targets have given some clues about the underlying physics. For such studies, experimental setups must be able to locate and identify all the states in a given nucleus, with the capacity to measure the corresponding single particle strength. This correlation effects can also be studied via heavy ion reactions, looking for the transfer of multiple nn, pp, and np pairs.[42]

The energy region far below the Coulomb barrier is another interesting area to investigate the role of nucleon-nucleon correlations via nucleon transfer reaction channels. At these energies, the nuclear-coupling is dominated by one-nucleon transfer and, therefore, the multi-nucleon transfer should proceed via a sequential reaction mechanism. Far below the barrier, the transfer strength should be concentrated in few states close to ground state, and odd-even staggering could be observed in the final yields, giving perhaps new evidence of the effect of nucleon correlations, Josephson effects or diabolic pair-transfer phenomena.[43]

Future studies to be carried out in a future high-intensity stable beam facility must use detector systems with improved gamma-particle coincidences in combination with large solid angle spectrometers. High-intensity stable beams of few particle-microamps are needed for the observation of these weak transitions, thus paving the road to the study of multi pair-phonon excitations. Sub-barrier fusion reactions are an important field of research as the different reaction channels associated with surface vibrations or nuclear rotations, breakup and nucleon transfer channels can strongly affect the behaviour of the fusion excitation functions. By selecting nuclear species with an increasing number of neutrons, one should expect a stronger nuclear interaction and an effective reduction of the Coulomb barrier, thus increasing the fusion probability. However, the addition of more neutrons does not necessarily lead to larger fusion cross sections, as demonstrated for the ^{40}Ca, ^{48}Ca isotopes. Coupling effects arising from specific details of the nuclear structure and dynamics of the involved systems can reduce the fusion yields for the richer neutron systems. An important reaction channel with strong effects on heavy-ion fusion is the two-neutron sequential transfer process, and a successful description of the data can be only achieved by including this process in the coupled reaction channel calculations.[44]

Sub-barrier fusion cross sections are at a level of some few nano-barns. To reach this level of sensitivity, a special detector system is required. Here is a recommended setup based on a recoil mass spectrometer with extremely high background suppression and a focal plane gas detector system with multiple

segmentation.[45] Increasing the beam intensity from present available particle-nanoamps to particle-microamps would allow exploring sub-barrier fusion phenomena at even lower bombarding energies and for a wider range of nuclear combinations.

Astrophysics

Nuclear astrophysics processes are intimately linked to the structure of reacting nuclei, which has a profound impact in the relevant reaction mechanisms present in the nuclear burning processes that take place in the stars, the associated nucleosynthesis and the corresponding energy production. These processes are governed by the values of nuclear masses, deformations, level densities and isospins. Therefore, many of the topics of interest mentioned above play a critical role in the context of nuclear astrophysics.

The new foreseen facility should provide intense heavy-ion beams for indirect astrophysical measurements based on transfer reactions, Coulomb break-up, or capture reactions in inverse kinematics. The latter case might bring a possible solution for reducing the background produced in measurements with radioactive beams, a persisting problem found in many measurements in astrophysics. In addition to these techniques, the traditional "direct" method based on accelerating light ions at low energies will still address a large variety of open fundamental issues with relevance in the field of nuclear astrophysics.[46]

Of particular interest are the key reactions involving Hydrogen, Helium, Carbon and Oxygen participating in the pp chain and CNO cycles, as they determine whether the star evolves into an early carbon-detonation supernova or into a type I or type II supernova. Another important topic of interest is to study the origin of the so-called p nuclei, which have been only observed in the solar system. Different scenarios occurring in exploding supernovae (SNII) or in He-accreting white dwarves have been proposed. In this case, abundance calculations must rely on the very few available experimental data about (alpha, gamma) reactions of interest, and by using systematic alpha particle optical potentials. However, these potentials have shown to be wrong by a large factor and, therefore, an important experimental effort must be dedicated to the measurement of alpha optical potentials with heavy targets at low collision energies, mainly in the $100 < A < 200$ region.[47] On the experimental side, the accuracy needed for nuclear astrophysics measurements demands time-consuming low-energy experiments very often; many of these are performed at small-scale astrophysics laboratories in Europe (mainly in Germany, such as Karlsruhe, Stuttgart and Bochum), which are already closed or will be closed in the near future. Therefore, there is an urgent need for an European first-class high-intensity low-energy stable beam facility with dedicated detection

equipment, such as a crystal ball and a recoil detector, that will complement the work carried out at current radioactive beam facilities.[9]

1.3 Applications

Traditionally these high-intensity ion facilities can be employed not only for basic research, but also for direct applications relevant to society. The production of clean energy by means of nuclear fusion is a main priority of the EU midterm energy policies. A large international collaboration is participating in international projects, such as IFMIF-EVEDA[48] and DEMO,[49] and at the ITER[50] demonstrator facility, which is being built in Cadarache (France).

Fusion Energy

The development of nuclear fusion energy is one of the most important technological challenges of humanity. For the European Union (EU) this field is considered within the main research programs, and an agreement was signed in June 2005 with USA, Russia, China, South Korea, Japan and India, for the construction of ITER (International Thermonuclear Experimental Reactor). The selection, development and testing of the materials and items composing the various reactor systems, together with the design of the energy extraction and tritium reproduction systems, are considered the most important challenges in the fusion research program.[50]

In the field of materials science, a main research line which will be carried out during forthcoming decades is dedicated to the study of the effect of neutron radiation on materials composing the reactor. Neutron radiation on materials will essentially produce two physical phenomena:

1. Ions displacement from their positions at the crystalline structure, causing point defects.
2. The generation of nuclear transmutation reactions, which lead to the generation of impurities in bulk material, with the most important cases being those of He and H production.

The ratio between the level of He and H and the number of point defects is one of the most important parameters concerning the effect of radiation in materials. Existing neutron sources have significant technological difficulties as well as low versatility. Therefore, alternative methods have been developed to simulate, in a simpler way, the effect of neutron radiation while also reducing the radiological risk during the operations.[51] Current computer simulation studies have demonstrated that the effect of neutron irradiation can be simulated

by using a set of three-ion accelerators, two of them implanting He and H beams, together with a heavy-ion beam able to produce point defects (e.g., Fe in the case of steel irradiation).[52] This type of application requires the use of several types of heavy-ion beams, from Hydrogen up to Tungsten and intensities ranging from $1\,\mu A$ for ^{184}W beams to $40\,\mu A$ for ^{16}O beams.

Aerospace

Heavy-ion accelerators can be used to study the response of electronic systems to radiation effects. Several collaborations involving the aerospace industry and research groups from universities and technological institutes are developing a number of R&D projects for the European Space Agency (ESA), the Spanish Institute for Aerospace Technology (INTA-Spain) and the Centre National d'Etudes Spatiales (CNES) in France, among many others. Specialized companies such as Thales Alenia Space, Eads Crisa, Eads Astrium, Alter Technology or Arquimea are interested in having beam time available for dedicated testing and development of on-board aerospace electronics.

The main contribution to the degradation process of electronic equipment in aircrafts and aerospace vehicles is due to the impact of energetic particles on the electronic circuits and components. These particles are mainly protons and electrons confined in the Van Allen belts around The Earth, although thermal neutron radiation also contributes in the case of more standard atmospheric flights. The continuous radiation bombardment can cause transient functional anomalies and other dangerous effects. Some of these, the so-called "Single Event Effects" (SEE), can cause the corruption of data processing and, over time, a full permanent degeneration of the electronic device. This radiation environment can be reproduced in the laboratory using a heavy-ion accelerator with typical fluences in the range of 10^8 ions/cm^2/s. The nature of the radiation (protons, helium, heavy ions), energy, and the beam fluence define the type of test, which in turn will depend on the internal structure, design and intended use of the device.[53] In Europe, the ESA-Space Components Coordination Group (SCCG) regulates the certification and qualification of electronic devices to be used in the aerospace industry. There are three accredited laboratories in Europe (RADEF, HIF, PSI).

For this purpose, proton beams in the range of [5-70] MeV are used, as in the case of the European laboratory LE-PIF (Low Energy Proton Irradiation Facility) at the Paul Scherrer Institute[54] (PSI) in Switzerland. Heavy-ion beams are also used in a wide range of energies up to 10 MeV/u, as in the case of RADEF (Finland) or HIF (Belgium). Table 1.2 shows the typical range of energies and LET in RADEF (Finland).

Nuclear Medicine

Table 1.1: Range of energies and LET in RADEF (Finland).

Ion	Energy (MeV/u) (MeV/u)	$\mathbf{LET^{MEAS}}$ @Surface ($\mathbf{MeV/mg/cm^2}$)	$\mathbf{LET^{MEAS}}$ @Bragg Peak ($\mathbf{MeV/mg/cm^2}$)
$^{15}N^{+4}$	139	1.87	5.92(@191 um)
$^{20}Ne^{+6‡}$	186	3.68	9.41(@138 um)
$^{30}Si^{+8}$	278	6.74	13.7(@114 um)
$^{40}Ar^{+12‡}$	372	10.08	18.9(@100 um)
$^{56}Fe^{+15}$	523	18.84	29.7(@75 um)
$^{82}Kr^{+22}$	768	30.44	41.7(@68 um)
$^{131}Xe^{+35}$	1217	54.95	67.9(@57 um)

Radioisotopes

During the last decade the production of radioisotopes has become an important source of income, as they have a large variety of applications in industry, science, military and medicine. In particular, the number of nuclear medicine prescriptions has tripled since 1996, and it is already exceeding 30 million procedures a day. In all of these prescriptions, radioisotopes play a key role in therapy as well as in various diagnostic methods.[55]

The increase of the worldwide demand, together with the closure of nuclear reactors dedicated to radioisotope production, has caused a global shortage in the supply of Mo-99 isotope. The importance of this radionuclide lies in the fact that it is the standard source for the production of **Tc-99m**, which is widely used in Single Photon Emission Computed Tomography (SPECT).[56] This situation is becoming extensible to other radioisotopes, such as I-123 and I-122. Therefore, it is considered that radiopharmaceutical production methods will be one of the most important lines of research in the field of nuclear medicine in the nearest future. Other radioisotopes of interest are C-11, N-13, O-15, F-18, Cu-64, Cu-67, In-111, Tl-201 and I-123; Table 1.2 shows the main radioisotopes. Most commercial isotopes are produced with proton beam energies up to 40 MeV, which has become a standard in commercial radioisotope cyclotrons. Higher energies are required for the production of some isotopes, such as Sr-82, Ru-97, Xe-122 and Ba-128, and for the use of thick targets that can increase the production, although controlling the ratio of impurities. Proton beam energies available can reach up to 66 MeV at the Ithemba laboratory (South Africa) or 70 MeV at PSI (Switzerland) and ARRONAX (Nantes, France). An advantage of LINAC accelerators is that energy can be varied in a large range and, therefore, they do not constitute a limiting factor in radioisotope production.[57]

Deuterium and alpha particle beams in the energy range proposed have also been used for the production of isotopes such as Sn-117m, Ac-225, As-73,

Table 1.2: Main Radioisotopes of medical interest).

Radionuclide	Half-life	E mean (keV)	Ey (keV)	Ey (keV)
Y-90	64 h	934 β		12 mm
I-131	8 days	182 β	4	3 mm
Lu-177	7 days	134 β	208, 113	2 mm
Tb-161	7 days	154 β 5, 17, 40 e^-	75	2 mm
At-211	7.2 h	5870 α		45 μm
Tb-149	4.1 h	3967 α	165,...	25 μm
Er-165	10.3 h	5.3 e^-		0.6 μm

Fe-55, At-211, Cd-109, Y-88, Se-75 and Po-210. Of particular interest is the production of Cu-64, Y-90, Tc-94m, I-124 and Re-188, which are becoming more relevant in nuclear medicine. Brachytherapy techniques involve the activation by irradiation of a thin sheet which is then implanted in the tumour area. This technique is widely used in modern hospitals to treat ocular tumours (glaucoma), lungs and critical organs. Cardiac ischemia is treated with sheets in which radioactive ions have been implanted.[58]

New technologies based in the use of two isotopes of the same element for simultaneous imaging and tumor targeted systemic therapy (theranostics) are in rapid development.[59] Some relevant radioisotopes are for example the different Tb isotopes (^{149}Tb, ^{152}Tb, ^{155}Tb and ^{161}Tb).

Proton therapy

Heavy-ion accelerators are currently used as the finest technique (with over 90% success) to treat tumours and cancer. Proton therapy is particularly appropriate in situations where conventional radiotherapy presents an unacceptable risk for the patient (e.g., in the case of eye cancer, and pediatric patients). The excellent definition of the penetrating power of the protons in the body allows an effective irradiation of the tumour with millimetre resolution. This technique was already developed about 30 years ago and it is already implemented in most modern EU countries.[60] At present, there are about seventeen EU hospitals routinely using proton beams for tumour treatment for more than 75000 patients a year, who suffer from this disease. The statistics show that proton therapy could treat around 11000 patients a year in Spain.

Prestigious proton therapy centres in Europe are the "Paul Scherrer Institute (PSI)" in Villigen (Switzerland, since 1984), the "Proton Therapy Centre" in Paris (France, since 1991), the "Helmholtz-Zentrum Berlin (HZB)" in Berlin orchestrating (Germany, since 1998), the "Westdeutsche Protonen- therapiezentrum Essen" in Essen (Germany, since 1999) and the "Proton Therapy Center

Czech" in Prague (Czechoslovakia), since 2016.

The LINCE project emphasizes radioisotope production and cancer treatment by proton therapy, and the team at the University of Huelva has promoted a number of very successful R&D projects on this area, funded by the Spanish Government, as complementary extension of the resent work.

New materials: Micro-membranes and Nanotechnologies

A membrane is a porous thin film (polymer, metal, ...) through which a fluid (liquid, gas) can be filtered to perform a separation process. Filter types are classified by the particle size or the technology employed. In the case of microfiltration, micropores are used in the range of 0.1 to 10 μm. For some applications, this range may reach some tens of nanometers (e.g., diffraction filters).[61]

The use of the tracks or paths left by accelerated ions when passing through the materials, for the production of porous membranes, was proposed almost immediately after the discovery of chemical etching by Fleischer in 1964. This chemical process is responsible for the formation of pores. In the process of ion irradiation, the track or trajectory of ions in the material generates a damaged region, in such a way that its content can be chemically removed, thus becoming a hollow channel or tunnel. There are basically two methods of heavy-ion material irradiation that can be later used to produce micropore membranes. The first method is based on the irradiation of the membrane with fission fragments produced by fission sources like uranium or californium.[62] The second method consists in the use of ion beams produced by accelerators fleisher-1975,.[63] The fluence should be at least $10^{11}/s$ to be able to compete in the industry of micro-membranes. Nowadays, most accelerators can provide much higher intensities. Commonly used heavy-ion beams are Xenon, Krypton and Argon, in a typical energy range between 1 and 5 MeV/u, depending on the requested ion and the material to be treated. In the case of irradiation of large areas, a heavy-ion scanner system is used. The main advantages of a heavy-ion accelerator are the following:

1. Absence of radioactive contamination (E <coulomb barrier).
2. High-purity beam, to ensure that the tracks have the same behavior in the chemical etching process.
3. Possibility of using higher and variable energies, enabling the irradiation of thicker films.
4. Better conditions to produce matrices with high-density tracks ($> 10^9 cm^2$).
5. Ability to use heavy ions in a wide range of masses and charges.

6. Production of parallel tracks.

Microporous membranes are produced in the accelerators of Brookhaven Laboratory (USA), Flerov Laboratory of Nuclear Reactions (Dubna, Russia), Cyclotron Research Centre (Louvain-la-Neuve, Belgium), and Berlin (Germany), among others. Development and research activities are ongoing at GSI (Germany), AVF cyclotron (Takasaki, Japan), IPN (Orsay, France), RIKEN (Saitama, Japan), GANIL (Caen, France), among others. The following are some of the relevant applications:

- Pharmaceutical, cosmetic and food industry: detection of bacteria and micro-organisms, micro-controlled emulsions.
- Health: biosensors, oncology, cytology.
- Energy: solar cells (exchange membranes).
- Nanotechnology: building "nano-reactors", e.g., systems for the production of nanoscale materials (metals, superconductors, polymers) in various structures such as wires, tubes or multilayers.
- Diffraction filters (X-ray astronomy).

2

Design Requirements

This chapter presents the design requirements of the LINCE facility.

2.1 Design requirements

The proposed CW multi-ion superconducting Linac should be able to accelerate a wide range of ions and energies, from protons up to Uranium. Overall design requirements from the point of view of the users are:

1. Maximum energy for heavy ions: 8.0 MeV/u.
2. Maximum energy for protons: 40 MeV.
3. Maximum intensities of 1 mA for light ions (protons and alphas) and 10 pμA for heavy ions.
4. Transverse emittance (normalized, rms): < 0.1 ·mm·mrad.
5. Longitudinal emittance (rms): < 1 ns·keV/u.

From the point of view of the machine, it was adopted that the maximum beam losses in the LINAC accelerator, due to the fact that the resonators are superconducting, should be < 1 nA/m. Details of the requirements and overall design have been published elsewhere,[3,14,15,16,64,65,66,67,68,69,70,71]

The beam dynamics studies were carried out with the code TRACK, using realistic electromagnetic fields obtained from the existing ATLAS superconducting accelerator, already in operation at Argonne National Laboratory (USA),[72] including space-charge effects,[66,65] These studies have provided optimum configurations using realistic working parameters, minimizing the length and complexity of the accelerator. A layout of the full accelerator system is presented in Figure 2.1. The solution combines two frequencies for the RFQ and SC cavities (72.75 and 109.12 MHz). Moreover, and due to the requirements of the experimentalists, a sub-harmonic of both frequencies (18.1875 MHz) was used as pre-buncher (in front of the RFQ) allowing a time gap between bunches of 54.98 ns. This timing is needed for experiments using time-of-flight. The main LINCE subsystems considered in the project are the following:

- Superconducting Electron Cyclotron Resonance (ECR) ion source with extraction voltage of 30 kV and focusing solenoid.
- High-voltage platform from 10 kV to 280 kV, where the ECR is placed.
- Low-Energy Beam Transport line (LEBT).
- A multi-harmonic buncher at the fundamental frequency F=18.1875 MHz He beams.

- RFQ to accelerate pre-bunched ions up to 500 keV/u operated at 72.75 MHz for q/A charge-to-mass ratios from 1/7 to 1.
- Four accelerating cryomodules (C1 to C4) housing superconducting quarter wave resonators (QWR) and solenoids.[64]
- Rebuncher section (C5).

An important element in this design is the choice of the factor q/A (charge-state / atomic-mass) characterizing the heavy-ion beam. In principle, the design of the main components (RFQ and SC cavities) is strongly related to this choice. The final beam energy per atomic mass unit (MeV/u) is proportional to both the total accelerating available voltage and the Q/A factor. For any configuration, it is required to reach an agreement for the Q/A value. Low-charge state ions, are obviously easier to obtain with an ECR Ion Source; however, this leads to lower Q/A factors, thus decreasing the final energy per unit mass.

The design goal chosen in this work is A/Q covering the range between 1 (protons) and 7 (heavy ions). It corresponds to accelerated beams of $H+$, $C3+$, $Ar8+$ and $Kr20+$, for example. Commercial Electron Cyclotron Resonance (ECR) ion sources can deliver high currents of several $p\mu A$ for many heavy-ion species and charged states. A convenient choice is an ECR with full permanent magnet construction, which reduces the power needs of the system at the HV platform. However, no commercial option is available at present to achieve high-charge states up to U $U30+$ at high currents of $10\,p\mu A$. A dedicated superconducting ECR working at double frequency (14/18 GHz) was under study during the ACELTEC project.[14] This will not be detailed in this work.

The fundamental beam bunch frequency of F=18.1875 MHz is an appropriate choice for achieving a minimum bunch spacing of 50 ns required in time-of-flight applications. For proton and helium beams, a second buncher working at the first harmonic F = 36.375 MHz is needed due to the space charge effects.

The normal conducting LINCE RFQ should operate at 72.75 MHz (4th harmonic of fundamental frequency) and is designed for A/Q=1-7, with an input energy of 40 keV/u. It is composed of a total of ten oxygen-free electronic (OFE) copper structures brazed in a high-temperature hydrogen atmosphere furnace, with a total length of 5.0 m. Each section has 500 mm length and should be machined with a high mechanical precision below $100\,\mu m$. The RFQ delivers a final energy of 500 KeV/u with a RF power consumption of 150 kW.[73]

For heavy ion accelerators, superconducting (SC) cavities represent the best choice to reach high energies with reasonable accelerator sizes and RF power levels, as the critical performance is the accelerating gradient, which is obtained with current state-of-the-art technologies. All these performances are the result of many recent technological developments, improving fabrication techniques

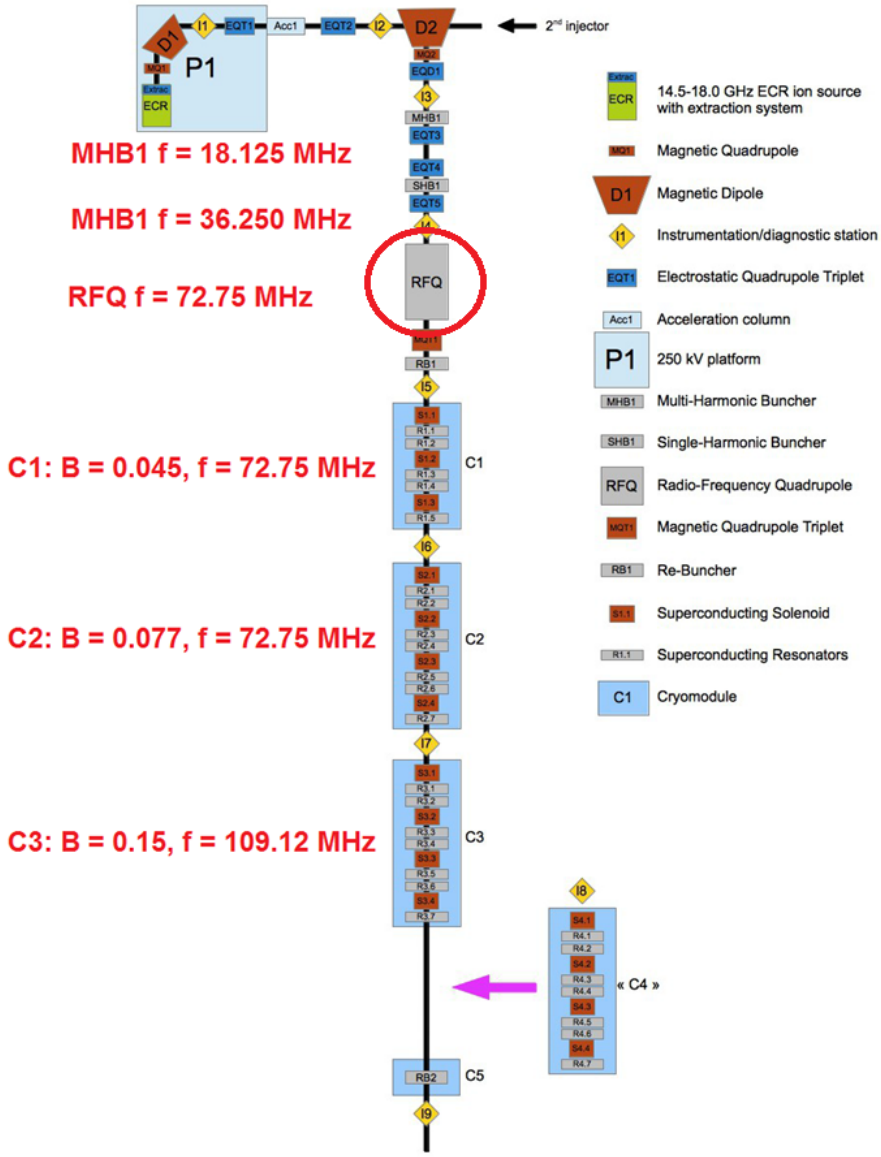

Figure 2.1: Proposed layout of the ECOS-LINCE superconducting linac[3]

and preparation of the surfaces. Four Heavy Ion Linacs these are the references used in this work: ATLAS upgrade phase[72] (ANL, USA), Spiral2[12] (GANIL, France), ALPI-LNL[74] (Legnaro, Italy) and FRIB[75] (Michigan, USA). The LINCE proposed resonators can take advantage of well-known high-performance resonators used in those facilities.

This study shows that the LINCE accelerator needs only 26 superconducting QWR cavities with three values of $\beta = 0.045$, 0.077, 0.15, working at 72.75 MHz and 109.125 MHz, to achieve very close figures of energy and intensity corresponding to the requirements. Those resonators are organized in only four cryostat modules, plus one for the re-buncher. The first cryostat has 5 resonators with $\beta = 0.045$ and frequency = 72.75 MHz. The second cryostat has 7 resonators with $\beta = 0.077$ and frequency = 72.75 MHz. The third and fourth cryostats have 7 resonators with $\beta = 0.15$ and frequency = 109.125 MHz. The beam dynamics of the whole accelerator are described in detail in chapter 4. The accelerating cryomodules provide reasonable compactness, less construction complexity and easy maintenance. Extra cryostat modules can be added to the system in the future.

The superconducting quarter wave resonators (QWR) chosen in this project are pure niobium bulk material, working at T=4.5 K. The fabrication technique was developed in the various laboratories cited above and are produced primarily by Nb sheet forming and precision machining. The resonator is to be assembled by using electron beam welding. Appropriate RF surface processing including buffer chemical polishing, electropolishing and high-pressure water rinsing are required prior to the installation of resonators into the various cryomodules.

Beam dynamics calculations were performed with TRACK code. With the present structure of the accelerator, all ion beams with mass-to-charge ratio from 1 to 1/7 can be accelerated with this structure as will be shown in the following chapters of this work.

No detailed studies of the cryogenics distribution were performed in this work; however, preliminary studies show that, in order to reliably operate the five cryomodules of LINCE at 4.5 K, a total cryogenic power of about 1 kW is needed. This dimensioning is based on the addition of realistic static losses, dynamic losses and margin for possible operations with higher voltages using known values of similar cryomodules. The expected dynamic cryogenic load is below 10 W per cavity, giving a total of 260 W. The static losses strongly depend on the cryostats design and the distribution of the infrastructure installation, and a typical margin level installed in other similar linacs is about 30%. Taking all these considerations into account, the cryogenic system should be designed for a minimum of 1 kW at 4.5 K.

Type of Installation.

According to Royal Decree 35/2008, the radioactive facilities are devices of any kind that contain a source of ionizing radiation:

(a) Ionizing radiation producing devices that operate at a potential difference of over 5 kV.

(b) Premises, laboratories, factories and facilities where radioactive materials are produced, used, possessed, treated, handled or stored, excluding their incidental storage during their transport.

According to their characteristics, radioactive facilities are classified in First, Second and Third class:

- First-class radioactive facilities:
  - Production factories for uranium, thorium and their compounds.
  - Production factories for natural uranium fuel elements.
  - Facilities that use radioactive sources for industrial irradiation purposes.
  - Complex facilities that handle large inventories of radioactive substances or radiation beams to produce very high power flow, which makes the potential radiological impact of the facility to be significant.
- Second-class radioactive facilities are (provided that it does not mean a first-class radioactive facility):
  - Facilities handling or storing radioactive nuclides which might be used for scientific, medical, agricultural, commercial or industrial purposes, whose total activity equals or exceeds 1000 times the exemption values set out in Instruction IS-05 of Nuclear Safety Council.
  - Facilities that use X-ray generating devices operating with a peak voltage over 200 kV.
  - – Particle accelerators and facilities housing neutron sources.
- Third-class radioactive facilities are:
  - Buildings and areas used for handling or storing radioactive nuclides whose total activity exceeds the exemption values set out in Instruction IS-05 Nuclear Safety Council, but no more than 1000 times.

– Facilities that use X-ray generating apparatuses whose peak voltage is below 200 kV

According to this classification, LINCE should be categorized within the SECOND class in its initial phase, but it might become a FIRST-class facility with the development of applications.

Safety and radio-protection.

High-intensity heavy-ion linear accelerator facilities are regulated in Spain by the law RD 35/2008, of January 18, for the Regulation on Nuclear and Radioactive Facilities, approved by Royal Decree 1836 of December 3rd 1999, and additional safety regulations established by the Nuclear Safety Council (CSN). The LINCE facility, mainly due to the applications program , requires a dedicated implementation study and special safety measures, due to the production of ionizing radiation through radio-isotope interaction with the environment, both voluntarily and involuntarily. This study must be done and delivered to the Government for approval prior to the start of construction of the building.

3

Radiofrequency Quadrupole Design

This chapter contains a brief theoretical background for designing Linear accelerators. A basic introduction to radio-frequency accelerators is presented in section 3.1 and 3.2. Section 3.3 describes in more detail the theory of radio-frequency quadrupole accelerators (RFQ). Section 3.4 focus on the methodology and tools used to carry out the simulations and RF test studies.

3.1 RF linear accelerators

A LINAC is a device used to accelerate bunches of particles (from now on just "bunch") while they are moving on a linear path. The bunching system is located between the ion source and the entrance of the LINAC. The acceleration is provided by time-dependent electromagnetic fields set at a specific frequency. The time-varying electric field applied to the bunches increases the velocity of the particles, provided they are at the right relative phase with respect to the field, as shown in Figure 3.1. Each bunch is accelerated into a cavity resonator which is excited by an external RF power source. An appropriate phase between each bunch and the fields is absolutely necessary to obtain the maximum energy gain and the correct timing for injection into the following resonator.[76]

The velocity $\beta = v/c$ of the particles at the entrance of the LINAC determines the size and the design of the cavites, as well as the drift tube between them. As the velocity of the particle bunch increases, the length of the drift tube must be increased in order to maintain the synchronization between the bunch and the maximum acceleration voltage.

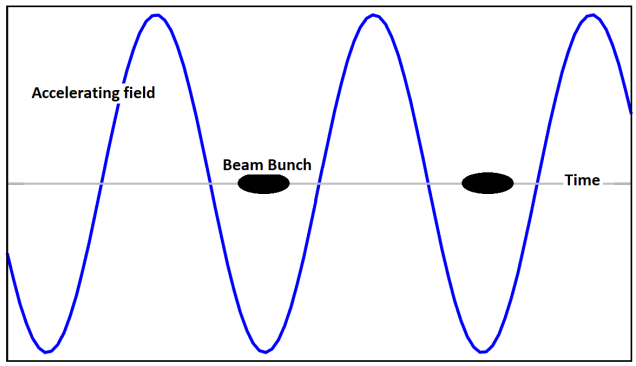

Figure 3.1: Particle beam bunch in an RF accelerating field.

In order to describe the amount of the supplied RF-energy that is effectively used to accelerate the particle, the concept of transit time factor (TTF) is introduced.

The "voltage" in a cavity along the particle trajectory (eq 3.2) is given by the integral along this path for a fixed moment in time (it will be in coincidence with the axis of the cavity), as shown in Figure 3.2:

$$V = \int_L E_{(z)} dz \tag{3.1}$$

The time variation of the field in the cavity is given by

$$E_z(z,t) = E_z(z) f(t) = E_z(z) cos(\omega t + \varphi) \tag{3.2}$$

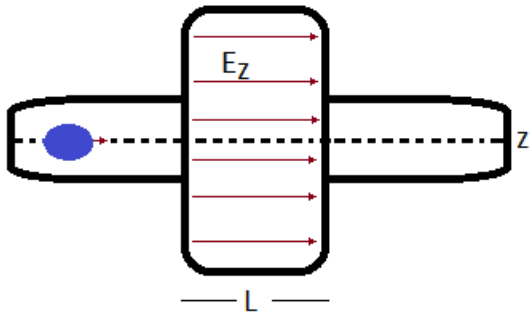

Figure 3.2: Constant electric field E010 mode.

Therefore, the field seen by the particle is

$$V = E_0 \int_{-L/2}^{L/2} cos(\omega t + \varphi) dz \tag{3.3}$$

The transit time factor is defined as

$$T = \frac{V}{\hat{V}} \tag{3.4}$$

where V is the voltage seen by the particle and V is the reference voltage. Usually, the reference is taken at the time when the longitudinal field strength of the cavity is at its maximum, $cos(\varphi) = 1$. A particle with infinite velocity passing through the cavity at this moment would see

$$\hat{V} = E_0 L \tag{3.5}$$

But the particle is sampling this field with a finite velocity $v = \beta c$. The resulting transit time factor is[77]

$$T = sin\left(\frac{L}{2}\frac{\omega}{\beta c}\right) / \left(\frac{L}{2}\frac{\omega}{\beta c}\right) \tag{3.6}$$

Figure 3.3 shows an example of the dependence of the transit time factor on beta for a different number of cells studied by Saini.[78]

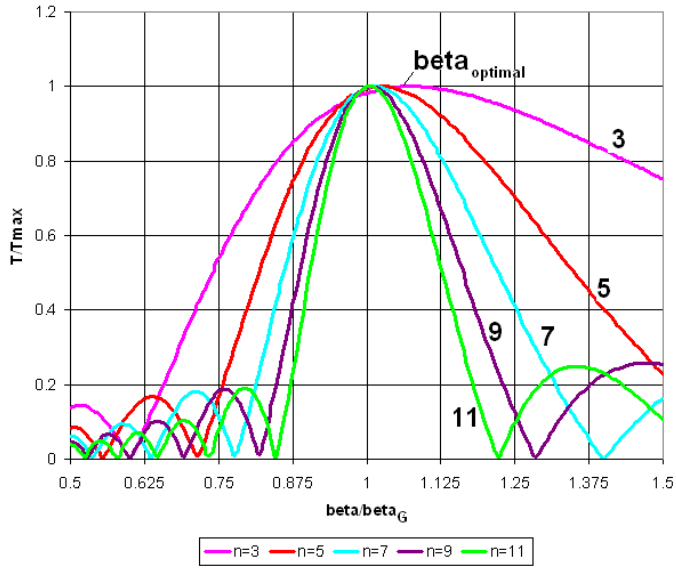

Figure 3.3: Dependence of transit time factor on beta for a different no. of cells.[78]

Modern linear accelerators are composed of different types of accelerating structures, the so-called "radiofrequency (RF) resonant cavities", that allow directing the beam while controlling its characteristics. The RF cavities are characterized by a high Q-value (a measurement of the cavity performance and stored energy available for acceleration, see Section 3.2), which are excited by RF electromagnetic fields at its resonance frequency mode using a RF-power source, such as Klystrons or RF power amplifiers. It is fundamental to conduct a very detailed geometric and electromagnetic design study of the cavities to obtain high values for the quality factor and the stored energy.

It is important to remark that, with the aim of reducing the cost and obtaining a practical design of the LINAC, a limited number of resonators, characterized by an optimum beta value, must be chosen. The resonators are usually grouped in acceleration sections (cryomodules in the case of superconducting linacs), containing the minimum number of resonator types with the same beta value needed for efficient acceleration, each section corresponding to each one of the selected values of beta.

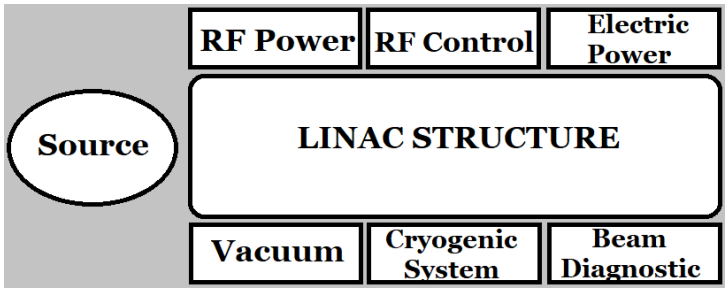

Figure 3.4: Scheme of a RF Linac Accelerator.

High-intensity heavy-ion beams are commonly generated at very low energies (few keV/u) in ion sources based on the electron cyclotron resonance principle (ECR). In most linac systems the particle beam is driven through a low-energy beam line (LEB) to a buncher system, an RF cavity that produces pulses of width and time structure optimized to match the LINAC input characteristics. The LINAC structure includes several elements: magnets (solenoids), that focus the beam on the Rf-cavities, the radio-frequency quadrupole (RFQ), a special type of RF cavity that provides both bunching and first acceleration at very low betas (~ 0.005), the main RF-cavities for higher beta values or energies, as well as the vacuum, electric, cooling and RF power systems.

The main advantages of RF accelerators are the capability to produce particle beams with high energy, high intensity, reasonable small diameter ($\sim 2\,\text{mm}$) and energy spread ($\sim 0.001\%$). A simple scheme of a RF Linear accelerator is shown in Figure 3.4. The beam is produced in an ion-source, e.g., Electron Cyclotron Resonance (ECR), and then it goes into Linac. The RF power is fed by the electrical power and controlled by a RF system. The cooling system depends on the type of accelerator. Normal conducting accelerators use water to maintain the temperature of the cavities, whereas superconducting (SC) accelerators use liquid helium. To achieve an optimal beam transmission a good vacuum system is needed ($\sim$ 10-7 mb), and becomes a critical part of the system in the case of SC accelerators due to the ultra-high vacuum requirements of the cavities. The beam parameters are measured with beam diagnostic systems such as Faraday cups, beam-current meters, beam-emmitance meters and beam position monitors.[79]

There are several types of LINAC structures, among which it is worth highlighting the following: super conducting linac (SC), quarter wave resonator (QWR), half-wave resonator (HWR), drift tube-linac (DTL), side coupled-linac (SCL), interdigital-H (IH), radio frequency quadrupole (RFQ) which is the most compact version. The RFQ focus, bunch and accelerate particles at the same time; they are often used in the very low velocity region, with beta values

ranging from about 0.01 to 0.006. The quadrupole mode is excited by four electrodes arranged symmetrically around the beam axis. The beam-focusing transverse electric field generated by RFQ is very strong, which makes it very useful also for driving ions and protons. The longitudinal electric field produced by the sinusoidal modulation in the electrode tip causes particle acceleration and bunching . The RFQ parameters and principles are explained in more detail in section 3.3.

3.2 RF acceleration

For each RF cavity type, there is a specific set of design parameters that must be analyzed to optimize the energy gain and beam transmission characteristics. A proper selection of this values will allow as well to deliver RF energy from the electric field to the beam more efficiently. The most relevant parameters used in the design are explained in this section.

To start with a description of a cavity resonator, it is fundamental to take the Maxwell's equations into account.

The laws expressed in differential form for a vacuum are:

Ampere's law

$$\vec{\nabla} \times \vec{H} = \vec{J} + \frac{\partial \vec{D}}{\partial t} \tag{3.7}$$

Faraday's law

$$\vec{\nabla} \times \vec{E} = -\frac{\partial \vec{B}}{\partial t} \tag{3.8}$$

Gauss's law (Electricity)

$$\vec{\nabla} \cdot \vec{H} = \frac{\rho}{\varepsilon_0} \tag{3.9}$$

Gauss's law (Magnetism)

$$\vec{\nabla} \cdot \vec{B} = 0 \tag{3.10}$$

where ρ is the charge density and J is the current density. It was also shown that the electromagnetic field can propagate as electromagnetic waves.

The acceleration can be expressed from the sum of the forces:

$$\frac{d^2\vec{z}}{dt^2} = \frac{q}{m} \cdot \left(\vec{E} + \frac{d\vec{z}}{dt} \times \vec{B}\right) \tag{3.11}$$

the relation ((3.11)) shows that particle dynamics depends on the charge/mass ($\frac{q}{m}$) relation and the electric field for acceleration, and on the magnetic field for focusing and/or bending ($\frac{d\vec{z}}{dt} \times \vec{B}$). On the other hand, the energy gain depends only on the electric field.

Another important aspect to take into account in the acceleration process are the resonant modes of the cavity. Homogeneous wave-guides have two basic modes of wave propagation,

- TE = H
- TM = E

TE modes are characterized by the absence of electric field components and only H-component (magnetic field) in the direction of the RF wave propagation. The TM modes have no magnetic field components, and only an electric field component in the direction of propagation. The different modes depend on the cavity shape.[76] For particle acceleration the TM modes are normally selected. For example, in a pillbox cavity, the TM mode (sometimes called electric mode) has the form:[80]

$$E_z(r,\theta,z,t) = E_0 J_m \cdot \left(y_{mn}\frac{r}{R}\right) \cdot exp(\pm im\phi) \cdot exp\left(i\pi p\frac{z}{L}\right)(i\omega t) \tag{3.12}$$

where J_m is the mth Bessel function, y_{mn} its $n-th$ zero and the parameters n, m, n, p are integers: m is the azimuthal-mode number ($m = 0, 1, 2$ for spherical, dipole and quadrupole symmetry, respectively), n is the radial-mode number (number of zeros along the radial direction), and p the longitudinal mode number ($p = 0$ gives longitudinally constant value). For a general cavity, the modes are defined in a similar way, as TM_{mnp}.

The specific mode for a RFQ is expressed in three independent azimuthal modes, one for a quadrupole mode TE_{21n} and two for dipole modes TE_{11n}, as shown in Figure 3.5. Typical accelerating modes in a RFQ cavity are TM210, and TM210, although the near dipoles modes $TE_{110}$and TE_{111} might also be present with reduced intensity due to the design characteristics.

Another fundamental aspect in RF acceleration is the phase.[81] The bunched particles should be in phase with the RF when it arrives to the next gap in

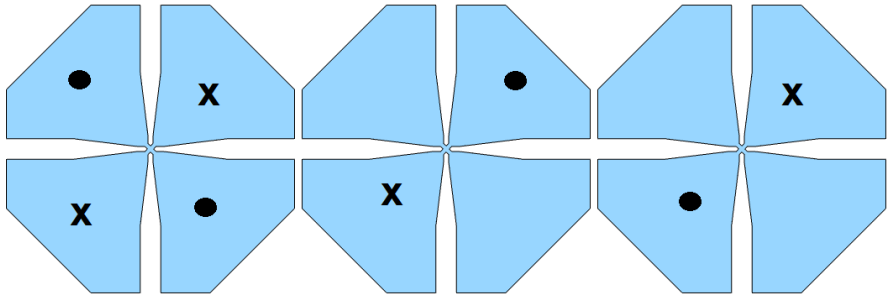

Figure 3.5: RFQ resonance modes. Quadrupole mode TE_{21n} (left), dipole mode TE_{11n} (center), dipole mode TE_{11n} (right)

order to reach the maximum voltage to accelerate. Therefore, the RFQ has an important asset in this regard, as it can automatically generate, from the continuous beam produced at the ion source , a bunched beam in phase with the RF field of the LINAC. Therefore the RFQ should be designed such that at the end of the structure, the phase is synchronized with the accelerator cavities.

On the whole, there are four fundamental aspects that must be taken in to account to carry out the acceleration:

- RF power source: It generates an electromagnetic wave of a specific frequency
- Cavity geometry: Closed metallic space that resonates at the same frequency as the RF power source.
- Beam: Flux of bunches of particles travelling through the cavity.
- Energy gain: Related to the adjustment of the field strength and phase to accelerate the beam.

Therefore, a typical design process requires both a beam dynamics study and a cavity design. The first involves optimizing the timing between fields and particles while maintaining the smallest beam size during the process. The second involves optimizing the field pattern inside the cavity and the ohmic losses on the walls. There are several important parameters to consider, such as energy gain, phase, quality factor and shunt impedance.

The energy gain is related to the capability of the cavity to transfer energy from a wave to a particle bunch, this process is efficient when both propagate at the same velocity. The relation to analyze this parameter is:

$$E = \frac{1}{L} \int E_z(z) cos\left(\frac{\omega z}{\beta c}\right) dz \tag{3.13}$$

As mentioned above, the phase is a relevant parameter to find the right acceleration. The particles that present the correct velocity at the entrance of the cavity will gain the predicted energy in order to keep the synchronization between the field ant the velocity. However, in reality not all particles contained in a bunch have the same velocity, but follow a certain velocity distribution. They are classified as follows:

- Synchronous particles: This is the name given to the particles with the correct phase and the exact synchronism with the accelerating field.
- Non-synchronous particle: Respect to the synchronous particle, the particle that arrives earlier occupies a smaller electric field from the correct field, and the particle that arrives later occupies a larger electric field. This is the principle to keep the particles around a stable phase. The particles will oscillate in phase about the synchronous particle. This oscillation is called a synchrotron oscillation.

The quality factor Q, or Q-value, is the ratio between the energy gain and the power loss in one RF cycle. Thus a high Q-value is a main objective in the design process. Q depends on the geometry and the surface resistance of the cavity material, and is given by

$$Q = \frac{2\pi f}{P} \cdot U \tag{3.14}$$

The effectiveness to produce an axial V_0 for a given dissipated power is measured by the shunt impedance parameter, and is given by

$$r_s = \frac{V_0^2}{P} \tag{3.15}$$

3.3 Radio-frequency quadrupole RFQ

The RFQ was developed in 1969 by Kapchinskiy and Tepliakov.[82] The idea was to modify the vane shape of a conventional RF quadrupole in order to obtain two effects on the particles: focusing and acceleration. This structure is a Low Velocity Accelerator, which accelerates particles without using a potential drop V between drift tubes. The acceleration is achieved instead by longitudinal RF

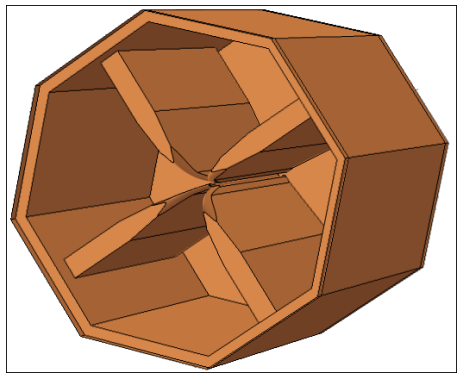

Figure 3.6: Four vane RFQ accelerator.

electric fields produced by the modulation on the vane tips, whereas the focus is produced by RF transversal electric fields generated by the vane geometry. The advantages of the RFQ compared with a conventional LINAC are:

1. Bunching particles.
2. Focusing bunches.
3. Accelerating bunches.

Most RFQs can be classified in two types: four-vane and four-rod RFQs. The four-vane RFQ is four-fold symmetric about the beam axis, and is generally used at frequencies above 200 MHz. This RFQ exhibit unwanted dipole modes, which can be eliminated including additional components (tuners), as well as cutting out RF windows along the vanes.[83] Figure 3.6 shows a model for RFQ vanes. The 4-rod RFQ is generally used at frequencies below 200 MHz. It is non-symmetric, requiring more attention to thermal expansion issues, although it has a simpler mode structure. Furthermore, the 4-vane RFQ presents handicaps as the high costs per meter, the complexity as well as the challenging RF tuning procedure of that structure due that the dipole modes tend to overlap with the quadrupole mode, and the high mechanical vane tolerances to have a safe beam operation conditions.[84] On the other hand, the 4- vane structures are the less consuming power so present less engineering difficulties and possible deformation in CW mode.[85] The RFQ is typically used at the first part of a LINAC, after the source, due to its capability to accelerate at higher energies.

Fundamental Principles

The acceleration in a conventional LINAC is produced in the gaps between the drift tubes, and the focussing process by magnetic quadrupole lenses placed in the drift tubes. Also, the facility uses a buncher in front of the LINAC to bunch the continuous beam. In the case of the RFQ, the special shape of the

electrodes generate an electric field able to accelerate, bunch and focus the beam at the same time. The process can be described by a potential function, which makes possible to study the electric fields using analytic formulae. In this way a better understanding of the beam dynamics between the four vanes can be obtained, as will be explained below.

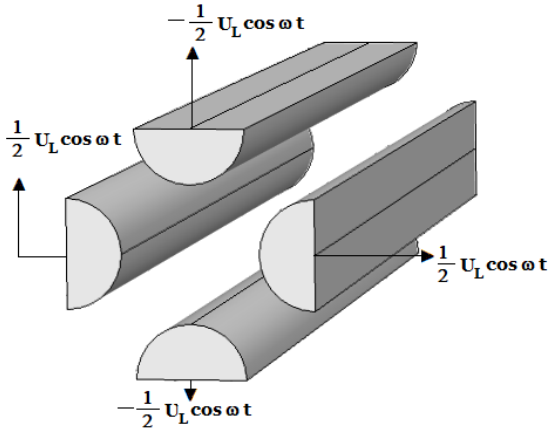

Figure 3.7: Electrostatic quadrupole.

Kapchinskiy and Tepliakov in their publication suggested that the effects of the focusing and accelerating electric fields could be obtained at the same time by giving a sinusoidal shape (modulation) to the electrode tip. Using the potential function they were able to describe how to apply a quadrupole electric field in low-velocity accelerators; as a result, a stronger hang effect (focusing and acceleration) was obtained in comparison with other accelerators. Subsequently, the authors introduced slow variations in the function parameters (modulation and cell length), which allowed a larger part of the beam to be captured, transported and converted into bunches. The final result of this development was an efficient acceleration of the bunch in the last part of the RFQ. This process is a result of the alternating gradient-focusing principle,[76] known as *Adiabatic bunching*.

In the RFQ cavity the longitudinal component of the electric fields produced by the modulation accelerate the bunches whereas the quadrupole component generate a transverse focussing effect. This effects can be easily understood by considering the simplified RFQ model of four cylindrical electrodes shown in Figure 3.7. In this model the ion beam travels through the symmetry axis, and each pair of opposed electrodes are electrically connected. If we apply a static potential U_L ($\omega t = 0$ in the figure), the system will operate as a standard electrostatic quadrupole, producing a transverse acceleration whose effect is to focus the beam over one of the symmetry-planes between electrodes, and

defocusing the beam over the other. Note that being a quadrupole system, the electric field along the longitudinal symmetry axis must always be zero, so there is no acceleration of the beam in the longitudinal direction.

If an alternating voltage $U_L\ cos(\omega t)$ is applied instead, the focusing/defocusing planes will swap in time with the frequency omega. By a suitable choice of omega, and depending on the specific geometry of the RFQ and the values of A/Q and beta of the particles, the beam can be radially confined within the RFQ electrodes. This "radial confinement" property of RF quadrupole systems is the working principle of the RFQ mass-filters,[86].[87]

On the other hand, we can in addition consider the inner surface of the cylindrical electrodes not to be flat but sinusoidally modulated along the beam direction, as shown in Figure 3.8. If the modulation between the two pairs of electrodes is shifted, a net component of the electric field will also appear along the longitudinal direction. The acceleration effect over the beam can be maximized by suitable selection of the variation of phase and radius of the modulation along the RFQ structure.

Transverse dynamics. Assuming that the potential applied at each of the electrodes is $V0$. The potential to satisfying $\Delta^2\phi_E = 0$ must be given by $E = \Delta\phi_E$. Neglecting the effects of space charge, we have

$$E_x = g_0 x, E_y = -g_0 y, \tag{3.16}$$

where $g_0 = \frac{V_0}{a^2}$ and a is the minimum radius from the axis to the vane tip.

Kapchinskiy and Tepliakov proposed in their publication[82] to give a sinusoidal shape to the tip of the vanes in order to simultaneously focus and accelerate particle bunches. With this modification, the equations for the transverse motion are,

$$m\ddot{x} = +qeg_0 x \tag{3.17}$$

$$m\ddot{y} = -qeg_0 y \tag{3.18}$$

where q is the ion charge of the particle. The voltage has the time dependence

$$U(t) = V sin(\omega t) \tag{3.19}$$

where $f = \frac{\omega}{2\pi}$.

Additionally, the period length β of the alternating linac structure, and so is the distance that a particle takes to travel one RF period with normalized velocity $\beta = \frac{v}{c}$. The equation of transverse motion is,

$$m\ddot{x} = qeE_x = qeg_0 sin(\omega t)x \tag{3.20}$$

Rewriting the equation ((3.20)),

$$\beta^2\lambda^2 \frac{d^2x}{dz^2} = B_0 sin(kz)x \tag{3.21}$$

where $k = \frac{2\pi}{\beta\lambda}$ and B_0 is

$$B_0 = \frac{qeV}{mc^2}\frac{\lambda^2}{a^2} \tag{3.22}$$

B_0 is called the focusing parameter. On the other hand, the beam is defocusing due to the quadrupole effect, so the equation in this case is,

$$\Delta_f = \beta^2\lambda^2 \frac{d^2x}{dz^2} \tag{3.23}$$

Δ_f represents the angle variation x' of the particles per focusing period. The final motion equation with the focusing and defocusing effects is,

$$\beta^2\lambda^2 \frac{d^2x}{dz^2} = [B_0 sin(kz) + \Delta_f]x \tag{3.24}$$

Equation ((3.24)) is the Mathieu's equation, and its solutions are well known. The stable solutions for the values of B_0 and Δ_f are the solutions of Floquet's equation.

$$x(z) = X(z)\sqrt{\beta(z)} \tag{3.25}$$

X should be satisfied,

$$\beta^2\lambda^2 \frac{d^2x}{dz^2} + \sigma^2 X = 0 \tag{3.26}$$

Where σ is the rate of phase advance of a particle in focusing structure, and is called tune.

Longitudinal dynamics. The form of the electric field on the beam axis should be,

$$E_z = E_o sin(kz - \omega t) \tag{3.27}$$

where f is the RF frequency. The relation between the increase of particle energy and the electric field is,

$$\frac{dW_s}{dz} = qeE_z cos(\phi_s) \tag{3.28}$$

where W_s is the synchronous particle energy with a synchronous phase ϕ_s. The variation of the energy for the synchronous particle is related to the variation of the transit time between gaps by,

$$\Delta W = \int_{S_0}^{S_0+L} qE_z(s) \cdot cos[\phi(s)] \cdot ds \tag{3.29}$$

where q is the particle charge, $\phi(s)$ is the cavity RF phase when the particle is at abscissa s. $\phi(s)$ is defined as

$$\phi(s) = \phi_0 + \frac{\omega}{c} \int_{S_0}^{S_0+S} \frac{ds'}{\beta_z(s')} \tag{3.30}$$

where $\phi_0 = \phi_{(S_0)}$ is the RF phase when the particle enters the cavity.

Writing $\phi_{(S)} = \phi_{(S)} + (\phi_S - \phi_S)$

ϕ_S is an arbitrary phase, using trigonometric relationships, one gets for the energy gain:

$$\Delta W = cos\phi_s \int_{S_0}^{S_0+L} qE_z(s) \cdot cos[\phi(s) - \phi_s] \cdot ds - sin\phi_s \cdot \int_{S_0}^{S_0+L} qE_z(s) \cdot sin[\phi(s) - \phi_s] \cdot ds \tag{3.31}$$

By defining ϕ_s as:

$$\int_{S_0}^{S_0+L} qE_z(s) \cdot sin[\phi(s) - \phi_s] \cdot ds = 0 \tag{3.32}$$

with the definition for a synchronous phase ϕ_s:

$$\phi_s = arctan\left(\frac{\int_{S_0}^{S_0+L} E_z(s)\cdot sin[\phi(s)]\cdot ds}{\int_{S_0}^{S_0+L} E_z(s)\cdot cos[\phi(s)]\cdot ds}\right) \tag{3.33}$$

finally the relation is,

$$\Delta W = \left(q\int_{S_0}^{S_0+L} |E_z(s)|\cdot ds\right)\cdot T\cdot cos\phi_s = qV_0\cdot T\cdot cos\phi_s \tag{3.34}$$

where T is the transit time factor,

$$T = \frac{1}{V_0}\int_{S_0}^{S_0+L} E_z(s)\cdot cos[\phi(s)-\phi_s]\cdot ds \tag{3.35}$$

As can be seen after the analysis, the energy gain varies in the same way as voltage V.

Acceleration in a RFQ. The vane tip must be sinusoidally shaped to produce longitudinal electric fields. The potential (3.36), can be expressed in cylindrical coordinates as,

$$U(r,\theta,z,t) = V(r,\theta,z,t)sin(\omega t+\phi) \tag{3.36}$$

where ϕ is the initial potential phase. The potential near the tips of the electrodes can be written as a Fourier Bessel series,

$$U(r,\theta,z) = \frac{V}{2}\left[\sum_{m=1}^{\infty} A_{0m}\left(\frac{r}{r_0}^{2m}\right)cos(2m\theta)+\right.$$
$$\left.\sum_{m=0}^{\infty}\sum_{n=1}^{\infty} A_{nm}I_{2m}(nkr)cos(2m\theta)cos(nkz)\right] \tag{3.37}$$

Taking the first two terms of the series, it is possible to obtain an approximation for the potential near the axis,

$$U_{two-term}(r,\theta,z) = \frac{V}{2}\left[\left(\frac{r}{r_0}^{2}\right) + AI_0(kr)cos(2m\theta)cos(kz)\right] \tag{3.38}$$

where A is the acceleration parameter, $L_c = \frac{\beta\lambda}{2}$ is the cell length, $k = \frac{\pi}{L_c}$, I_0 is the zero order modified Bessel function, $A_{01} = 1$ and A_{10} are the two term

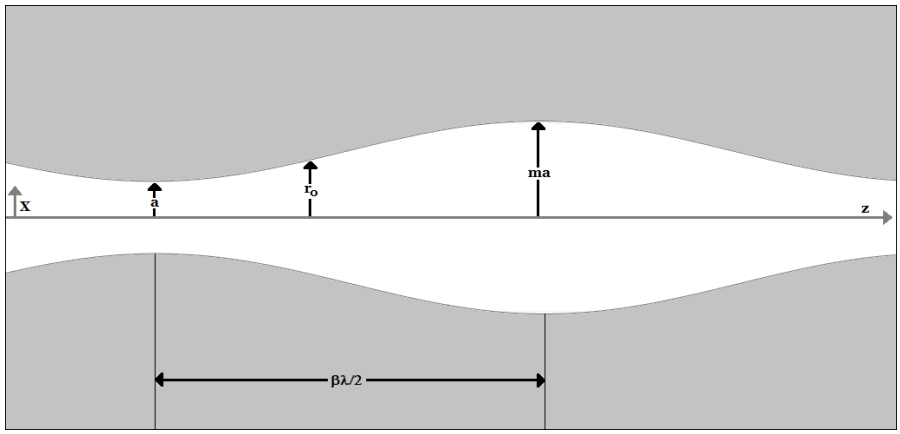

Figure 3.8: Vane tip profile (longitudinal).

potential acceleration parameters determined by the geometry of the electrode tip, and r_0 is the radius, as shown in Figure 3.7.

A sinusoidal pattern for electrodes modulation is shown in Fig 3.7, where a is the minimum distance from the axis to the tip, ma is the maximum distance from the axis to the tip, m is the modulation parameter or modulation depth and $\frac{\beta\lambda}{2}$ is the unit cell length.

The potential must satisfy the corresponding boundary conditions at the electrode tip profiles, at the end of each cell at $L_c = 0$ and $\frac{\beta\lambda}{2}$. Therefore, for the even electrodes,

$$U(a, 0, 0) = U(ma, 0, L_c) = \frac{V}{2} \tag{3.39}$$

and for the odd electrodes,

$$U(ma, \frac{\pi}{2}, 0) = U(m, \frac{\pi}{2}, L_c) = -\frac{V}{2} \tag{3.40}$$

replacing in equation (3.38),

$$\left(\frac{a}{r_0}^2\right) + AI_0(ka) = 1 \tag{3.41}$$

and

$$\left(\frac{ma}{r_0}^2\right) - AI_0(mka) = 1 \tag{3.42}$$

where $k = \frac{\pi}{L_c} = \frac{2\pi}{\beta}$. The solution of the equation for A and the radius r_0,

$$A = \frac{m^2 - 1}{m^2 I_0(ka) + I_0(mka)} \tag{3.43}$$

The focusing efficiency χ is obtained from equation (3.41),

$$\chi \equiv 1 - AI_0(ka) \tag{3.44}$$

The radius R_0 located in the middle of a cell is also the place of symmetry of the quadrupole, from Eq (3.41) and Eq (3.44),

$$r_0 = a\chi^{\frac{1}{2}} \tag{3.45}$$

In order to find the relations for the components of the electric fields, Eq (3.38) is derived, and Eq (3.38) is replaced by,

$$E_r = -\frac{\chi V}{a^2} r cos2\theta - \frac{kAV}{2} I_1(kr) coskz \tag{3.46}$$

$$E_\theta = \frac{\chi V}{a^2} r sin2\theta \tag{3.47}$$

$$E_z = \frac{kAV}{2} I_0(kr) sinkz \tag{3.48}$$

where $k = \frac{2\pi}{\beta\lambda} = \frac{\pi}{L_c}$ and I_0 is the first-order modified Bessel function.

The components E_r and E_θ represent the quadrupole electric field. It is possible to observe in E_r (3.46) that the second term corresponds to the defocusing parameter seen above. On the other hand, the component E_z produces the acceleration of the particles. The axis voltage in a cell for $r = 0$ is,

$$\Delta V_c = \int_0^{L_c} E_z dz = AV \tag{3.49}$$

The energy gain of a particle in a cell depends on the voltage variation $V = V_0 sin(\omega t + \phi_s)$. The synchronous particle phase ϕ_s is the phase reference for particles around it, which will follow the Principle of Phase Stability.[81] Accordingly, the energy gain for a particle in a cell is,

$$\Delta W = qe\int_0^{L_c} E_z sinkzdz = qe\frac{\pi}{4}AVcos\phi_s \tag{3.50}$$

Transit Time Factor

An important concept in the dynamics of an RF is the Transit Time Factor. It is the relation between the energy gained in the RF field cycle and the energy gained in a dc field of voltage $V_0(\pi)$.[76] It is a relevant parameter to determine the reduction of the energy gain due to the sinusoidal time variation of the field along the gap.

$$\Delta W = qeAVTcos\phi_s = qe\frac{\pi}{4}AVcos\phi_s \tag{3.51}$$

$$T = \frac{\pi}{4} \tag{3.52}$$

RF Defocusing

$$\Delta = \frac{\pi^2}{2}\frac{qeV}{mc^2}\frac{A}{\beta^2}sin\phi_s \tag{3.53}$$

Focusing strength

$$B = \chi\frac{qeV}{mc^2}\frac{\lambda^2}{a^2} \tag{3.54}$$

Relevant RFQ's in accelerators

Nowadays there are several RFQs in operation around the world. A list of RFQ systems with similar characteristics to the one considered in this study (energy, geometry and/or technology) are listed below.

ATLAS-ARGONNE

Table 3.1: Characteristics of 60.625 MHz CW RFQ for Atlas upgrade.[88]

Parameter	Value	Units
Type	4-vane	
Input energy	30	keV/u
Output energy	295	keV/u
Frequency	60.625	MHz
Vane Voltage	70	kV
Power	60	kW
Average radius	7.2	mm
Charge-mass ratio	1/7	
Length	3.81	m

LINAC 4 - CERN

Table 3.2: Characteristics of 352.2 MHz CW RFQ for Linac4 at CERN.[89]

Parameter	Value	Units
Type	4-vane	
Input energy	95	keV/u
Output energy	3	MeV/u
Frequency	352.2	MHz
Vane Voltage	87.32-121.61	kV
Power	210	kW
Average radius	3.69-5.13	mm
Charge-mass ratio	H^-	
Length	5.954	m

SPIRAL2

Table 3.3: Characteristics of 88 MHz CW RFQ for Spiral2 at Ganil.[85]

Parameter	Value	Units
Type	4-vane	
Input energy	20	keV/u
Output energy	0.75	MeV/u
Frequency	88	MHz
Vane Voltage	100 - 113.7	kV
Power	240	kW
Average radius	8.1 - 10.0	mm
Charge-mass ratio	1/3	
Length	5.077	m

Table 3.4: Characteristics of 80.5 MHz CW RFQ for ReA3 at Michigan State University.[90]

Parameter	Value	Units
Type	4-rods	
Input energy	12	keV/u
Output energy	600	keV/u
Frequency	80.5	MHz
Vane Voltage	86.5	kV
Power	160	kW
Average radius	0.6	mm
Charge-mass ratio	0.2-0.5	
Length	3.3	m

3.4 Materials and methods

In this section, the detailed methodology used to carry out this study is presented, along with some basic information about the instruments and software used in each relevant stage.

3.4.1 Methodology

The development of a RFQ system is a very complex project, which requires many iteration loops between physical simulations and engineering practices. On the physics side the design started by specifying the input and output beam characteristics. The beam dynamics study was then carried out by considering the range of mass-over-charge ratios and the required energy gain working at a maximum inter-vane voltage. These studies were performed with the code DESRFQ.[5] The RF modelling process was performed using Comsol,[7] following several design stages from the shape of the resonator to the final vane modulation, the windows and the RF tuners. Three-dimensional field maps for the electromagnetic fields were extracted and used in particle tracking studies performed with the codes GPT[91] and TRACK.[4] The chosen vane modulation has a sinusoidal shape for most of the RFQ length. This structure could be improved by by using trapezoidal cells instead, as it has been recently demonstrated,[92],[88] enhancing the transit time factor and, ultimately, the energy

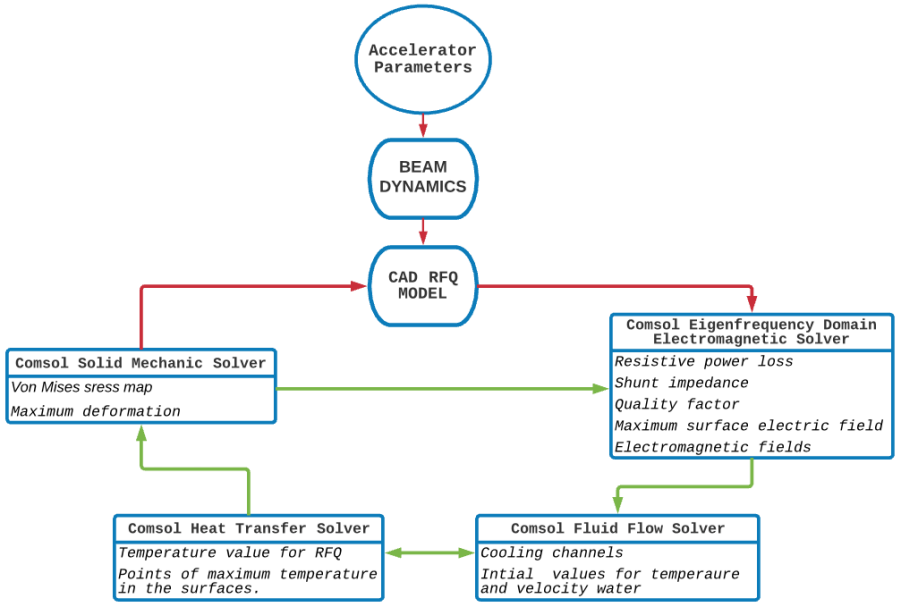

Figure 3.9: RFQ design workflow along two complementary development paths: (1) Initial parameters, beam dynamics and RF modelling can be fulfilled along the red path, whereas (2) technical parameters from the electromagnetic field can only be evaluated along the green path. The deformed structure can be further evaluated for the main RF parameters and the process can be repeated if necessary.

gain. This will be the subject of future developments. The overall development stages are presented in Fig. 3.9.

For the numerical computation of the 3D distribution of the resistive losses on the surfaces, the electric field distributions are scaled in order to meet the particle injection and acceleration requirements. This calculation is coupled to the thermal study for the evaluation of the heat transfer rate through the copper RFQ structure. In this way it was also possible to calculate the water flow needed to cool down the structure. This scaling depends on the $^{A}/_{Q}$ ratio, energy gain, maximum allowed energy spread and bunch length.

3.4.2 Detailed study

Software

Some dedicated software packages were used to carry out specific research. Among them, the most important are DESRFQ and TRACK, both described above in Chapter 2, and COMSOL Multiphysics. DESRFQ was used to obtain

the RFQ parameters and modulation file, whereas the study of the beams through the RFQ was conducted with TRACK.

The codes used to develop the beam dynamics studies for LINCE, taking each element into account, were DESRFQ and TRACK. These codes were developed by the Argonne National Laboratory. Next, a brief description of them is presented.

DESRFQ

The DESRFQ[5] code was developed to study the RFQ structure geometry and its parameters. As its main advantages, this code enters input parameters of the accelerator, analyses the output graphics, studies the main RFQ characteristics and can generate a sinusoidal modulation. The RFQ design with DESRFQ is an interactive process that shows accelerating and focusing parameters while the code is running.

DESRFQ creates RFQ vane modulation in terms of cell length and aspect ratio factor, which poses a permanent comparison between the depth and length of each cell. The code uses energy input and output levels, as well as a number of parameters that control the longitudinal phase advance, energy spread, inter-vane voltage, etc. It was used repeatedly in order to produce and refine the RFQ vane modulation. An example of a DESRFQ output file is presented in Figure 3.10, which shows a snapshot of the longitudinal phase space distribution in the separatrix.

DESRFQ considers the following RFQ structure to build the geometry:

- Input radial matcher.
- Prebuncher.
- Gentle buncher.
- Accelerator section.
- Output radial matcher.

Accordingly, the frame for beam input and RFQ parameters, contains:

- Mass number in atom mass units.
- Charge number in electron charges.
- Normalized transverse emittance in *cmmrad*.
- Average beam current in *A*.
- Initial energy spread of particles in %.

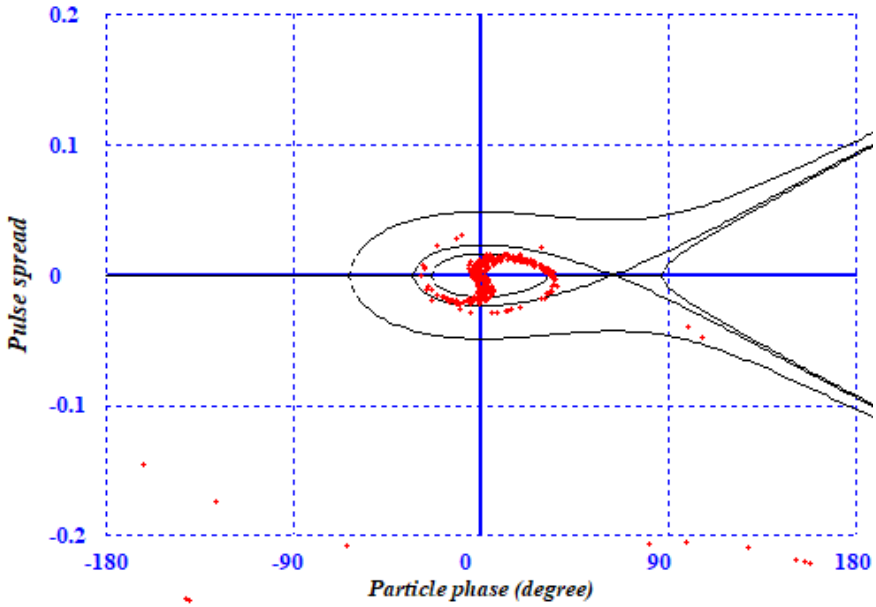

Figure 3.10: DESRFQ output while it calculates RFQ geometry.

- Initial phase length of bunch at RFQ input in *degrees*.
- Design maximum field on electrode surface in Kilpatrick units.
- Input particle energy in MeV/u.
- Design value of RFQ output energy in MeV/u.
- Curvature of electrode tip as its ratio to RFQ average radius R_e/R_0.

The next section presents information related to modulation, such as number of cells, initial values for modulation and phase, and number of oscillations.

TRACK

TRACK[4] is a particle-tracking code written in Fortran. It can handle a complete chain of accelerator components and beam-line magnetic devices. It was used for the beam dynamics studies carried out on the RFQ due to its ability to couple with the output of the DESRFQ code. As Figure 3.11 demonstrates, the outcome of this code was the complete characterization of the transverse and longitudinal beam dynamics along the RFQ.

The TRACK code works in Windows, performing beam dynamics simulations of multi-component ion beams in linear accelerators. As the main advantages, TRACK can study multiple component ion-beams in 6D phase space, import 3D electromagnetic fields of RF cavities from codes such as CST MWS or COMSOL

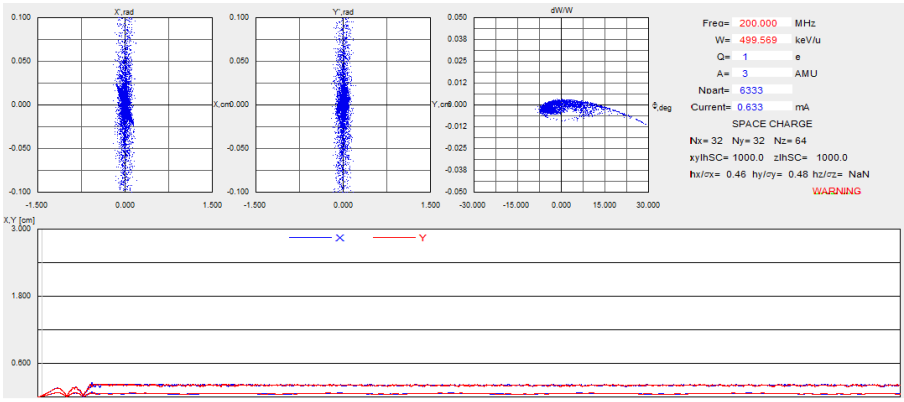

Figure 3.11: Snapshot of TRACK code.

Multiphysics, use realistic fields in solenoids, and study misalignments and random errors, among others.[4] Space charge calculations are performed by the integration of motion equations of all the tracked particles for a short distance. The code uses a number of macro-particles with a given q/A; in the case of beam current, each multi-particle will carry the same charge for the space charge calculation routines.

TRACK includes several elements to use in a LINAC simulation, including: acceleration cavity resonators with realistic 3D fields (imported), Radiofrequency Quadrupole, solenoids, bending magnets, quadrupoles, sextupoles, multi-harmonic bunchers, and electrostatic lenses, among others.

COMSOL Multiphysics

Comsol Multiphysics[7] is a finite elements code which allows calculations and coupling of various physical phenomena such as electromagnetic wave resonances, fluid flow and heat transfer. A snapshot of a Comsol interface which displays the RFQ vane modulation is shown in Figure 3.12. Its mesh distribution and setup were used to compute the electric potential pattern. Comsol was mostly used to model and optimize basic geometry, RF simulations, heat transfer, cooling, mechanical and frequency shift studies.

Inventor

Autodesk Inventor[8] is a mechanical design program that allows integrating Autocad and 3D data. The code was used to obtain the 3D files in order to bring these to COMSOL for specific situations, such as the modulation design. It was also used to generate drawings as can be shown in the last chapter of the present document.

JAVA

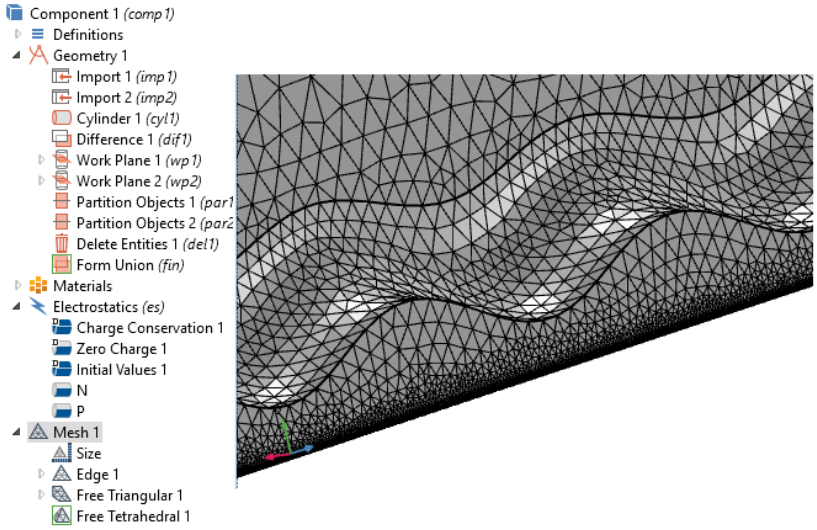

Figure 3.12: Snapshot of COMSOL code.

Oracle Java SE[93] was the language of choice for all programs written to process numerical simulations data or to handle repetitive calculations. Taking the RFQ work as an example, Java was used to provide cubically and quartically shaped beam matchers as well as the sinusoidal modulation profiles of the vanes. Due to its object-oriented formulation, Java was used to organize codes in types of methods that approach various aspects of the beam dynamics simulations, such as beam emittance, rms size, energy spread etc.

The RF Laboratory at the University of Huelva

The laboratory[94] is equipped with a dedicated test-bench for RF measurements, which includes high-power RF generators, network analyzer, amplifiers and power meters. A clean room is also available with a dedicated space for high-precision mechanical metrology and cavity mounting, together with a vertical cryostat for superconducting cavity tests.

The main interest of implementing a Radio-Frequency RF Laboratory at the University of Huelva is to test the performance of RF cavity prototypes, which will allow improving the electromagnetic and thermo-mechanical design, mainly focused on heavy-ion accelerators in the framework of the ongoing projects. The RF laboratory is complementary to a cryostat system foreseen for testing superconducting cavities. The main equipment of the laboratory is listed below:

- Agilent CX N9000A spectrum analyzer.

- Agilent 53181A, Frequency counter.
- Rhode and Swartz Network analyzer .
- 3 kW power-amplifier from DB-Elettronica.
- Analog RF signal generator MXG N5181AEP from Keysight Technologies.

The laboratory is also equipped with a remotely operated bean pull system for field measurements. The clean room is close to the test cryostat, where superconducting cavities can be tested. The space dedicated to the clean room has been prepared for the assembly and testing of both particle detector systems and RF cavity systems. The total surface is $50\,\mathrm{m}^2$, divided into three main areas, as shown in Figure 3.13.

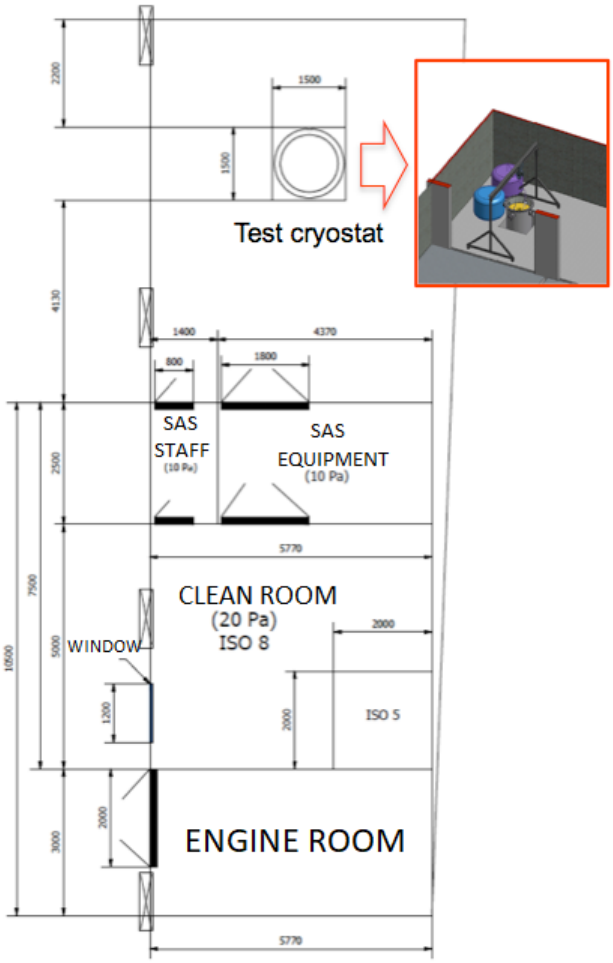

Figure 3.13: Sketch of the clean room built for RF cavity assembly and testing.

- An over-pressurized area of $20\,\mathrm{m}^2$ for the entry of personnel and equipment (SAS).
- An ISO8 area of $30\,\mathrm{m}^2$ containing a metrology system for the quality control of mechanical elements.
- An ISO5 area of $4\,\mathrm{m}^2$ prepared for the assembly and handling of special systems .

The associated auxiliary equipment was installed in a separate area of $18\,\mathrm{m}^2$ near the research complex. The first activity of the laboratory was to build and test a cold model (aluminum) of a RFQ cavity, as is shown in Figure 6.9. This process is explained in more detail in Chapter 6.

4

Beam Dynamics for LINCE

This chapter describes the main results of the beam dynamics together with the tools used for this study. Section 4.1 introduces the beam characteristics and requirements of the LINCE facility. Section 4.2 presents an overview of the codes used for the design of the RFQ. Section 4.3 is dedicated to the beam dynamics of the whole facility, focusing on transport beam studies for protons and heavy ions through LINCE.

4.1 Overall specifications of LINCE

LINCE must be a light- and heavy- ion accelerator with the capacity to accelerate virtually any isotope of all elements. An exemplary set sample of requirements for a selection of ion beams, with the intensities, are listed in Table 4.1. These have been determined from the fundamental and applied physics program.

The final transverse emittance of any beam should be better than $0.1\,\pi \cdot mm \cdot mrad$ normalized (RMS), for a pulse length below 100 ps with a longitudinal emittance of 1 keV/u $\cdot$ ns(RMS). The beam intensity stability of the LINCE facility should be better than 5% for any beam for a period of 6 hours (measured with an integration time below 2 ms).

Another important point is that beam tuning should be straightforward and beam changing between species should not exceed 24 hours. Finally, beam energy changing should not exceed 1 hour.

The design of this facility can benefit from the state-of-the-art technologies and expertise recently acquired in the construction of high-intensity linacs for SPIRAL2[12] (GANIL, Caen, France), ALPI[74] (LNL, Legnaro, Italy), ATLAS[95] (ANL, Chicago, USA) and FRIB[75] (MSU, Michigan, USA).

Table 4.1: Selected beams intensities and energies for LINCE.

Ion	**Q**	**A/Q**	**E [MeV/u]**	**I [pμA]/I [eμA]**
H	1	1	40	1000/1000
^{4}He	2	2	10	500/1000
^{28}Si	9	3.1	12	10/90
^{48}Ca	8 or 10	6 or 5	7.5	10/80 or 100
^{184}W	27	6.8	2.5	1/27
^{238}U	34	7	7.5	0.5/17

In this way the Linac will rely on proven technology and use as much tested equipment as possible. For this reason, the choice was to fix the frequency of the whole machine to already existing, proven, reliable and best-performing resonators. The frequency and main characteristics of the RFQ was also determined by this method.

Moreover, for some physics experiments involving time-of-flight measurements, the bunch spacing should be above 50 ns (20 MHz fundamental frequency) for heavy ions. For protons and alphas, the time between bunches can be

shorter, which can significantly reduce space charge effects per bunch. The beam fundamental frequency for heavy ions was chosen to be 18.1875 MHz, corresponding to about 55 ns between bunches. This beam frequency will be produced by using a multi-harmonic buncher (MHB) with at least 4 operational frequencies. For proton and helium beams, the beam frequency is increased to 36.375 MHz, to reduce space charge effects per bunch.

This choice of the fundamental frequency benefits from the use of the quarter-wave resonators (QWR) already developed by the Argonne National Laboratory (ANL, USA),[95] for most of the betas needed in the layout of the accelerator. The frequency of the cavities will be 72.75 MHz (4th harmonic) and present the best performance (MV/m) known worldwide for heavy ions. The results obtained recently at ATLAS projects[72] confirm the possibility to obtain accelerating total voltages up to 5 MV,[96],[9798] operating in a safe nominal point between 1.2 and 5.6 MVwith quality factor values $> 10^9$. The frequency of the RFQ will be the same and its particular design is based on the ANL 60 MHz model, which is already commissioned and operates at an overall transmission of about 80%.

The required intensities are about 1 mA for protons and $[10 - 100]$ pμA for heavy ions with a maximum mass-to-charge ratio of 7. The intensities for heavy ions are achievable using an Electron Cyclotron Resonance Ion Source (ECRIS) at a maximum frequency of 18 GHz,[14] which is similar to the system of INFN-Legnaro National Laboratories.[99]

ECR ion sources are very reliable, highly efficient and easy-to-tune ion sources that provide full compatibility with the specifications of the LINCE project. In particular, high efficiency is a very important feature for the production of multi-charged ions of isotopes with low natural abundance, such as ^{48}Ca or ^{36}S.

As is shown in Table 4.1, the beam intensities and charge states are somehow conservative for ECRIS. Therefore, the performance requested for the source does not correspond to maximum available intensities of 28 GHz ECRIS. However, the running conditions of the LINCE project require high reliability, stability and easy tuning. These three requirements are only fulfilled when the ECRIS is not running close to its maximum performance.

4.2 Beam dynamics studies of LINCE

The beam dynamics studies for the whole accelerator was performed using the TRACK code.

Table 4.2: Accelerator cryo-module types with their specifications: Frequency, harmonics, beta and accelerating voltage. The resonators used in cryo-modules from 2 to 5 were already developed by ANL; only the resonator in cryo-module 1 needs to be developed for LINCE.

Cryo-module	Type	Frequency (MHz)	Harmonic	Beta	Vacc (MV)	Nº Resonators
C1	QWR	72.75	4	0.045	1.39	5
C2	QWR	72.75	4	0.077	2.38	7
C3	QWR	72.75	4	0.077	2.38	7
C4	QWR	109.25	6	0.15	3.30	7
C5	Rebuncher	109.25	6	0.15	3.30	1

For the simulations, real accelerating potentials were used for the RF cavities everywhere whenever available, otherwise replaced by results of the electromagnetic simulations (ideal). In particular, the structure of each cell of the RFQ was simulated using the DESRFQ code and integrated in the TRACK code. The number of RF cavities of the LINAC was optimized by taking in to account the multi-beam requirement of LINCE.

The final configuration consists of 27 Quarter Wave Resonators (QWR), packaged into 4 cryostats (C1-C4), with three different betas (0.045, 0.077 and 0.15) working at two harmonics (4, 6) of the reference frequency. Table 4.2 shows a summary of the characteristics of the resonators used in the beam dynamics simulation; V_{acc} represents the maximum acceleration voltage seen by a particle with the geometric beta. This value is of paramount importance, since it defines the total number of resonators, i.e., the length of the accelerator. With the present structure, all beams with a mass-to-charge ratio between 1 and 7 can be accelerated with overall efficiencies around 80%.

The values used in the simulations of the LINAC for all cryo-modules, with the exception of cryo-module C1, are the results from recent field measurements at ANL. The betas were optimized not only for heavy ions but also to accelerate very light ions, such as protons. Moreover, the resonators used in cryo-modules 2, 3, 4 and 5 were already developed. Only the resonator for beta 0.04 (cryo-module 1) needs to be developed specifically for LINCE at this frequency. It should be noted that FRIB developed resonators with beta $\beta = 0.041$ at the frequency of 80.5 MHz. Those resonators can be a very good starting point for the development of LINCE resonators.

Cryo-modules C2 and C3 consist of seven QWR $\beta = 0.077$ at 72.75 MHz SC cavities, and C4 is composed of seven QWR $\beta = 0.15$ at 109.125 MHz, with four 9- Tesla SC solenoids. These cryo-modules were already developed in ANL. Cryo-module C1 consists of five QWR $\beta = 0.045$ at 72.75 MHz SC cavities with

three 9- Tesla SC solenoids. These resonators, as mentioned above, need to be specially designed and developed for LINCE, taking as reference the QWR used in FRIB, with $\beta = 0.41$ at 80.5 MHz.

The focusing of the beam is driven by superconducting solenoids placed inside each cryostat. In this way a very compact linac structure was chosen, integrating 5 or 7 resonators per cryo-module, together with the superconducting solenoids. This makes the total length of the accelerator to be about 20 m. A layout of the final design is shown in Figure 4.1.

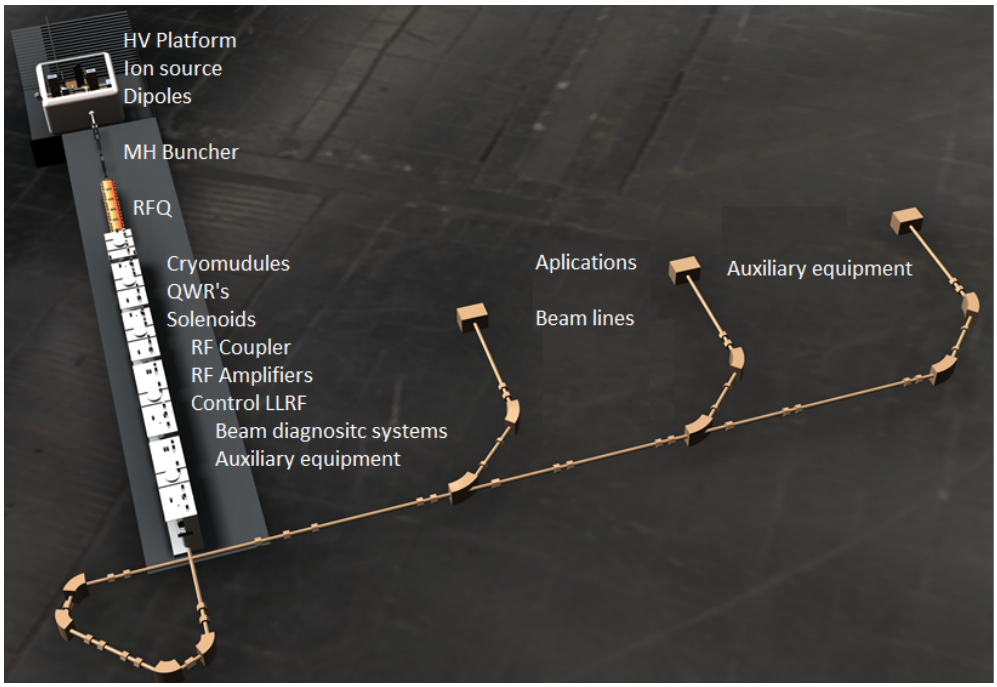

Figure 4.1: LINCE layout.

The construction of the accelerator could be divided in two phases. Phase 1 would comprise the machine installation and commissioning up to the third cryomodule, C3, and can provide already beams to start the physics program. In phase 1, the beam energy of $A/q = 5$ (^{48}Ca beam) is 7.5 MeV/nucl, and the beam energy from protons (25 MeV) is already relevant for most applications. The addition of a 4th cryomodule allows reaching the target energies, like 40 MeV for protons and 4.5 MeV/u for U. The beam energy at the exit of each cryomodule, as a function of A/q, is indicated in Figure 4.2 and Figure 4.3.

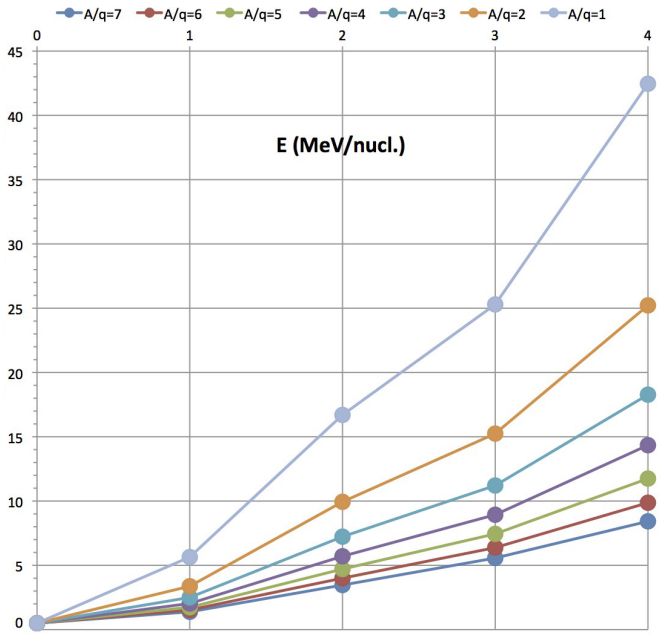

Figure 4.2: Beam energy as a function of A/q

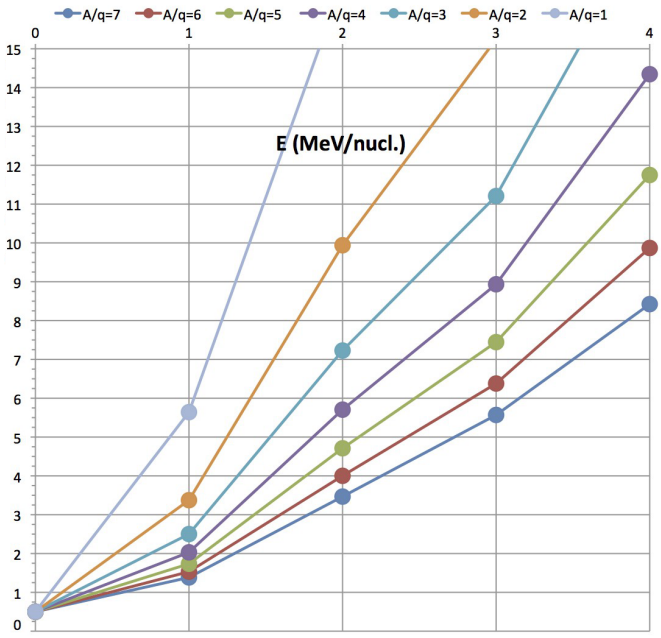

Figure 4.3: Zoom of the low energy region of Figure 4.2

Table 4.3: RFQ main characteristics.

Characteristic	Value	Units
Frequency	72.75	MHz
Input kinetic energy	40	A keV
Output kinetic energy	500	A keV
Design mass-to-charge ratio	1-7	
Maximum vane voltage	82	kV
Maximum field strength	1.5	Kilpatric
Length	5	m
Average radius	6	mm

Optimum injection into the SC-linac imposes a maximum normalized transverse and longitudinal emittances of $0.125\,\mathrm{cm}\cdot mrad$ and $25\,\mathrm{ns}\cdot keV/u$, respectively.[73] Therefore, the design of the RFQ becomes critical for the efficient operation of the linac. The values of the average radius, total length, voltage and field strength were determined by beam dynamics simulations using DESRFQ. The main characteristics of the RFQ to be designed are shown in Table 4.3. The main objective of the study is to reach the maximum transmission with the given beam specifications.

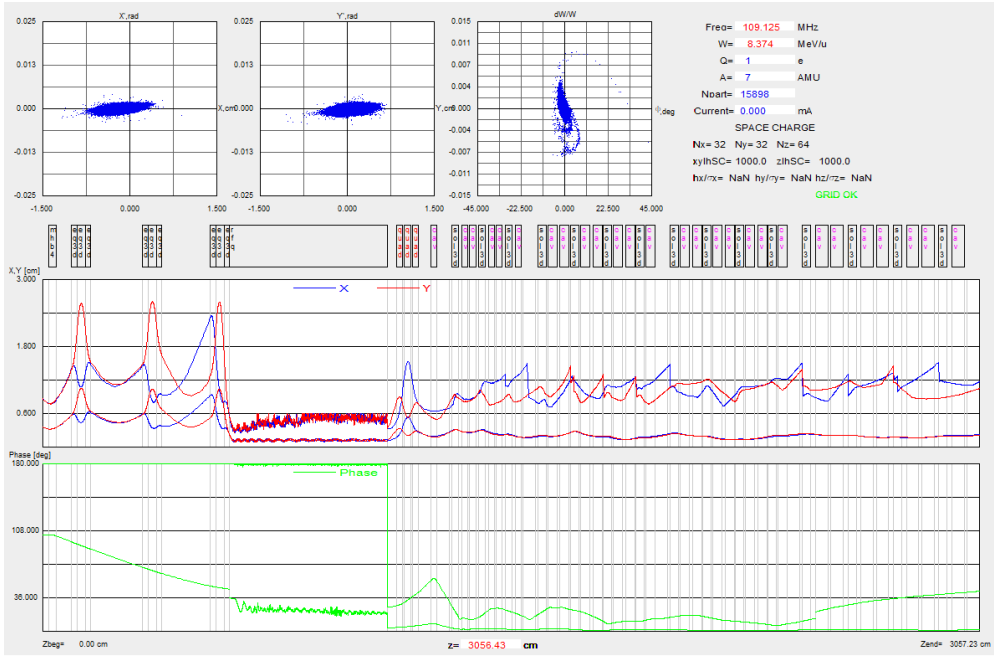

Figure 4.4: Beam transport of heavy ions ($A/Q = 7$) along LINCE without space charge effects. The final beam energy in this case is $8.37\,\mathrm{A}\cdot\mathrm{MeV}$.

Simulations for the LINCE facility use realistic data for QWR cavities, RFQ and solenoids. To perform this task properly, information was gathered about the values used in laboratories that are currently working or that are in an advanced design stage, for instance, the QWRs for the ATLAS upgrade at the Argonne National Laboratory,[96100] with $\beta = 0.15$, F=109 MHz, and SC solenoids of 9 T or QWR with $\beta = 0.041$, F=80.5 MHz at FRIB.[101] As an example, the track input file for a heavy-ion beam (without space charge) using the specific parameters for each element is shown in Appendix A of the present document.

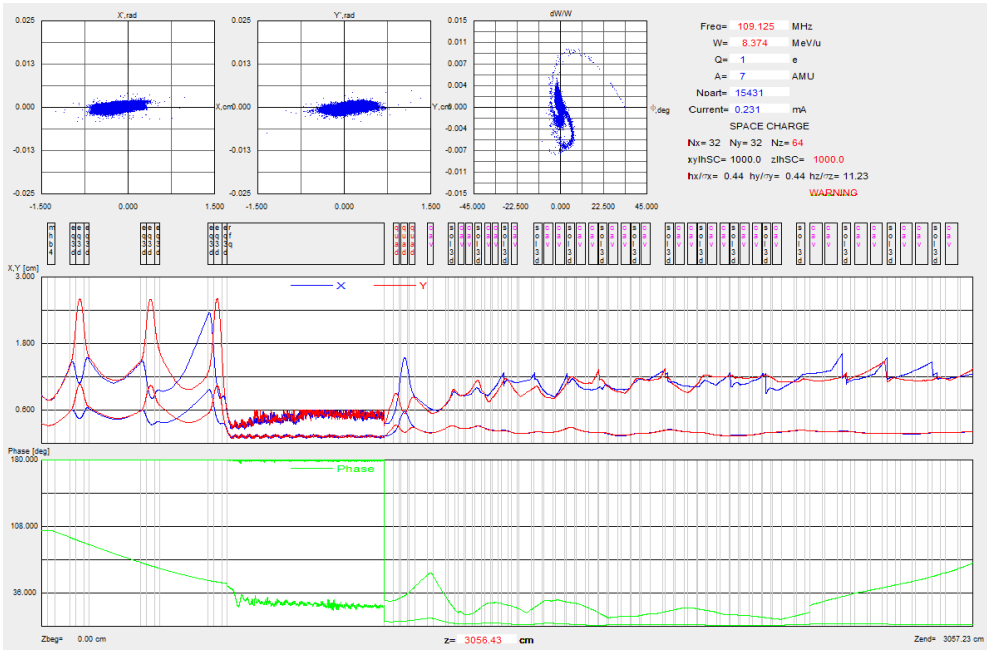

Figure 4.5: Beam transport of heavy ions ($A/Q = 7$) along LINCE with space charge effects. The current and final energy upon exiting the linac are 231 μA and 8.37 A $\cdot$ MeV, respectively.

The beam dynamic studies revealed that most of the losses occur in the Medium Energy beam Transport (MEBT) line, just after the RFQ and before the first cryomodule. This corresponds to particles in the tail of the bunches, which do not have the adequate phase to be accepted in the first accelerating resonator; this is a common characteristics of this kind of Linac.

In order to understand in more detail the beam transport in the LINCE facility, a sequence of simulations were carried out. Firstly, simulations for heavy ions (without and with space charge) were conducted, taking into account considerations about the input and output matcher of the RFQ, and the

possibility to build cryostat 4. Several iterations were carried out in order to optimize the overall system and using realistic tunings of the cavities and solenoids. Two simulation results using TRACK, after beam optimization, are shown in Figure 4.4 and Figure 4.5, where the beam parameters along the Linac are described. Those simulations were performed with an initial beam of 20000 particles.

A typical simulation without space charge effects for heavy-ion beams shows 15,898 particles at the Linac exit, corresponding to a transmission efficiency of 79.4%. The beam is accelerated at 8.37 A · MeV, as shown in Figure 4.4.

A second simulation shown in this work corresponds to a heavy-ion beam with an initial current of 0.3 mA. This calculation is shown in Figure 4.5, and it has 15431 particles at the Linac exit with an energy of 8.37 A · MeV/u, corresponding to a transmission efficiency of 77.1%. As can be observed, the total efficiency of the accelerator is very high and the effects of space charge for heavy ions are relatively small.

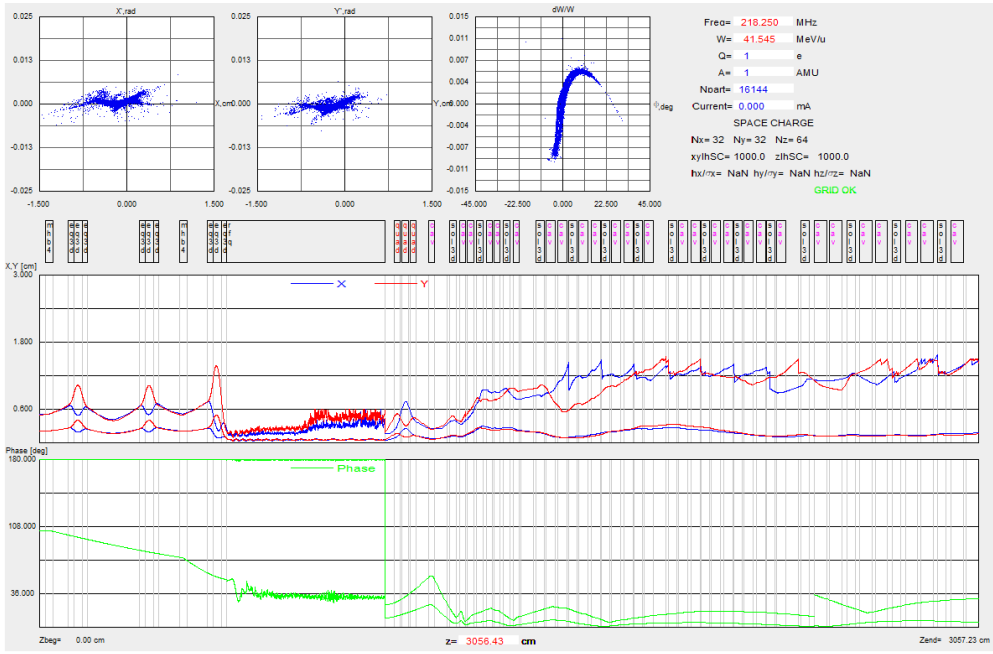

Figure 4.6: Beam transport of protons along LINCE without space charge effects. The final beam energy in this case is 41.54 A · MeV.

Simulations for protons (without and with space charge) were also carried out, taking into account similar considerations as for heavy ions. When a proton beam with 20,000 particles is accelerated, there is a total of 16,144 particles

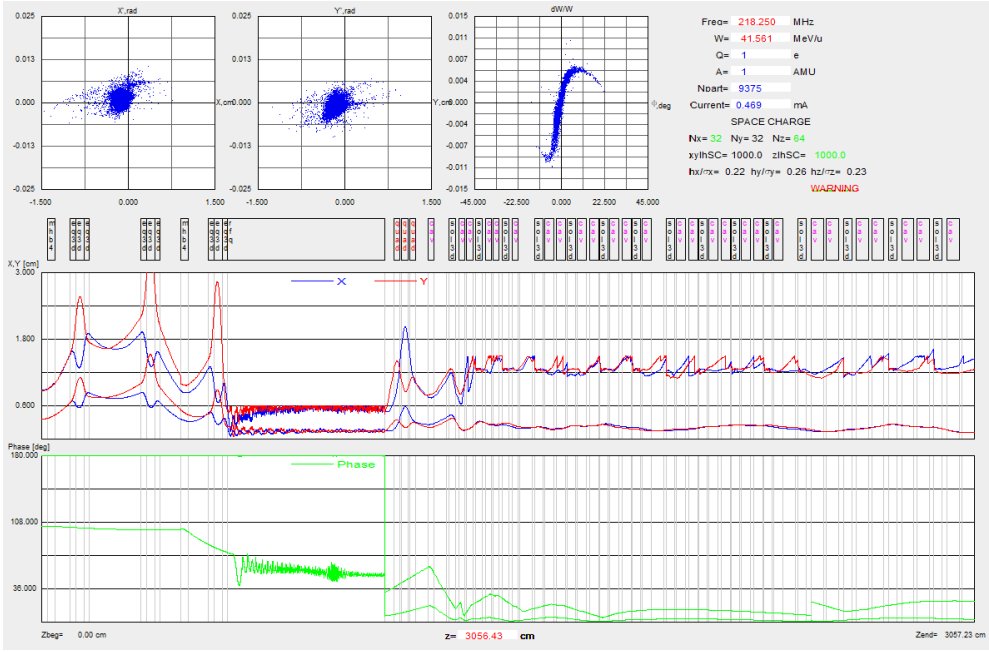

Figure 4.7: Beam transport of protons along LINCE with space charge effects. The current and final energy in the exit of the linac are 469 μA and 41.56 A $\cdot$ MeV, respectively.

at the exit of the linac, thus the transmission efficiency through the linac is 80.7%, as shown in Figure 4.6. It is important to remark that the magnetic flux was increased in some solenoids for proton beams up to 4 T. The beam energy reached for a proton beam is about 41.54 A $\cdot$ MeV.

When including space charge effects the simulations reveal that about half of the proton intensity is lost when the current is close to 1 mA (which is still within the design requirements of LINCE). The beam dynamics is shown in Figure 4.7. In the case shown, the proton beam at the exit has 9,375 particles, starting with an initial beam of 20,000 particles, which corresponds to a loss of 50.3%. However, the beam transmission only in the linac section is 95.78%.

The main loss occurs in the last cell of the RFQ, showing the need to re-design this section of the RFQ for protons, or even better, the need to have a dedicated RFQ for this beam. With the present design of the RFQ, proton beams with 0.1 mA (Figure 4.8) are transported with an efficiency of about 64%.

A specific study for a proton beam was conducted to determine the maximum transmission as a function of the voltage of the RFQ for the specific design developed. This study was carried out with the objective of optimizing the

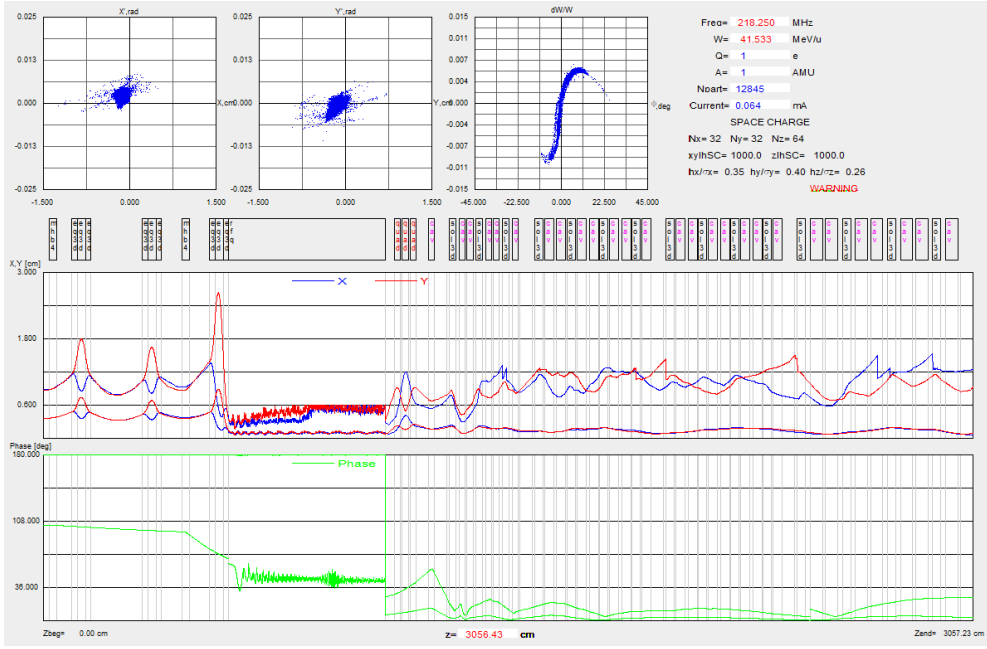

Figure 4.8: Beam transport of protons along LINCE with space charge effects. The current and final energy in the exit of the linac are 64 μA and 41.53 A $\cdot$ MeV, respectively.

transmission of protons in the designed RFQ, following the process performed in accelerators operating as ReA in MSU. The transmission percentage was calculated while the voltage value varied in the operational range from 15 kV to 35 kV.

The maximum transmission was obtained at 23.08 kV, as shown in Figure 4.9. Using this voltage value, the simulation for protons was performed again including the full LINAC, and the results are shown in Figure 4.10. The beam at the input contains 20,000 particles and I =1 mA, whereas at the LINAC exit contains 10,332 particles with I =517 μA. The transmission achieved for the LINAC system alone (excluding the RFQ) was close to 100%, which could be achieved after proper tuning of the quadrupole and the rebuncher to maximize the transmission.

With the aim of getting a better understanding of the beam transport through the LINAC, a heavy-ion beam with A/Q= 7 without including the effects of space charge was selected. The simulated beam consists of bunches of 1 ns length and 2% energy spread, with a total of 20,000 particles. The results are shown in Figure 4.11. At the exit of the RFQ there are 15,916 particles, which means that the transmission efficiency through the RFQ for heavy-ions in the

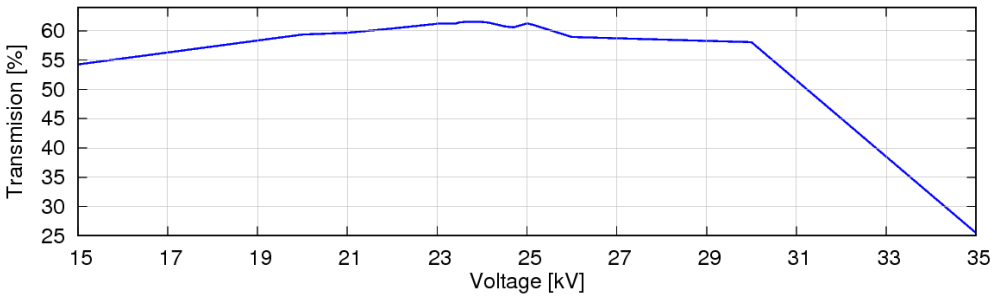

Figure 4.9: Transmission as a function of the RFQ voltage.

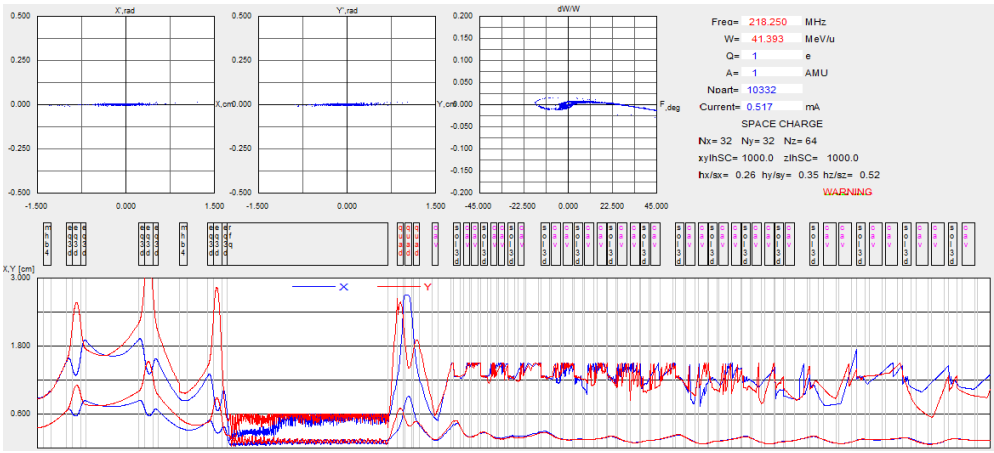

Figure 4.10: Beam transport of protons along LINCE with the RFQ voltage at maximum transmission and an initial current of $1000\,\mu$A. The current and final energy in the exit of the linac are $517\,\mu$A and $41.39\,\mathrm{A}\cdot\mathrm{MeV}$, respectively.

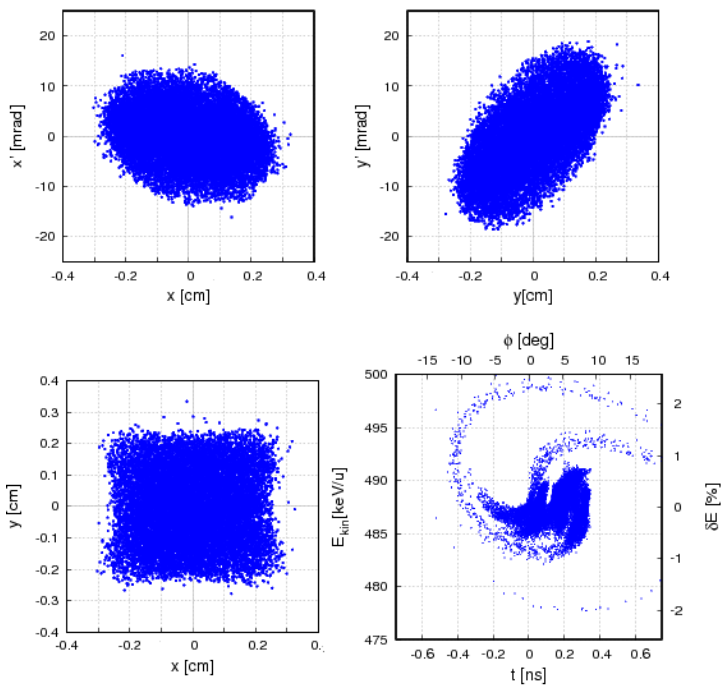

Figure 4.11: Screen after RFQ

absence of charge space effects is 75.98%.

Figures 4.12 and 4.13 describe the evolution of the beam through the linac. The transverse phase space for the horizontal plane is at the top of the figures and the longitudinal phase space is at the bottom. The output beam length and energy spread after the first cryostat are 0.6 ns and 6 %, respectively, and 0.4 ns and 2 % after the second cryostat. In fact, the length and energy spread are reduced as the beam passes through the cavities and solenoids.

For the beam after the third cryostat, shown in Figure 4.13, the length obtained is 0.4 ns and the energy spread is 1.5 %, which is consistent with the last results and with the theory. Finally, the output beam length and energy spread after the fourth cryostat, that is, at the linac exit, are 0.2 ns and 1 %, respectively.

The normalized transverse and longitudinal emittances at the end of the facility are $0.075\,\pi \cdot \text{mm} \cdot \text{mrad}$ and $0.4 \cdot keV/u \cdot ns$, respectively, as shown in Figure 4.14. It is remarkable how the beam evolves as it crosses each element, noting that the value is almost constant in the RFQ. These results are in accordance with the qualities required by the project mentioned above.

Finally, the result obtained for the energy gain per distance through the facility is shown in Figure 4.15. The energy gain increases after the RFQ, as expected,

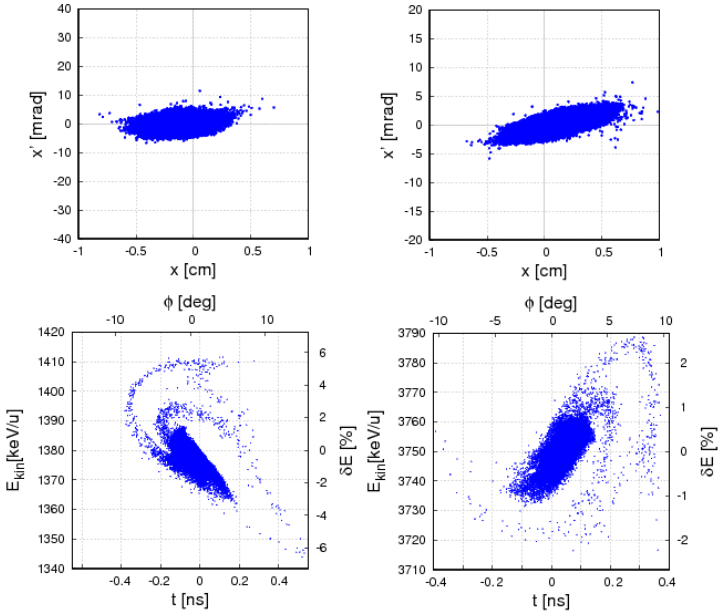

Figure 4.12: Transverse (top) and longitudinal (bottom) phase space at the exit of cryostats 1 (left) and 2 (right).

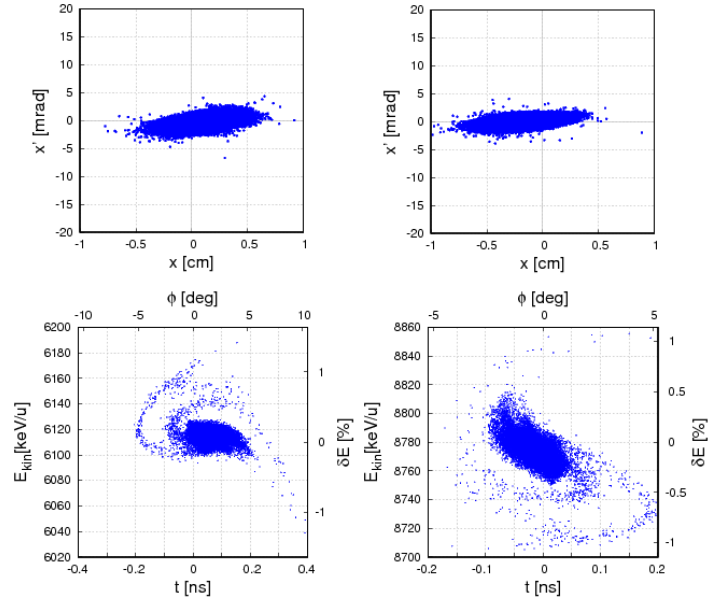

Figure 4.13: Transverse (top) and longitudinal (bottom) phase space at the exit of cryostats 3 (left) and 4 (right)

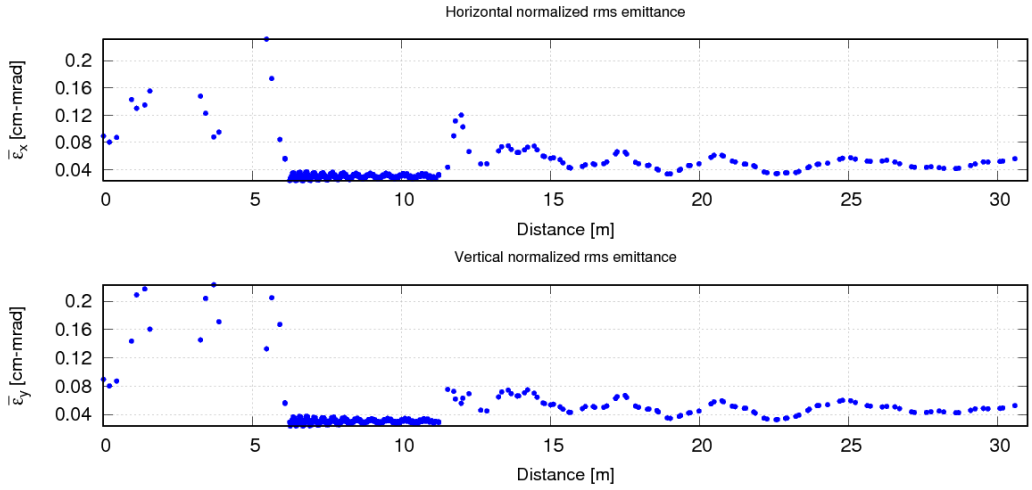

Figure 4.14: Transverse emittance in the horizontal plane (top) and in the vertical plane (bottom) through LINCE.

and reaches the target energy at the end.

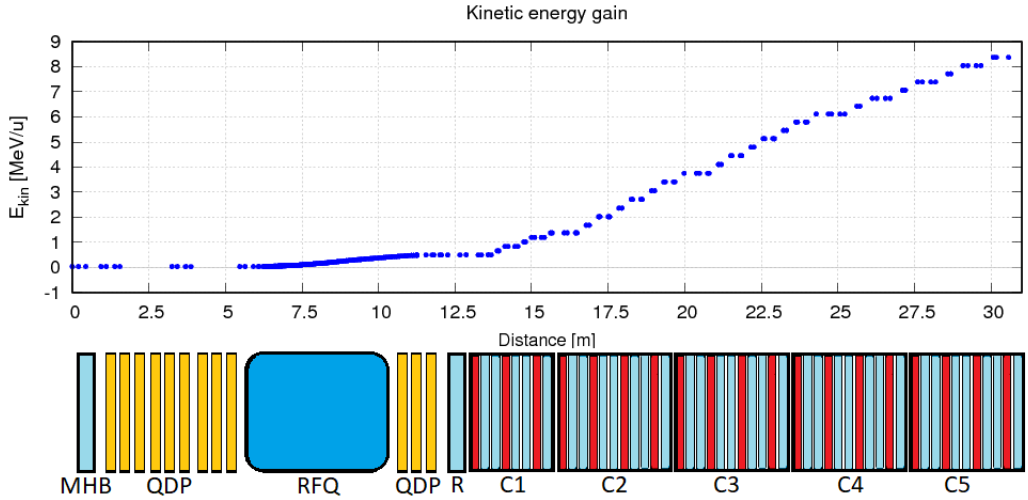

Figure 4.15: Lince Energy gain per distance

5

Design of RFQ Linear Accelerators

This chapter presents the results of the radio-frequency quadrupole. Section 5.1 shows a detailed description of the beam dynamics for the RFQ. The process followed for the cavity design is presented in more detail in section 5.2. Section 5.3 contains the results for the electromagnetic studies, including the power losses. Finally, section 5.4 presents the main results of the thermal study, including maximum values of temperature and displacement.

5.1 Detailed Beam Dynamics

In order to generate the modulation shape and evaluate the main parameters of the RFQ, the DESRFQ code was used. The input data is entered as shown in Figure 5.1.

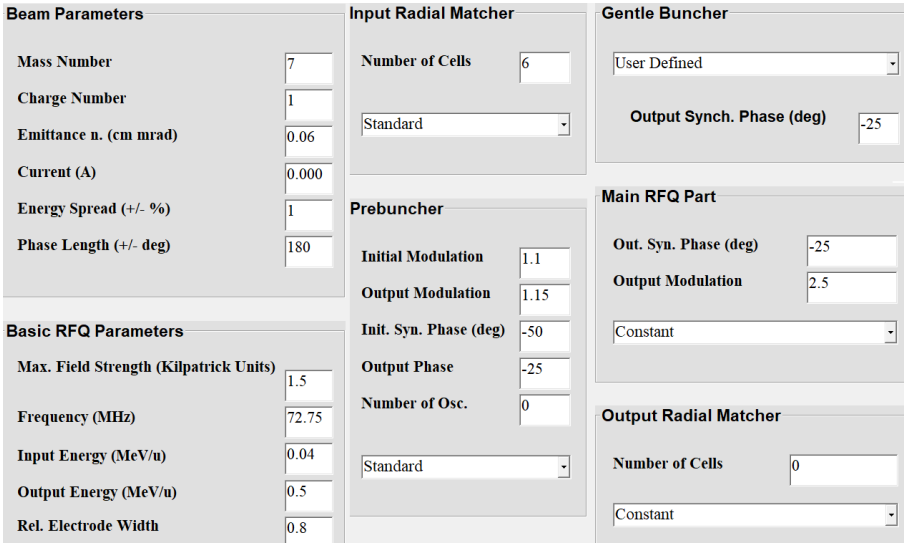

Figure 5.1: DESRFQ input data interface.

The parameters in the first frame are: the mass number in atomic mass units, the charge number in electron charges, $q/A = 1 - 7$, the normalized transverse emittance (0.6 cm−mrad), the average beam (0.0 A), the initial energy spread of beam particles (set at 1 %) and the initial phase length of the bunch at RFQ input (180 ±deg). For the frame called Basic RFQ Parameters, the input values are: the design maximum field on each electrode surface in Kilpatrick units (1.5), the operating frequency (72.75 MHz), the input energy (0.04 MeV/u) and desired output particle energy (0.5 MeV/u) and, finally, the curvature of the electrode tip as its ratio to RFQ average radius ($\frac{R_e}{R_0} = 0.8$).

For the input matcher, it is optional to insert the number of cells and the type of calculation for it, in this case the number of cells is 6 in standard calculation,[5] which poses a total length of 15.36 cm for the input matcher. The parameters for the prebuncher box are the following: the value of the initial modulation (1.1) the output for this section (1.15), and the synchronous phases −50 deg and −25 deg for the input and output sections, respectively. The desired phase advance of the longitudinal oscillations along the prebuncher, as well as the number of oscillations of the period, are also required.

At the end, it is possible to define the prebuncher calculation section as for the input matcher mentioned above.

In the next frame, there is the option to select the gentle buncher calculation and the output synchronous phase (−25 deg). The output synchronous phase for the RFQ acceleration section (−25 deg) and the final output modulation factor (2.5) are required in the box. Finally, it is possible to introduce the number of cells and the calculation for the output matcher.

With the aim of obtaining the modulation shape for the specified parameters, DESRFQ performs several iterations between the modulation factor and the synchronous phase until the desired output energy is reached. Figure 5.2 shows the relevant parameters obtained using DESRFQ. It can be observed that the phase is approximately constant, and that the acceptance decreases as the modulation factor increases

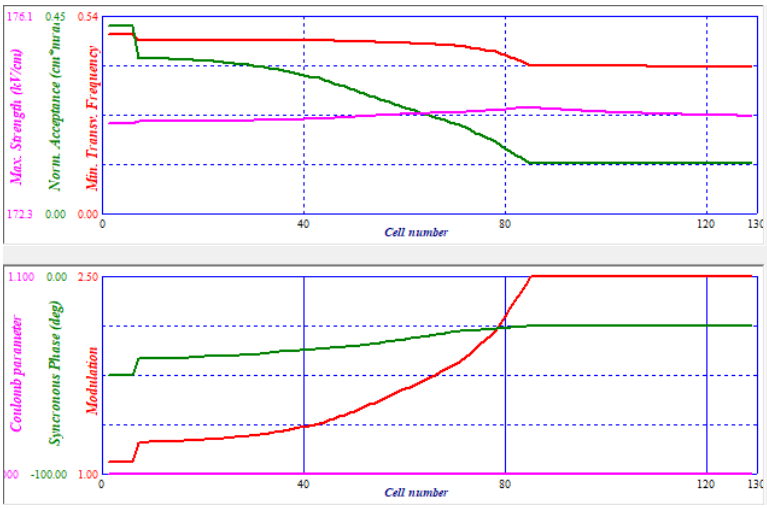

Figure 5.2: Output parameters from DESRFQ

DESRFQ generates the specific output file rfq.00, which is the input file for the TRACK code. It includes the following information.

- Cell number
- Cell length
- Inter-vane voltage
- R_0 - Average radius
- Factor modulation
- Cell type
- Function Bessel's eight parameters

The DESRFQ output file rfq.00 is added to the TRACK folder to be simulated, in order to obtain the transport dynamics along the RFQ length. After the simulation, the transverse and longitudinal phase spaces for each bunch in any position along the RFQ are obtained. The separatrix at the end of the RFQ is shown in Figure 5.3 and the total transmission obtained is about 76%.

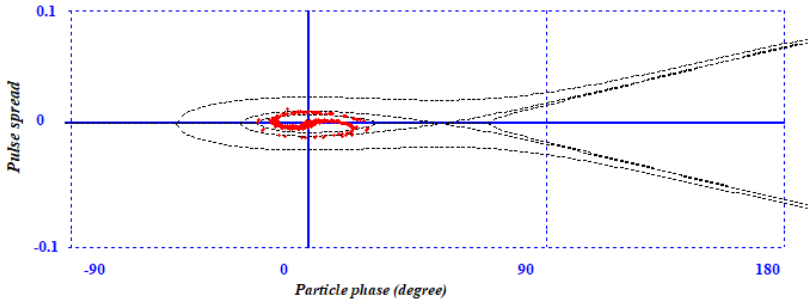

Figure 5.3: Snapshot of the separatrix at the RFQ end.

5.1.1 Transversal and Longitudinal Dynamics

Complete beam dynamics simulations were carried out using TRACK in order to verify that the target energy is achievable, while keeping the beam transverse size within the inter-vane region. The electric RFQ quadrupole fields are generated internally by the numerical code for an inter-vane potential of 82.06 kV and the sinusoidal modulation obtained previously. Snapshots of the transverse phase space are shown in Figure 5.4 for the entrance and exit of the RFQ. It can be observed that the transversal size and phase space decrease along the RFQ, as expected.

In addition, snapshots for longitudinal dynamics are shown in Figure 5.5 with the same effect in time, phase and energy spread. The input beam consists of bunches of about 2 ns in length and 4 % total energy spread of 20,000 particles; for the output beam, the length and energy spread are 1 ns and 2 %, respectively. This is the result of a multi-harmonic buncher[15] which induces longitudinal energy modulation. At the RFQ exit, there are 15,916 particles, which means that the transmission efficiency through the RFQ is 75.98%

Figure 5.6 shows the energy evolution through the RFQ per cell and on each cell. The first part of the RFQ is used for bunching rather than acceleration. Starting with the $80th$ cell, the aspect ratio remains constant, which allows a linear energy growth in this part of about 260 keV/u. Normalized RMS transverse emittance estimation along the RFQ structure is shown in Figure 5.7.

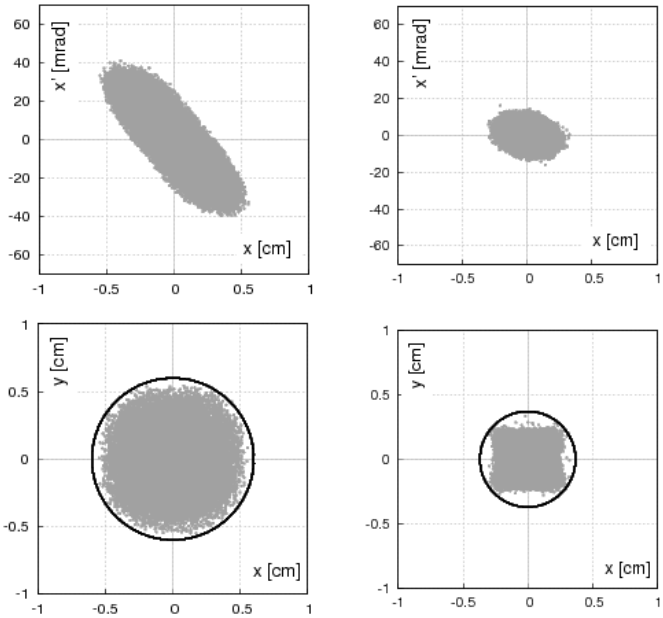

Figure 5.4: Transverse dynamics at the entrance (left) and exit (right) of the RFQ. The black circle represents the inter-vane aperture.

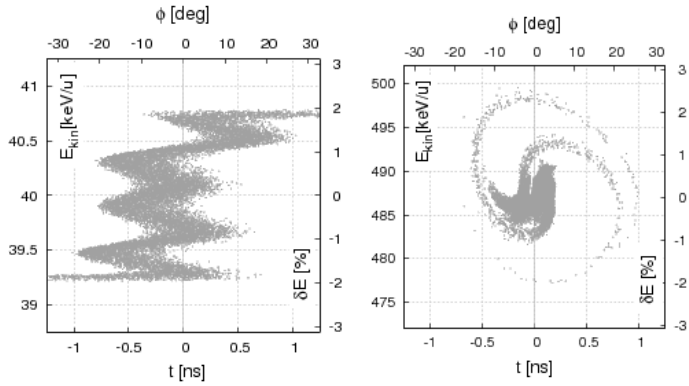

Figure 5.5: Longitudinal dynamics at the entrance (left) and exit (right) of the RFQ. The particle transmission rate is around 76 %.

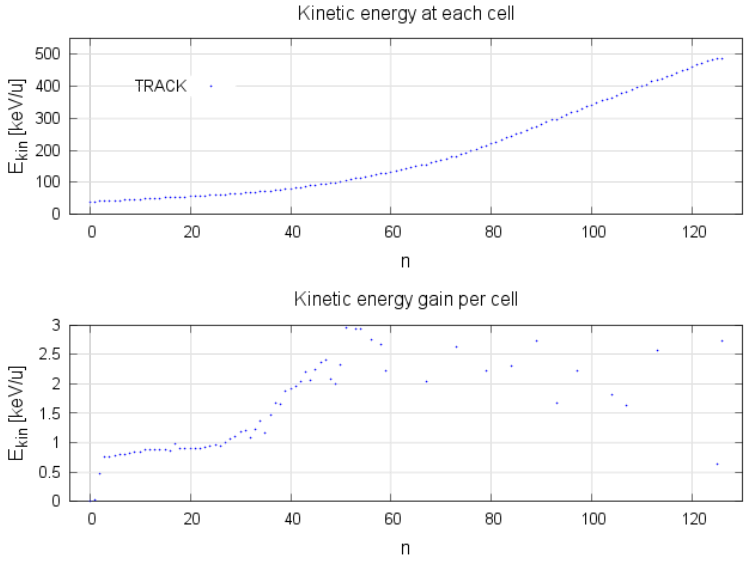

Figure 5.6: Kinetic energy along the whole RFQ structure.

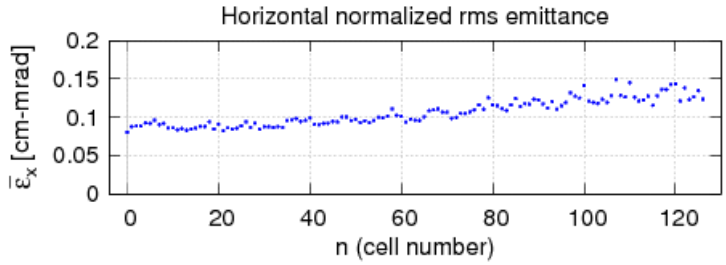

Figure 5.7: Normalized RMS transverse emittance.

The longitudinal RMS emittance is defined by the MHB and is constant along the RFQ.

5.1.2 Modulation

The modulation process begins from the DESRFQ code. Among its output files, rfq.00 is related to the most relevant data of the modulation, such as energy gain, distance, potential, etc. This file is reorganized to obtain two files with horizontal and vertical span corridors separately. The final objective is to obtain a 3D file of the electrodes (vanes). The detail process is explained below.

Modulation

Since the RFQ will be used with various ion species, a design mass-to-charge ratio of $A/Q = 7$ was chosen with the aim of having a normalized transverse emittance of $0.5\,\pi\text{mm} - \text{mrad}$ and a longitudinal emittance of $2\,\pi/\text{keV/u} - \text{ns}$.

The vane profile was generated using the DESRFQ code and implemented into the Comsol model. The vane modulation was generated mathematically based on a numerical implementation of the two equations defining its sinusoidal profile as a function of each cell length L_{ci} and the average radius R_0.[4]

$$\begin{aligned} x_i &= R_0\left(1+\frac{m_i-1}{m_i+1}\sin\left(\pi z/L_{ci}\right)\right) \\ y_i &= R_0\left(1-\frac{m_i-1}{m_i+1}\sin\left(\pi z/L_{ci}\right)\right) \end{aligned} \tag{5.1}$$

Cell	Lenght	Voltage	R0	m	t	Eight parameters define two-term potential approximation							
1	15.36618	82.06000	0.60000	1.00000	-1	0.97326	0.02838	0.95471	11.37690				
2	1.92074	82.06000	0.60000	1.16100	-2	0.97508	0.10760						
3	1.92957	82.06000	0.60000	1.16100	0	0.97505	0.10788	0.02793	0.02224	0.00171	-0.00011	0.00000	0.00001
4	1.94723	82.06000	0.60000	1.16100	0	0.97501	0.10874	0.02792	0.02214	0.00167	-0.00012	-0.00001	0.00001
5	1.96494	82.06000	0.60000	1.16200	0	0.97498	0.11022	0.02791	0.02217	0.00164	-0.00013	-0.00001	0.00000
6	1.98272	82.06000	0.60000	1.16400	0	0.97496	0.11169	0.02790	0.02220	0.00162	-0.00014	-0.00001	0.00000
7	2.00054	82.06000	0.60000	1.16500	0	0.97492	0.11285	0.02789	0.02217	0.00159	-0.00015	-0.00002	0.00000
8	2.01839	82.06000	0.60000	1.16600	0	0.97489	0.11401	0.02788	0.02214	0.00155	-0.00016	-0.00002	0.00000
9	2.03737	82.06000	0.60000	1.16700	0	0.97486	0.11551	0.02787	0.02217	0.00153	-0.00018	-0.00002	-0.00001

Figure 5.8: DESRFQ output file.

where m is the cell aspect ratio. While R_0 was set at 6 mm, cell length L_{ci} and aspect ratio m were obtained from the DESRFQ output file, which is shown in Figure 5.8.

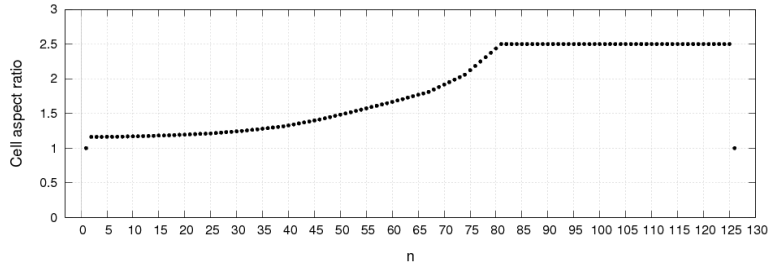

Figure 5.9: Cell aspect ratio along the RFQ structure.

As shown in Figure 5.9, the modulation aspect ratio has a gradual increase up to the $80th$ cell, after which it remains constant at 2.5, which is the accelerator section. The first part has the focus and bunch effects, thus it is important to control the phase in each cell. To obtain the geometry it is necessary to

produce two files with coordinates for the horizontal and vertical planes. The coordinates file was brought to Comsol in order to create a sinusoidal shape with the dots. The final result for the vanes is shown in Figure 5.10.

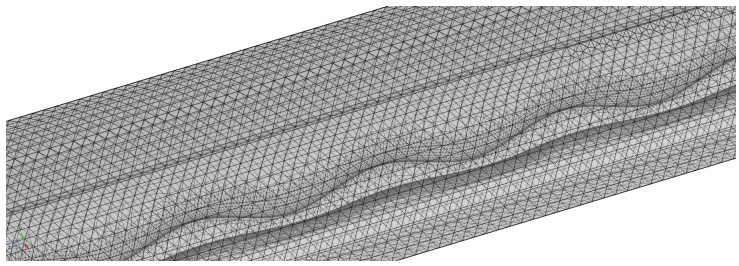

Figure 5.10: Modulation section in Comsol.

5.2 Cavity Design

The RFQ length was adjusted from the RFQ parameters simulated with DESRFQ. Taking in to account the process followed at the Argonne National Laboratory to design the 4-vane RFQ, the design of the cavity starts from the CW RFQ model 60.625 MHz[102] developed for the Argonne Tandem Linac Accelerator System (ATLAS). With this model as a reference, changes were made in order to reach the values and final parameters desired. The process is described below.

2D Analysis

An optimization process of the quality factor, resistive power loss and resonant mode frequency TM_{21} was carried out, following a loop of simulations in two stages. The first stage was dedicated to the optimization of the vane height and thickness using only the transverse shape of the vane without windows (2D), and the second one to the optimization of the RF window parameters (3D).

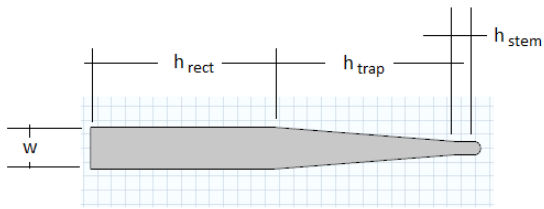

Figure 5.11: Geometrical parameters of the vane.

Figure 5.11 shows the main parameters of the vane shape, which was divided into a “rectangle”, a “trapezoid” and a “stem” shape. As an example of the first stage optimization process, Figure 5.12 shows a scan of the parameters h_{rect} (height of the rectangular shape) and h_{trap} (height of the trapezoidal shape), for three values of the vane thickness W (“rectangle width”). In these calculations, the values for the tip radius (r_1=4.8 mm), stem height (h_{stem}=14 mm) and the inter-vane distance between electrodes (R_0=6 mm remained constant. The selected values were W=40 mm, h_{rect}=130 mm and h_{trap}=130 mm, taking into account the quality factor results, the mechanization and the robustness of the vane.

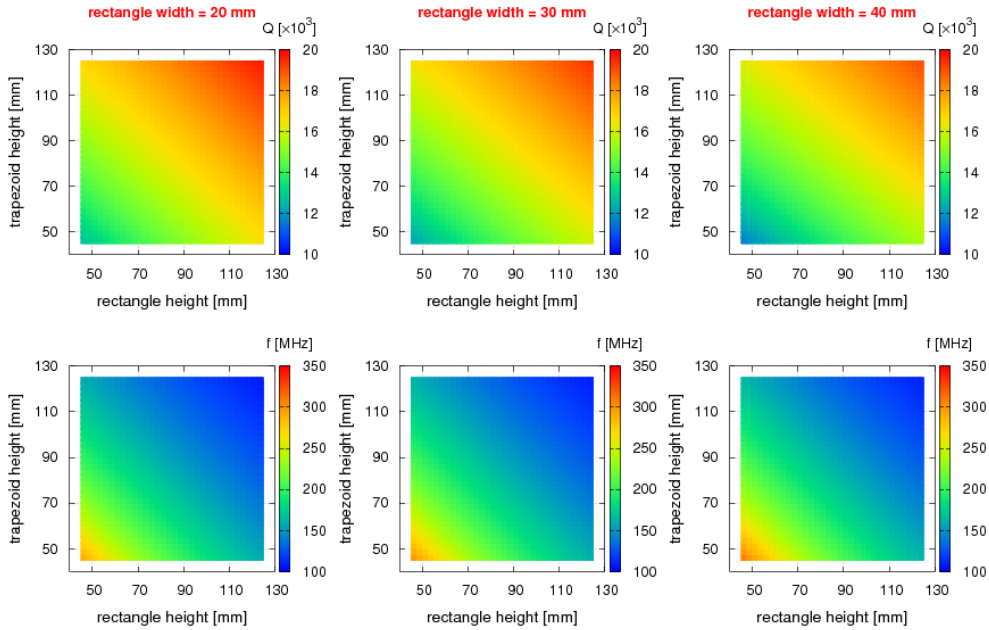

Figure 5.12: Evaluation of the quality factor Q and resonance frequency as a function of vane geometry.

3D Analysis

In the second stage, different shapes of the varying RF windows (a_1) and (b_1)were simulated in order to obtain the maximum quality factor at the design frequency; some results of this simulation are shown in Figure 5.13. The best result is obtained by using the elliptical window, with quality factor $Q \sim 10^4$ and shunt-impedance $r_s \sim 400$ kΩm.

The process followed for the optimization of elliptic parameters is illustrated in Figure 5.13. The two plots at the top of Figure 5.13 show the variation of the value of the quality factor and resonant frequency as a function of the

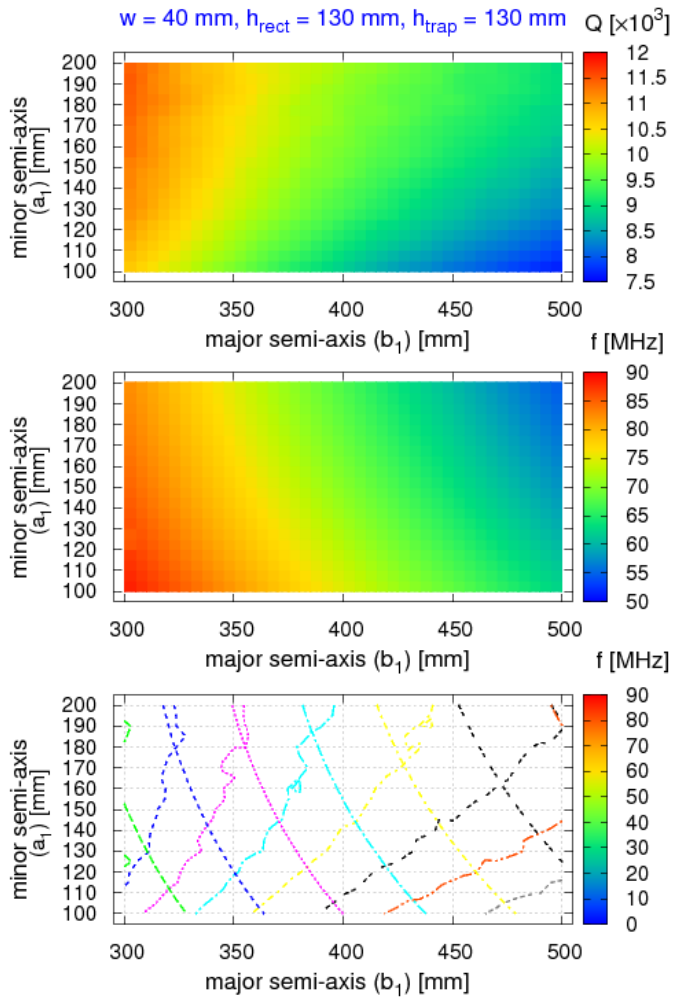

Figure 5.13: Evaluation of the quality factor Q and resonance frequency f as a function of the semi-axes a_1 and b_1 length of the elliptical shapes.

major (b_1) and minor (a_1) semi-axis. The cavity Q value increases drastically by increasing a_1 and reducing b_1, while increasing the resonant frequency. For example, for $b_1 = 375\,\text{mm}$ and $a_1 = 200\,\text{mm}$, $Q \sim 10200$ is obtained.

5.2.1 Error Analysis

In order to study the effect of random errors in the mechanization of modulation, the output file $rfq.00$ from DESRFQ is selected to change the cell length and, eventually, to be simulated in TRACK. The chosen parameter is the one that

can go wrong after the final machining of the RFQ, which can also generate more beam loss and changes in the beam transport within the RFQ.

The simulation was conducted for charge-to-mass ratio = 1/7, 20,000 particles at the RFQ entrance and 40 keV/u input energy. The cell length L_c parameter was simulated for two cases: a machining precision of 100 μm and $4\sigma = 50\,\mu$m, and a machining precision of 200 μm and $4\sigma = 100\,\mu$m. The original values at the entrance and the exit of the RFQ for emittance, energy and number of particles are shown in Table 5.1.

Table 5.1: Original values for the RFQ structure.

Original values		
Parameter	**Entrance values**	**Exit values**
$4\times\varepsilon[x, rms][mm \cdot mrad]$	0.08794	0.08305
$4\times\varepsilon[y, rms][mm \cdot mrad]$	0.09250	0.08535
$4\times\varepsilon[z, rms][keV/u \cdot ns]$	2.44116	1.17838
$E_{out}[KeV/u]$	40.02	500.7
Particles [N°]	19999	15916

The results of the simulations carried out with variations in the cell length Lc parameter are summarized in Table 5.2. The results are also expressed in percent over the original values at the exit of the RFQ mentioned above. The results show that random errors produced by 100 μm machining precision in the cell length L_c modulation have no relevant impact on the beam dynamics along the RFQ. The maximum change is observed in the longitudinal emittance, which is below 1% with respect to the initial value.

On the other hand, in the case of a machining accuracy of 200 μm, it can be seen that its effects on beam transport, as expected, represent more significant changes in the beam. With an increase of about 10% in the longitudinal emittance, less beam transmission and increased energy gain were obtained, which affects the focusing and bunching processes of the next cavity.

Table 5.2: Effect of random errors in the RFQ structure.

Error values				
Precision	**100 µm**		**200 µm**	
Parameter	**Exit values**	**%**	**Exit values**	**%**
$4\times\varepsilon[x, rms][mm \cdot mrad]$	0.08292	0.16	0.08229	0.92
$4\times\varepsilon[y, rms][mm \cdot mrad]$	0.08536	0.01	0.08470	0.76
$4\times\varepsilon[z, rms][keV/u \cdot ns]$	1.17716	0.10	1.29383	9.80
$E_{out}[KeV/u]$	501.87	0.23	504.82	0.82
Particles [N°]	15895	0.13	15811	0.66

5.3 Electromagnetic Analysis

The complete RFQ structure of 5 m in length was simulated using the RF Module of COMSOL Multiphysics; the main resonance modes are shown in Table 5.3. The process starts with the simulation for the octagon. Then, step by step, the vanes, windows, and modulation are introduced, in that sequence. The fundamental value of the resonance frequency decreases to 71.89 MHz. The working frequency is reached by using the tuning system, as is discussed at the end of this section.

Table 5.3: Resonance modes and degeneracies.

Geometry stage	**Modes & Degeneracy**	**Frequency [MHz]**
Cavity	TE_{111}	306.41
	TE_{112}	310.61
Cavity with vanes	TE_{211}	107.74
	TE_{111}	113.67
Cavity with vanes	TE_{211}	72.02
and windows	TE_{212}	78.78
Cavity with modulated vanes	TE_{211}	71.89
and windows	TE_{212}	78.10

For structural and heat transfer simulations, it is necessary to increase the size of the mesh, in order to obtain optimal results. Accordingly, the simulation to obtain power losses was conducted only for the first section. The same geometry will be used for heat transfer and structural studies as is explained in section 5.4.

5.3.1 Electromagnetic Fields

Introducing the four vanes into the resonator enables the appearance of a quadrupole mode TE_{211} resonating at around 107.74 MHz and one doubly degenerated dipole mode at 112.3 MHz. On the other hand, the mode TE_{211} results for the cavity with vanes and windows and its double degenerated dipole are 72.02 MHz and 78.78 MHz, respectively. Therefore, the separation mode increases approximately 2 MHz when the windows are specially cut in the vanes. The quadrupole electric field pattern in a transverse cross-section for mode 72.02 MHz is shown in Figure 5.14.

The magnetic field is directed longitudinally along the structure with its sign alternating from one quadrant to another as can be seen in Figure 5.15. It is important to highlight that the direction of the magnetic field is only for a RFQ cavity with vanes without windows.

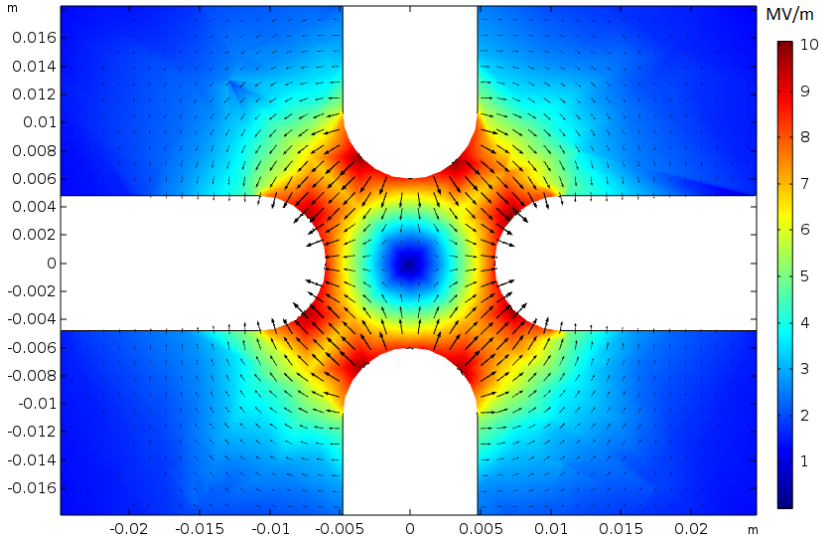

Figure 5.14: Quadrupole electric field patterns for the vanes without windows at $TE_{211} = 72.02\,\text{MHz}$.

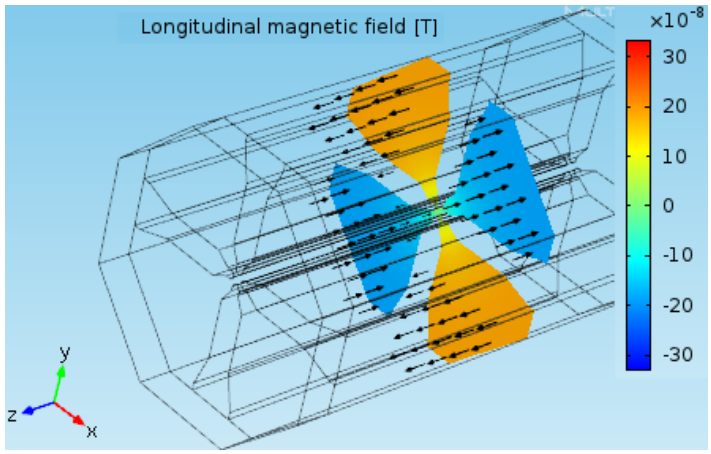

Figure 5.15: Magnetic electric field pattern for the vanes without windows.

Cutting RF windows through the vanes leads the magnetic field lines to loop around window corners, as shown in Figure 5.16 resulting in a reduction of the

quadrupole mode frequency and a clear separation from the dipole modes[102] from 71.89 MHz to 78.10 MHz. This also brings the next order quadrupole mode into the range of the fundamental one. The electric field distribution for the fundamental mode frequency in the middle of the RFQ is shown in Figure 5.17.

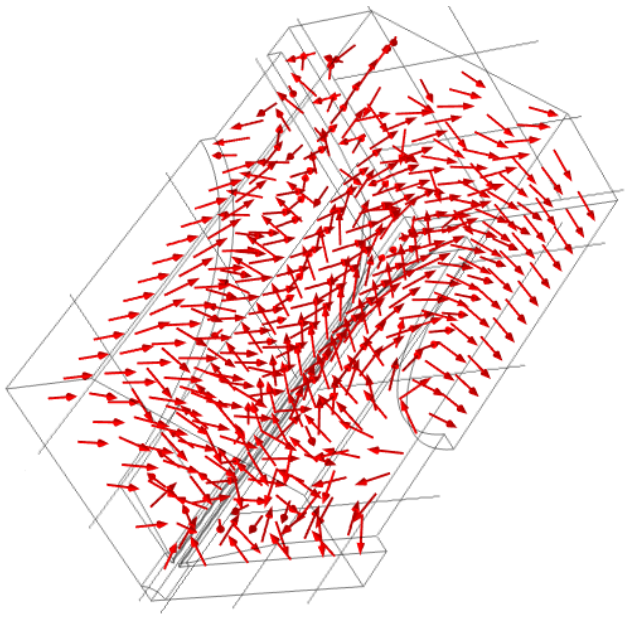

Figure 5.16: Magnetic field pattern for the vanes with windows.

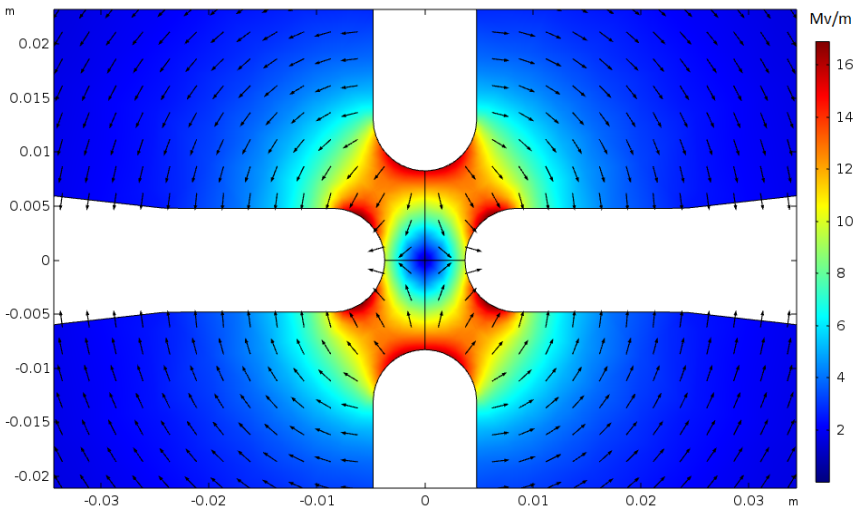

Figure 5.17: Quadrupole electric field pattern for the vanes with windows.

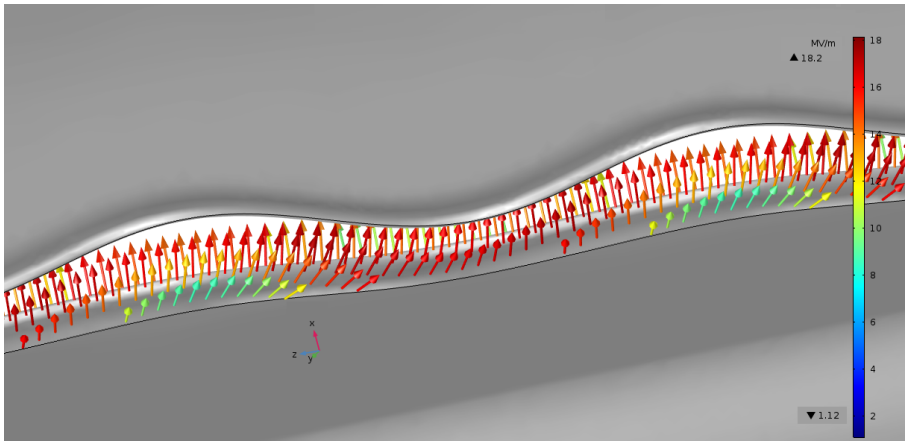

Figure 5.18: Pattern of electric field intensity vectors at the surface of one modulated vane tip.

The longitudinal component produces the effect of acceleration in a particle bunch. The distribution of the electric field vectors near the vanes shown in Figure 5.18 appears as the modulation is introduced. The longitudinal electric field pattern between the vanes from 2.525 m to 2.565 m is shown in Figure 5.19. As can be observed, the result is in agreement with the accelerator theory, since the axial field is maximal at the halfway locations, where the gradient of the potential is maximal and the four electrodes also have equal displacement.[76]

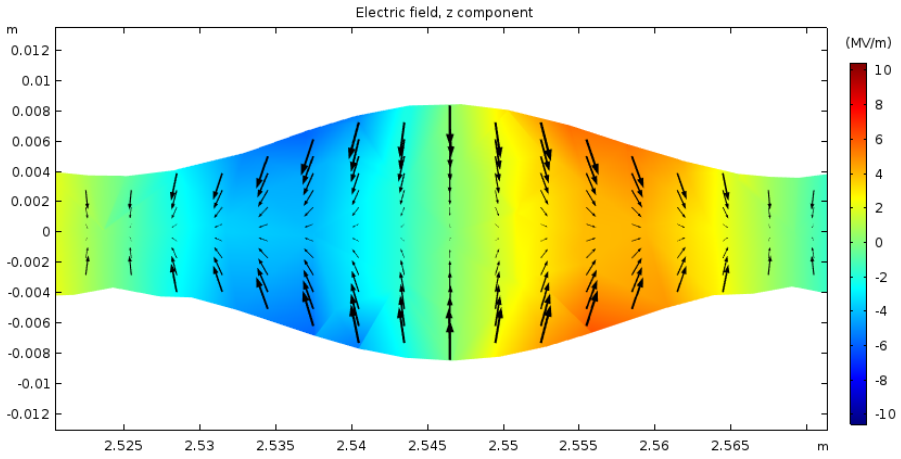

Figure 5.19: Longitudinal electric field pattern in two cells between modulated vane tips.

Figure 5.20 shows the on-axis electric field distribution along the RFQ. This

result is consistent with the pattern for this split-coaxial structure and a sinusoidal modulation shown for the 60.625 MHz RFQ for the Argonne Tandem Linac Accelerator System (ATLAS).[102] The peak surface field at specific zones of the vane tip increase up to 6.52 MHz, although still below the kilpatrick limit. Simulations showed an electrical discharge peak at the ends of the RFQ in a 5 cm gap between the flanges and the extremities of the vanes. It is important to note that between the end vanes and flanges there is a longitudinal component field. However, its effect in beam dynamics is not significant due to two reasons: the window cuts and the fact that the next element is a SC linac.[88]

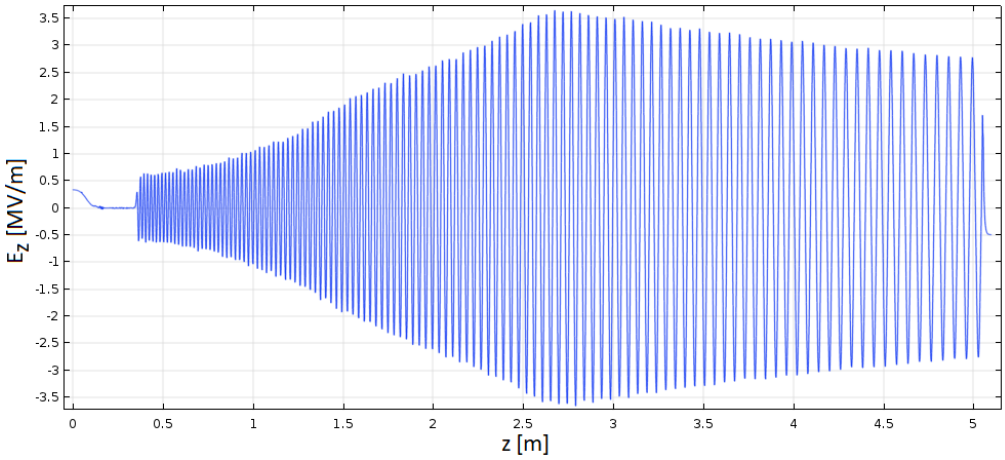

Figure 5.20: On-axis longitudinal field along the RFQ.

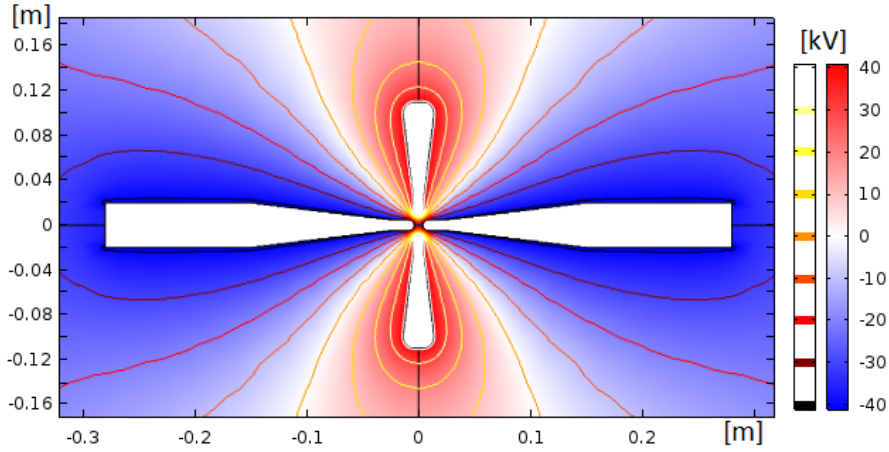

Figure 5.21: Pattern of the electric potential between the vane tips for an inter-vane potential of 80.06 kV.

With the aim of obtaining the pattern of the potential of 80.06 kV between the vane tips, a transverse view at the RFQ center was selected. The results of the potential pattern are shown in Figure 5.21.

5.3.2 Power Loss Map

Resistive power losses are calculated from the electromagnetic study in section 5.3 for a quarter RFQ section, assuming total symmetry in the model. The results showed maximum losses of 25.7 W/cm^2 located on window corners as can observed in Figure 5.22. The total resistive power dissipated by the RFQ working mode 75.95 MHz for cavity RFQ is 9.67 kW. The results are consistent with similar thermal studies conducted by T.J. Schultheiss,[103][104] for a 57.5 MHz CW RFQ and 60.625 MHz, with maximum losses at the same location of 8.28 W/cm^2 and 11.7 W/cm^2, respectively. It is important to note that the maximum inter-vane voltage for these RFQs is about 70 kV.

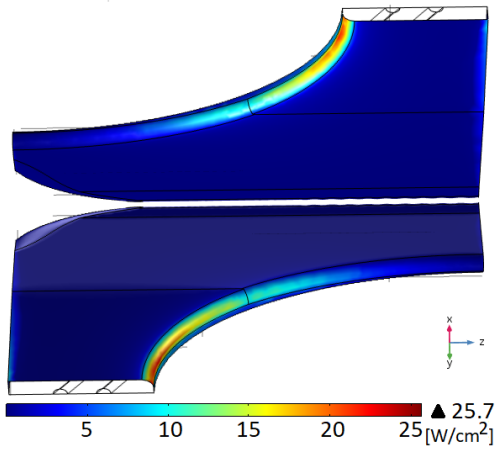

Figure 5.22: Resistive power losses in W/cm^2.

Once the result from the power losses was obtained, the coupling of the RF module with the thermal and CFD modules was carried out. The main purpose of the coupling method is to obtain the heat map and solve the problem of high temperature with an efficient cooling system. Then, the thermal results will be extrapolated to structural and moving mesh studies to obtain the final frequency shift for a quarter symmetry model of the RFQ section.

5.3.3 RF Parameters

Main RF parameters as frequency mode, quality factor, power loss, shunt impedance, stored energy among others obtained from the electromagnetic study are presented below. RF parameters for the whole RFQ are shown in Table 5.4. In addition, the RF parameters for one section were included to compare the results with the whole RFQ.

Table 5.4: RF characteristics for the whole RFQ.

Parameter	**Value RFQ**	**Value section RFQ**
Operating frequency	71.89 [MHz]	75.95 [MHz]
Nearest mode frequency	78.10 [MHz]	79.83 [MHz]
Second nearest mode frequency	82.75 [MHz]	84.15 [MHz]
Quality factor	10898	10832
Total RF power losses	119.45 [kW]	9.67 [kW]
Stored Energy	2.8817 [J]	0.21948 [J]
Impedance shunt	280.50 [$k\Omega m$]	351.09 [$k\Omega m$]

5.3.4 Tuner Design

The typical tuner shape is cylindrical and it moves into the cavity resonator to change the frequency. It is made from the same material as the cavity and the movement is usually performed by a stepper linear actuator, which depends on the range and use of the tuner. The tuner shape was designed as is shown in Figure 5.23.

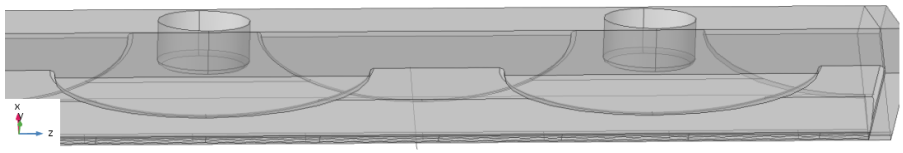

Figure 5.23: Frequency shift of the whole RFQ as a function of tuner diameter and depth (left) and position offset (right).

Then, in order to find a good combination for the working mode frequency, a quarter RFQ was simulated with five tuners placed on the free side. The main frequency is reach for a combination of 6 cm, 5.1 cm, 5 cm, 5.1 cm with a final frequency of 72.75 MHz. The sensitivity of the frequency with respect to the tuner depth is 30 KHz/cm. However, a detailed study of the tuner geometry was also conducted varying its penetration depth, diameter and position on the wall with respect to the beam entrance. The results of this study are shown in Figure 5.24.

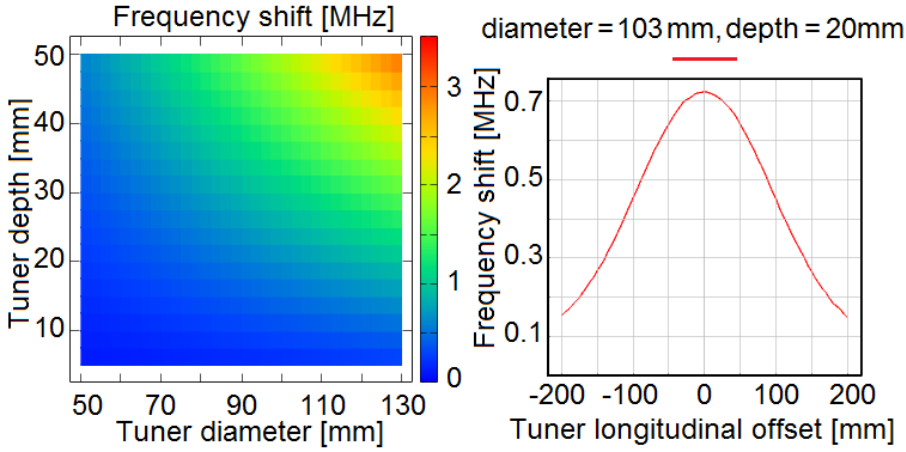

Figure 5.24: Frequency shift of the whole RFQ as a function of tuner diameter and depth (left) and position offset (right).

The graph on the right shows the frequency change with respect to the depth and the diameter of the tuner, whereas the graph on the left describes the maximum frequency shift with respect to the position movement on the RFQ side. As can be observed, the maximum frequency change occurs when the diameter and depth of the tuner reach their maximum values. Taking into account the size of the structure and the commercial values, a tuner of 103 mm in diameter was selected with a possible maximum depth of 20 mm, which may vary according to the frequency needs. Two main conclusions were extracted from the study: the bandwidth of the tuner increases with the diameter and penetration depth, and the maximum effect occurs when the tuner is on the center of the cavity wall, equidistant from both ends.

5.4 Heat Transfer Study

The 72.75 MHz RFQ is designed to function at room temperature. The effective functioning of the RFQ cavity requires efficient water cooling in order to dissipate significant resistive power non-uniformly distributed on the copper walls and vanes. This amounts to about 10 kW for one 0.5 m long RFQ section.

A complete loop of coupled numerical studies is achieved as shown in Figure 5.25. The RF Analysis was carried out with Comsol,[7] resulting in an estimate for the resistive power losses. These are scaled and coupled with Heat Transfer model in order to obtain a temperature map at the vanes surface. The next

step is the optimization of the cooling system according to the heat map. Optimizations to study the fluid and velocity temperature are carried out. The final heat flux is coupled to a solid mechanics study to estimate the stress and displacements caused by thermal expansion. The frequency shift is obtained through a new RF study of the deformed structure.

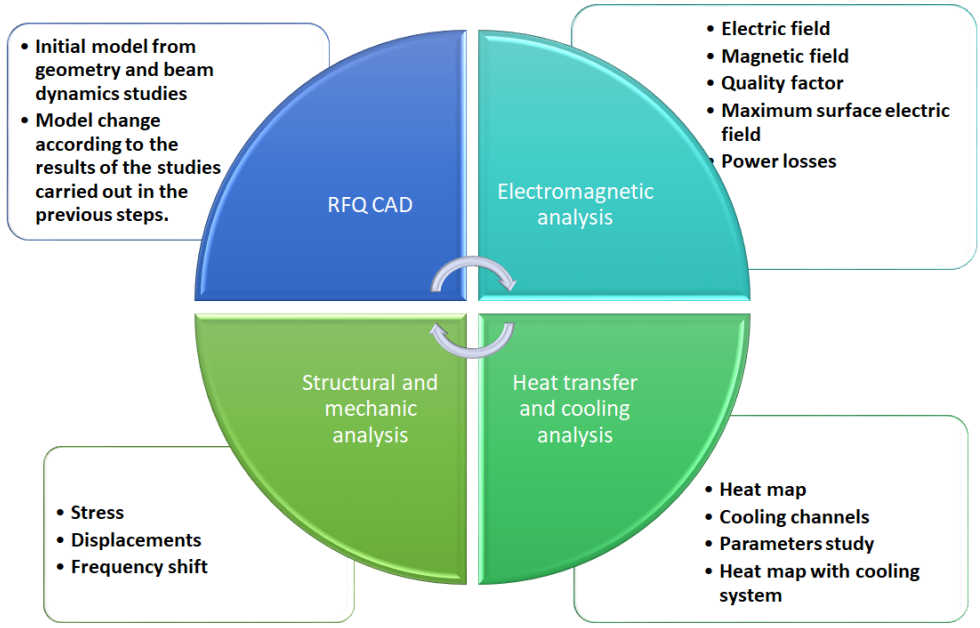

Figure 5.25: Technical study workflow.

5.4.1 Heat Map and Cooling Design

The temperature distribution map for one section of the RFQ is obtained from the power loss results presented above. It is assumed that the temperature is symmetric for both the remaining cavities and the three remaining parts of the section. The resulting heat map is shown in Figure 5.26. As can be seen, high temperature appears at the window corners and it increases as the surface is further away from the corners, which is where the maximum power is concentrated. It is important to emphasize that in order to obtain the real power loss value for a section, it is essential to perform a scale process. The electric field result is multiplied by the ratio between the result with and without scale.

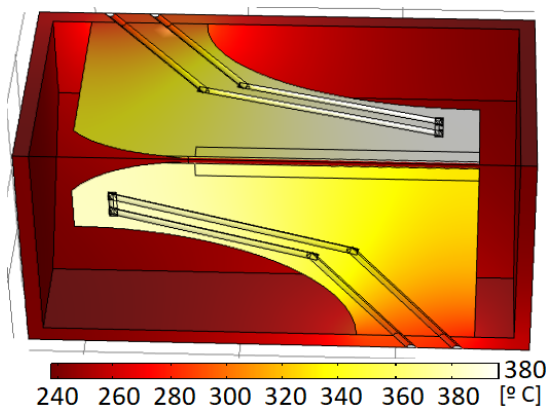

Figure 5.26: Temperature without cooling system.

Once the heat map is obtained, appropriate cooling channels on the vanes should be designed in order to have an optimal cooling of the vanes and total structure.

Cooling Channels

To tackle the problem of resistive power losses, two models were proposed as shown in Figure 5.27. An initial cooling channel of rectangular profile was considered in an initial RFQ model due to its mechanical simplicity, as shown in the left part of the figure, although it proved unsatisfactory in the vane tips. Therefore, the second model, at the right part of Figure 5.27, was based on the model provided by Schultheiss,[104] with better results in the tip, corners and total structure.

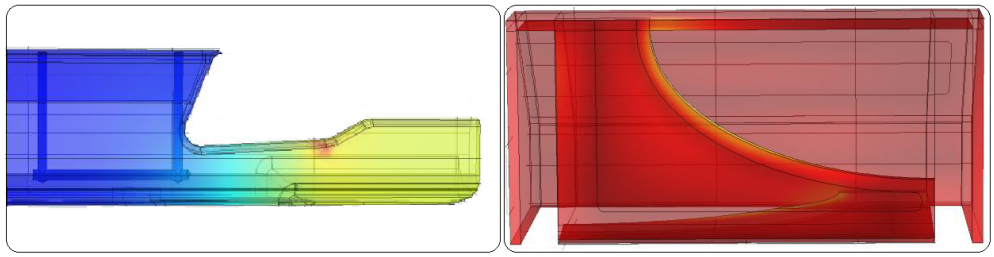

Figure 5.27: System cooling models.

Subsequently, cylindrical cooling channels were designed and included in the system, coupled to the total design with RF. Power loss simulations were conducted to study their consequences on the RFQ performance in terms of resonant frequency and thermal deformations. Finally, the cooling channel was

adapted to a real form derived from the mechanisation process, taking into account the studies previously carried out by Schultheiss.[103]

The criteria to select the pipe diameter was the maximum possible considering the structure. For this reason, the cooling channels have an inlet and outlet diameter of 6.5 mm and 7.5 mm, respectively. These diameters were implemented in the 3D COMSOL design. Similarly, the channel position was placed as close as possible to the curvature of the window in order to obtain the maximum heat dispersion. In addition, cooling channels were implemented on the sides of the octagon, with a diameter of 5.0 mm. The final model is shown in Figure 5.28.

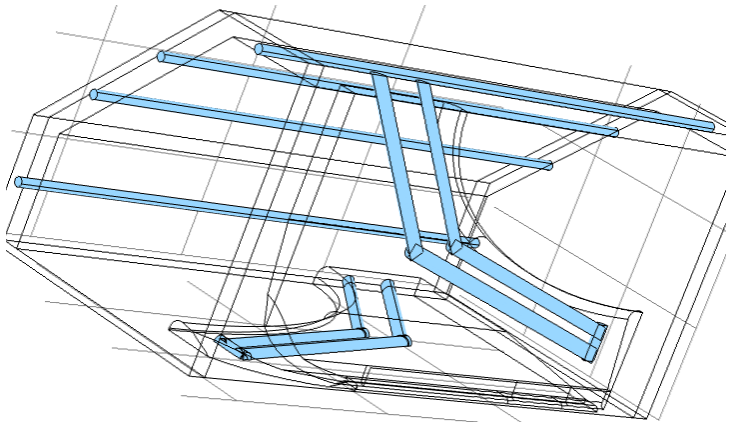

Figure 5.28: RFQ cavity cooling system.

Cooling Design Parameters

Special attention is paid to the dynamics analysis for the total structure temperature as a function of the initial fluid conditions, temperature and velocity. The results obtained show that for higher temperatures of the liquid, the heat dissipation is lower; proportionately, when the temperature decreases, the dissipation is greater. Likewise, if the fluid velocity is low, the dissipation is lower, and it increases proportionately when the velocity is increases. The dissipation is greater as shown in Figure 5.29.

In view of the results, a value range can be suggested for the initial velocity and temperature of the liquid. It is important to highlight that the values were selected considering the reference market values of the chillers for both temperature and velocity. The ranges are shown in Table 5.5. As can be observed, the structure temperature will be lower if the velocity value is greater and the temperature of the cooling liquid is lower.

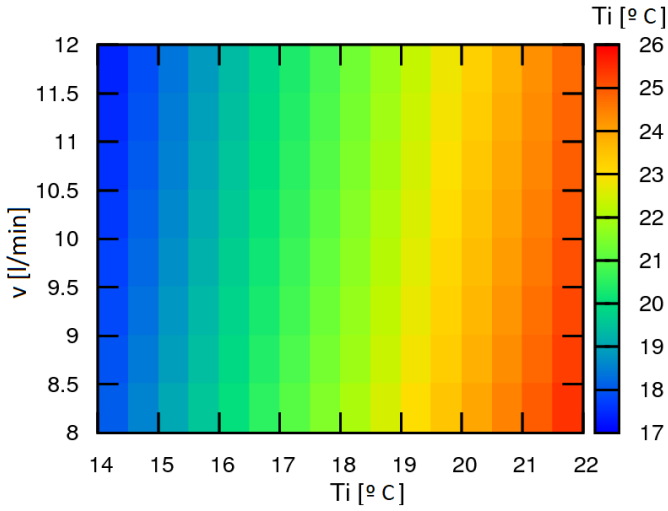

Figure 5.29: RFQ cavity temperatures as a function of the initial temperature and velocity of the fluid.

Table 5.5: Parameters

Parameter	Value	Interval	Units
Initial Temperature	20	14-22	° C
Vanes Initial flux	14	8-14	l/mim

Cooling RFQ

Once the parametrization simulations to study the final combination of temperature and velocity at the entrance of the refrigeration channels were concluded, a several iterations between heat transfer and fluid models were carried out. The purpose of the simulations is to reduce the RFQ heat through the cooling system using a combination of the values mentioned above.

As can be observed in Figure 5.30, the temperature of the cavity has maximum values located at the vane tip and minimum in the lateral side, with 41 °C and 33 °C, respectively.

The results for the velocity of the cooler and pressure into the channel are shown in Figure 5.31. As expected, fluid velocities in the cooling channels shown in the left part of Figure 5.31 reflect maximum values of 7 m/s at the entrance and channel corners. In the right side of Figure 5.31, it can be observed that the pressure drop between the input and output cooler is about ≈ 90 kPa with an initial value at the input cooling channel of 483 kPa, which is consistent with the value observed in the study for the CW RFQ of ATLAS.[103]

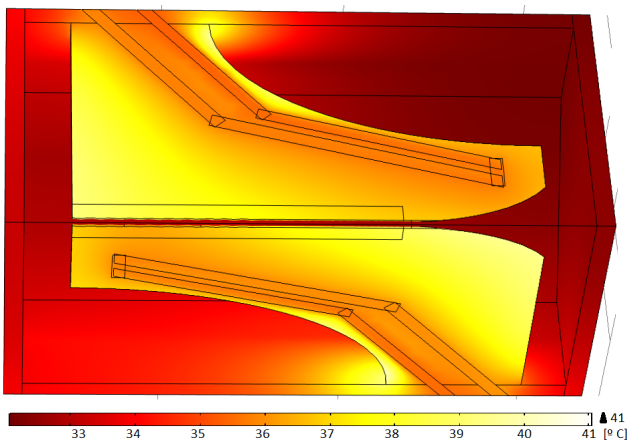

Figure 5.30: RFQ cavity temperatures as a function of the initial temperature and velocity of the fluid.

It is important to remark that the mechanization of the cooling channel located on the input matcher vane can cause some problems due to the small space available to do the holes into the copper. In this case, the cooling channel can be moved up in order to return the cooler. The results obtained for a simulation with these parameters are in line with the results presented above. Furthermore, the cooling channels used for the simulations are made with an ideal shape due to the needs of the mesh and the time for the simulations.

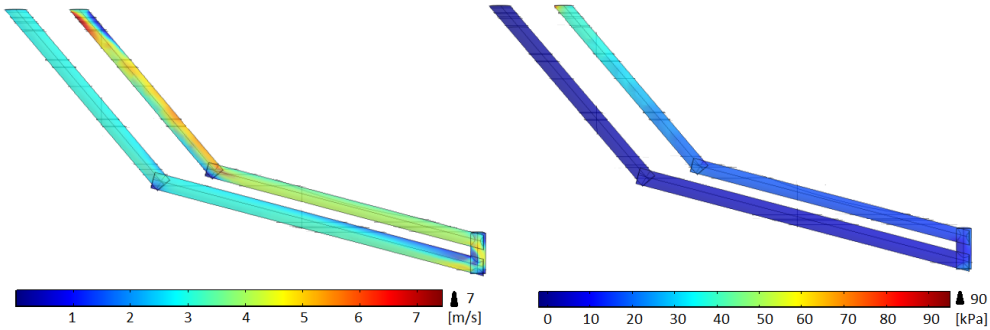

Figure 5.31: Velocity of the cooler and pressure in the RFQ cooling channel. (Left) Velocity in [m/s] (Right) Pressure in [kPa].

Consequently, the selected values for the cooling channels on the vanes to carry out the structural analysis are 20 °C and 14 l/min for the initial temperature and initial velocity, respectively. Furthermore, the liquid temperature on the cooling channels located on the octagon sides is the same and the velocity is 2.5 l/min.

5.4.2 Structural Analysis

Once the cooler parameters are fixed, these results are coupled with the solid mechanics module in order to find the displacements caused by the power loss. Then, as was mentioned above, the displacement results are coupled with mesh moving and frequency modules in order to study and obtain the frequency shift caused by the thermal expansion.

Deformations and displacements

The results obtained for the displacements show maximum values at the vane tips of 0.1 mm in the x axis and 0.12 mm in the y axis, both in the direction of the beam, as shown in Figure 5.32 for y axis. Finally, the results obtained for the whole structure showed a maximum displacement of 0.2 mm located on the vane tips of the cavity.

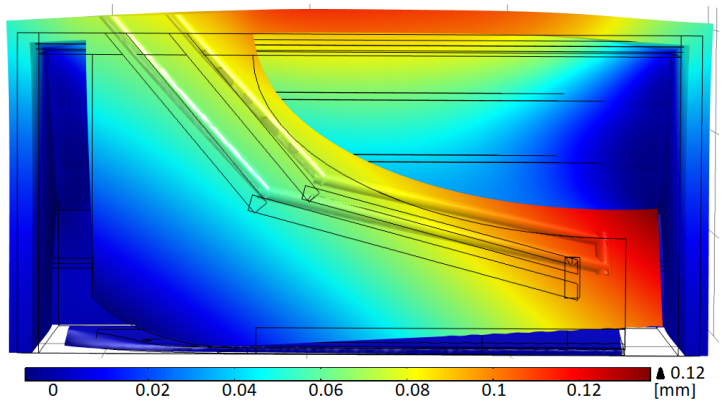

Figure 5.32: Displacement in the y axis in [mm] on the RFQ section.

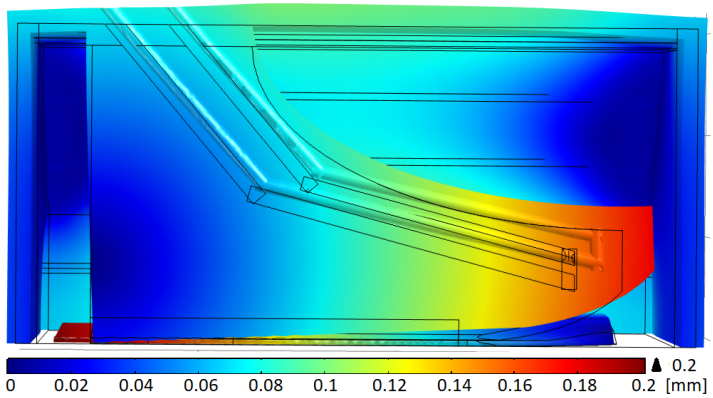

Figure 5.33: Total displacement in [mm] on the RFQ section.

In view of the results, it can be deduced that the difference between the displacements in the x and y axes is due to the fact that the RFQ support area is considered a fixed constraint in the structural model simulation, located at the corners of the cavity. Likewise, Figure 5.33 comprises the total cavity deformations.

As can be observed, the octagon corners (sides and flange) present the maximum deformations between 0.1 mm and 0.12 mm. On the other hand, the maximum deformations in the vanes are located towards the beam line direction with maximum values of 0.2 mm.

Frequency Shift

In view of the results, Table 5.6 presents the final parameters selected for an optimum heat dissipation. Finally, the **frequency shift**, determined by combining solid mechanics results with the moving mesh and frequency module, is **366 kHz**.

Table 5.6: Parameters

Parameter	**Value**	**Units**
Input Radius	6.5	mm
Output Radius	7.5	mm
Side Radius	5.0	mm
Initial Temperature	20	°C
Vanes Initial Flux	14	l/min
Side Initial Flux	2.5	l/min
Initial pressure	483	kPa
Max Displacement	0.2	mm
Frequency Shift	366	KHz

Finally, as part of the thesis into the frame of the R&D projects, a study for the design of a dedicated 4-rods radio-frequency to accelerate protons and very light ions for medical applications has been carried out. A brief description and the main results are shown in Appendix B.

6

Radiofrequency Quadrupole Prototypes and Tests

This chapter is dedicated to the mechanical design and construction of the RFQ prototypes, the RF measurements and the comparison with the electromagnetic simulations. In Section 6.1 details of the work carried out to design and build a section of the RFQ in aluminum, are given. The RF measurements and the results of the simulations are discussed in Section 6.2. The study of the RFQ model fabricated in copper is presented in Section 6.3, which also includes a summary of the brazing process carried out at LNL, Italy.

6.1 Aluminum prototype

In order to test the quality and reliability of the calculations, a simple aluminum prototype of a RFQ section was built in collaboration with local Spanish companies. The system was assembled and tested in the RF Laboratory of the University of Huelva. The electromagnetic model is shown in Figure 6.1. The companies FAYSOL S.A.L.[105]and MECA-TECA S.L[106] were in charge of producing the fabrication drawings and delivering the various parts of the aluminum cavity. At the University of Huelva we carried out the electromagnetic study, mechanical design, assembly and radio-frequency measurements.

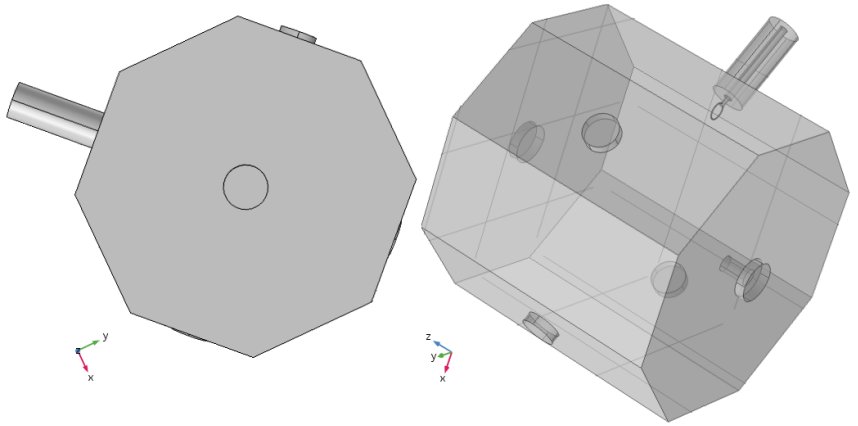

Figure 6.1: RFQ section without vanes.

6.1.1 Electromagnetic model and simulations

The aluminum prototype was built with the aim of testing the electromagnetic model and the results of the simulations using code COMSOL MULTIPHYSCS. The main goal was to produce a prototype with similar characteristics to a real RFQ, but with an easier fabrication process, simple assembly and cost effective, using materials already available in the workshop.

The frequency was chosen in the range of RFQ resonance frequencies used for heavy ions in other projects, as mentioned above in chapter 5. A first series of simulations were carried out to define a convenient geometry. The final result is a structure of 540 mm length, with octagonal cross section and 236 mm side length (Figures 6.1 and 6.3), which resonates at 157 MHz. The mechanical design study produced an arrangement of 14 pieces: eight rectangular walls, two end-caps and four vanes with specific shape (Figures 6.5-).

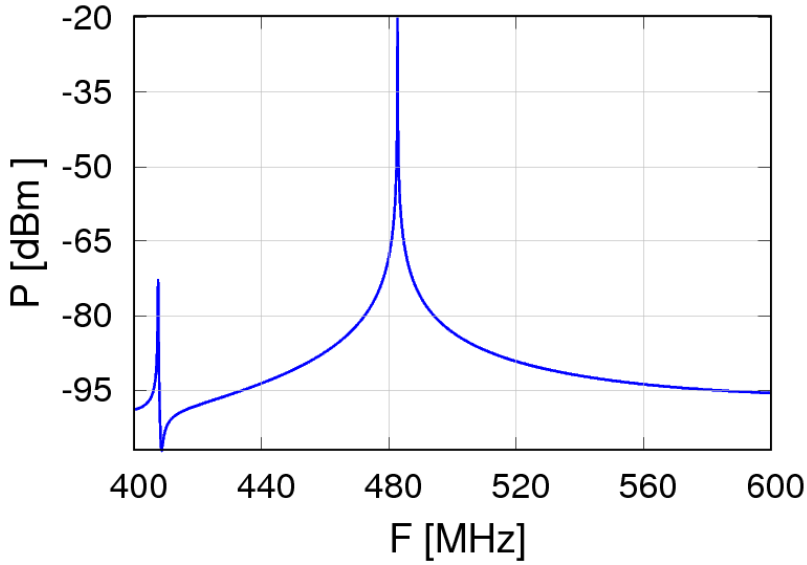

Figure 6.2: Frequency simulation for the RFQ section without vanes.

The system could also be mounted in two stages, the first one producing an empty octagonal cavity, and the second one by inserting the vanes. Therefore an additional test could be carry out by using the empty cavity shown in Figure 6.1, which according to the simulations should resonate at 483 MHz. It is worth highlighting that the vanes do not have the windows and modulations included in the design study.

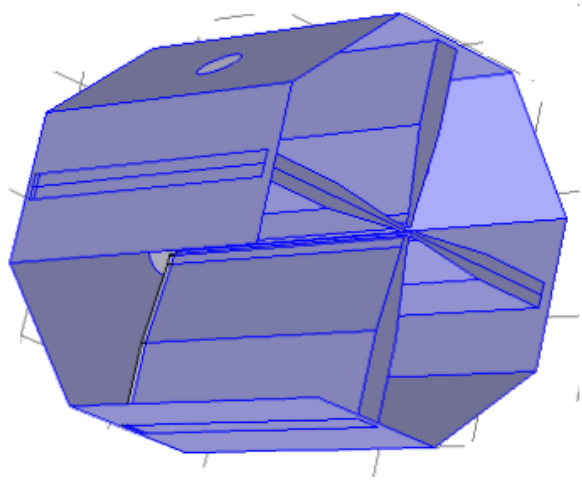

Figure 6.3: RFQ section with vanes.

The simulations were carried out using the Frequency Domain module of COMSOL MULTIPHYSICS. The designs of the coupler and the pickup are based on already existing models, to obtain a good value of the transmission. The pickup is the cylindrical shape shown in the upper parts of the RFQ in Figure 6.1.

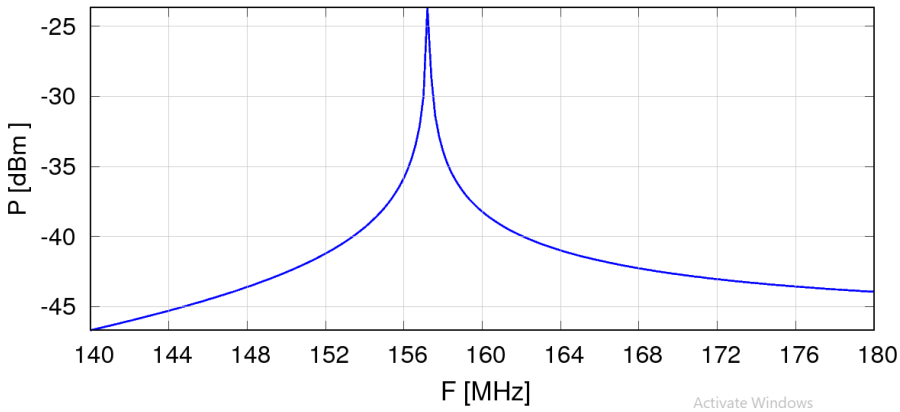

Figure 6.4: Frequency simulation for the RFQ section with vanes.

The result of the simulation of the empty section is presented in Figure 6.2. As already mentioned above, the resonance frequency predicted for this structure is 483 MHz.

The electromagnetic model of the RFQ section with vanes is shown in Figure 6.3 The resonant frequency obtained is 157 MHz, as shown in Figure 6.4.

6.1.2 Mechanical design and fabrication

The mechanical drawings of the RFQ prototype were elaborated from the geometry used in the electromagnetic model of the simulation. The main set of drawings are included below, in Figures 6.5-. The final prototype is shown in Figure 6.9.

Figure 6.5 shows the drawing of two octagonal end-cups. The flange drawings with a radius of 304.88 mm, 16 screws with a diameter of 10 mm and a 92 mm separation between them. The flange is 20 mm thick. There is a hole in the center with a diameter of 70 mm.

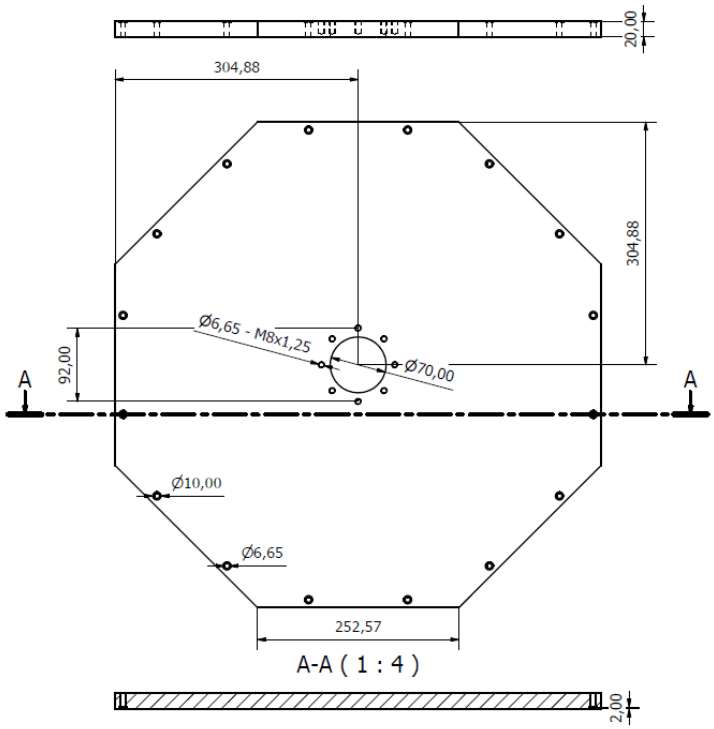

Figure 6.5: Drawing of two octagonal end-cups. The circular aperture is foreseen to allow the passage of a bead-Positioning System for electric field measurements.

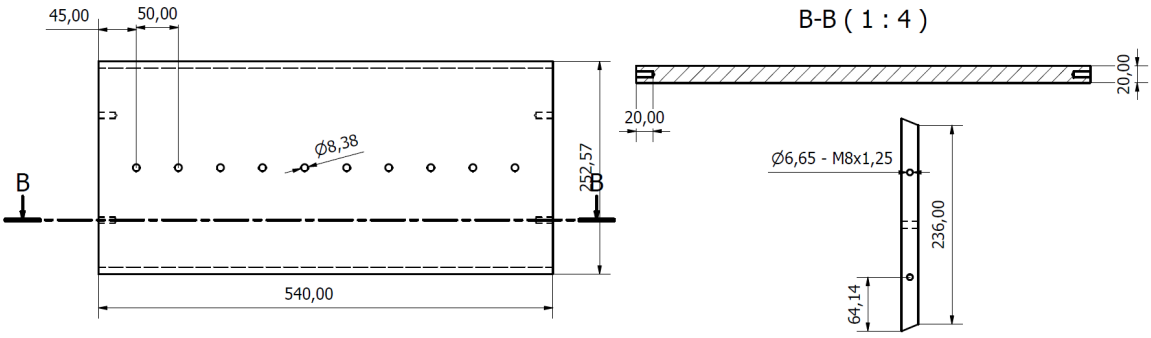

Figure 6.6: Drawing of a set of 4 rectangular walls. Each vane is fixed using 10 x M8 bolts

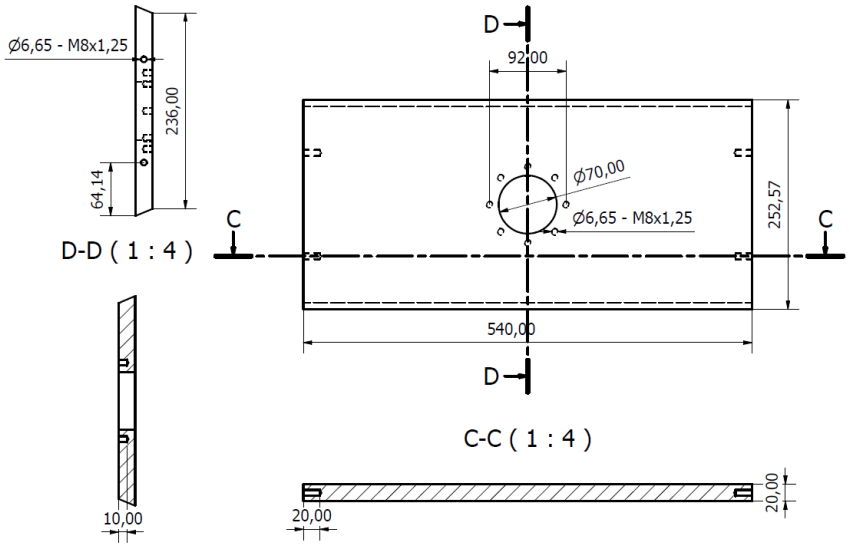

Figure 6.7: Set of 4 rectangular walls, where the circular aperture is foreseen to hold either the pickup, coupler, vacuum pump or the RF tuner.

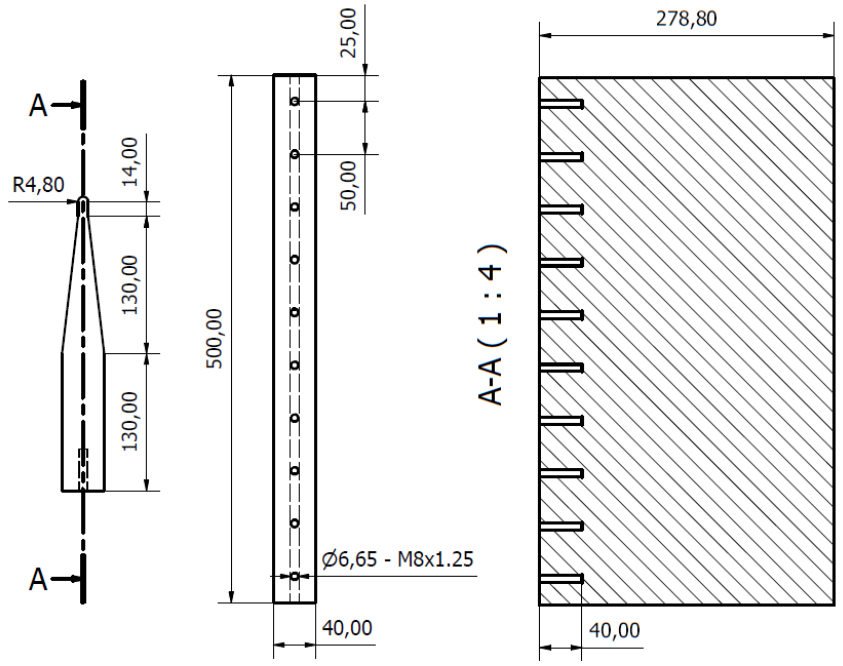

Figure 6.8: Drawing of the set of four RFQ vanes.

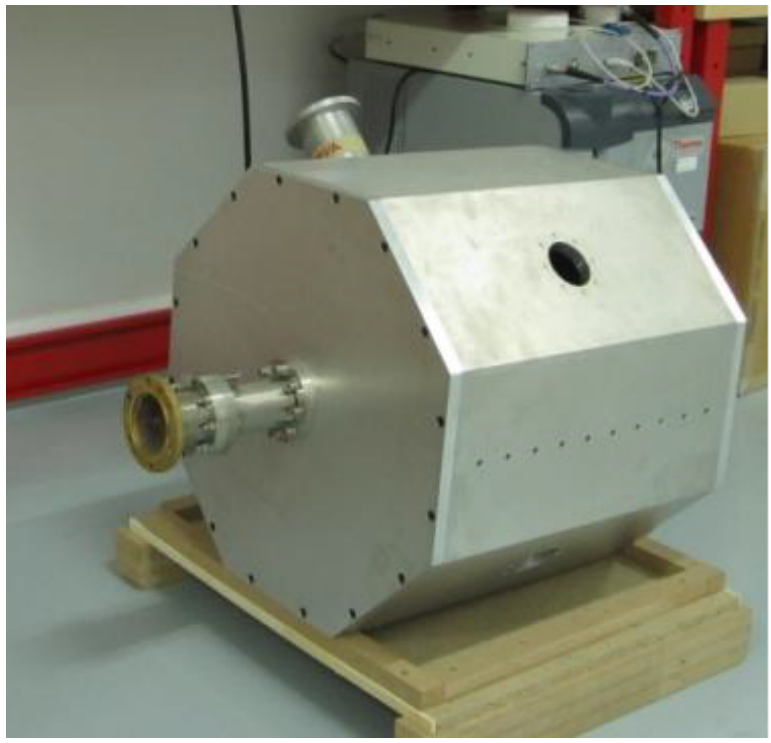

Figure 6.9: Picture of the final prototype of the RFQ fabricated in aluminum.

6.1.3 RFQ test.

Once the model in aluminum for one RFQ section was built, the RFQ section was tested in the RF Laboratory of the University of Huelva. The experimental setup is shown in Figure 6.10. The frequency response of the cavity was performed with an Agilent N90000A CXA spectrum analyzer.

The first measurement was carried out using the empty octagonal cavity. The transmission curve P (in dBm) as a function of the frequency is depicted in Figure 6.12, which shows a narrow resonance at 485 MHz. This result should be compared with the 483 MHz predicted by the simulations using COMSOL MULTIPHYSICS.[67]

The second measurement was carried out with the full RFQ prototype, and the result is shown in Figure 6.12. In this case, the transmission curve P (in dBm) shows a large maximum (P ~ -20 dBm) at 156.3 MHz, but also a small component (P ~ -24 dBm) at 158.2 MHz. However, the simulation predicts only the expected TE_{211} mode resonating at 157 MHz.

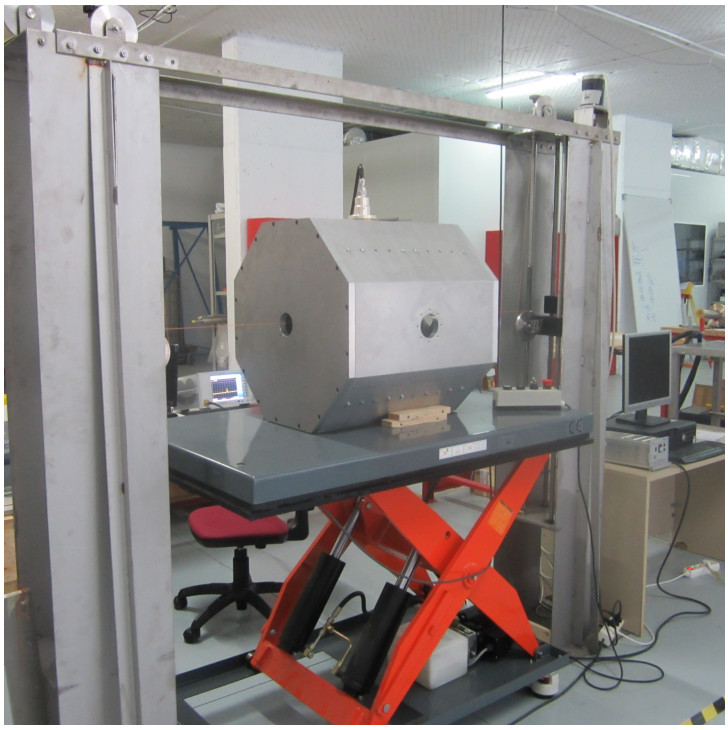

Figure 6.10: Experimental set up used for measuring the RF response of the aluminum prototype.

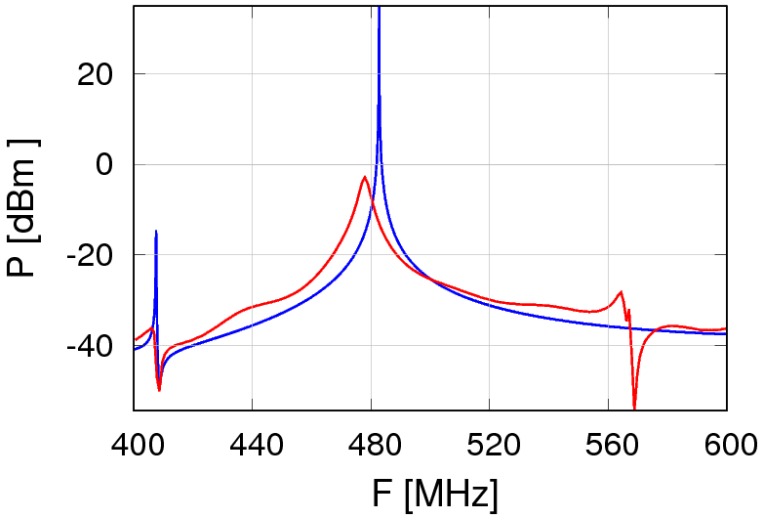

Figure 6.11: Experimental (red) and simulated (blue) RFQ frequency frequency response for the RFQ model without vanes.

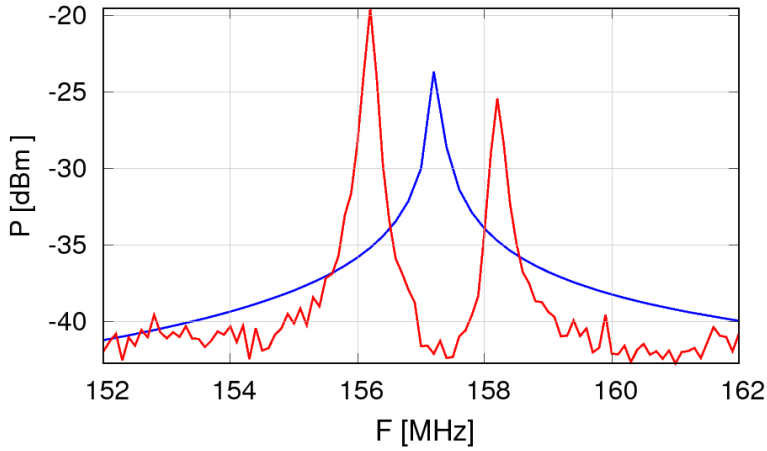

Figure 6.12: Experimental (red) and simulated (blue) RFQ frequency mode with vanes.

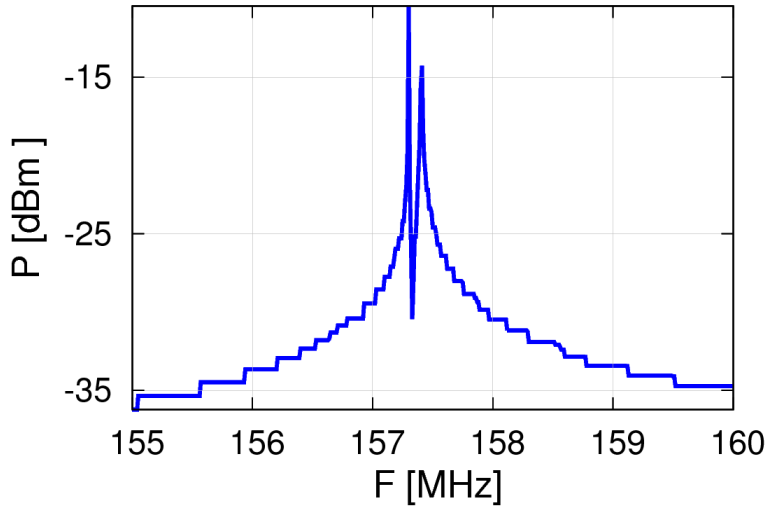

Figure 6.13: Simulated RFQ frequency response with vanes (zoom of Figure 6.4).

Although a tuners system can in principle solve this frequency shift of 2 MHz, the appearance of the second mode should be investigated, as it should be related to errors in the construction process.

In order to understand this effect, we check the first simulation and we found that there are two peaks very close, as shown in Figure 6.13. In view of the results, it can be concluded that the double pick is the result of the quadrupole and dipoles modes.

6.2 Cooper Prototype

Once the electromagnetic model and the software was tested with the aluminum model, a copper prototype was designed, built and tested.

6.2.1 Electromagnetic model and simulations

The design study carried out for the LINCE RFQ have delivered a resonant structure of 5 m length and octagonal cross section. In this case, the RFQ with vanes, windows and the proper modulation, should resonate in at 72.25 MHz. Small deviations from this value could be corrected by using dedicated RF tuners. In order to build this complex apparatus, the full mechanical system was divided in 5 sections of approximately equal length $\sim$ 1000 mm. The prototype foreseen in this work is the first half of the first acceleration section, which includes the full input matcher and the gentle buncher, altogether with a total length of 520 mm.

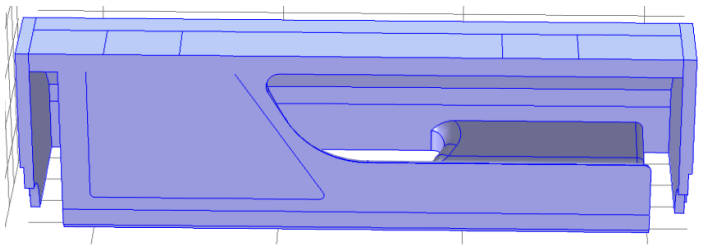

Figure 6.14: Electromagnetic model of the copper prototype of the RFQ.

In a similar manner as before, the simulation of the prototype was carried out using the COMSOL Frequency Domain module, the frequency range adjusted as described in chapter 5. The electromagnetic model is shown in Figure 6.14.

The results obtained from the simulation for the RFQ section in copper are presented in Figure 6.15.The resonance mode obtained for this structure is 72.05 MHz.

6.2.2 Mechanical design and fabrication

The design and fabrication process was carried out in collaboration with the Spanish companies FAYSOL S.A.L.,[105] MECA-TECA,[106] Added Value Solutions (AVS)[107] and the Laboratori Nazionali di Legnaro (LNL).[99] The

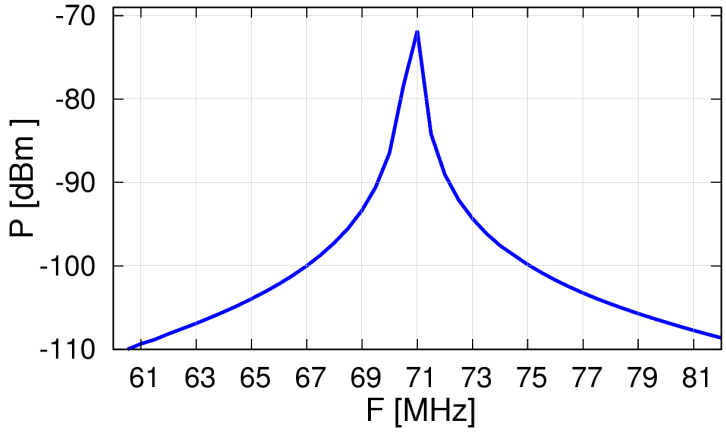

Figure 6.15: Simulation of the frequency response of the copper prototype.

main parts of the system are the four rectangular walls, the four vanes, two rings and two end-caps, as depicted in Figure 6.16.

The model was fabricated in high-purity oxygen-free copper material grade Cu-HCP CW021A EN13599. The standard material used to build resonators is the more expensive Cu-OFE C10100 grade (CERN) and this project gave the opportunity to test a more cost-effective option.

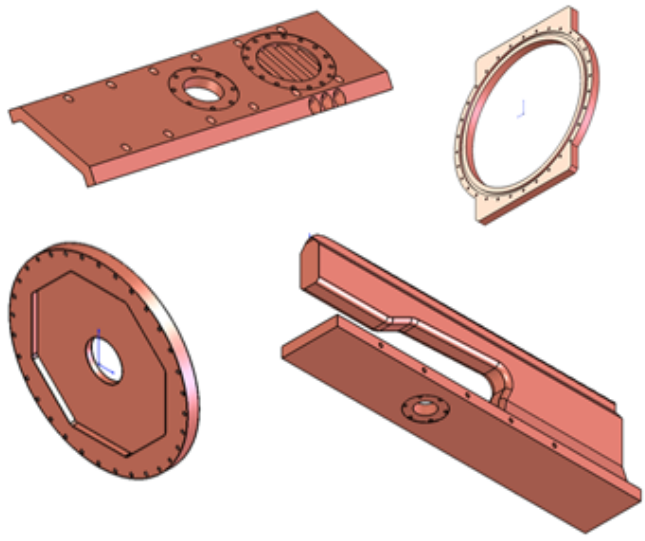

Figure 6.16: Parts of the copper prototype of the RFQ.

The fabrication process can be divided in the following eight general stages:

1. Annealing tests of the material. Preparation of probes for stress-strain tests to ensure that the copper quality is appropriate for building the cavity.
2. Preliminary machining of vanes, quadrants, flanges, drilling water cooling channels. Chemical cleaning. Metrology inspection-1.
3. Performing first annealing, including high-temperature furnace brazing of water channel plugs.
4. Final, high-precision machining of all parts including vane tip modulation. Metrology inspection-2.
5. First mechanical assembly and RFQ test. Metrology inspection-3.
6. Brazing process of the RFQ, fully assembled. Metrology inspection-4.
7. Post-brazing machining to match the end-caps.
8. Final metrology inspection and RFQ test.

In this work we accomplish all steps from 1-5. After the high-precision machining (stage 4), the RFQ parts were sent to the University of Huelva. The metrology inspection was performed using the CNC test-bench and a high-precision (10 micron) squareness comparator. The measurements included the geometrical dimensions of all pieces, including the vane tip modulation. A picture of the test-bench is shown in Figure 6.20.

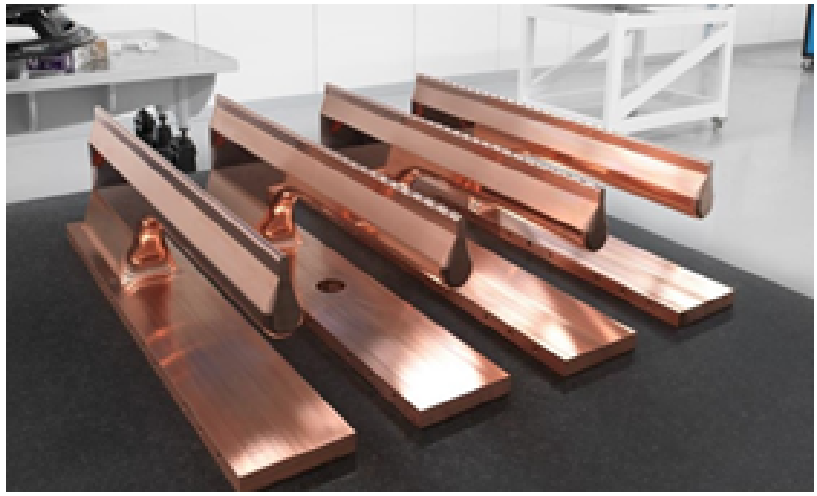

Figure 6.17: Copper vanes at stage 4 of the fabrication process.

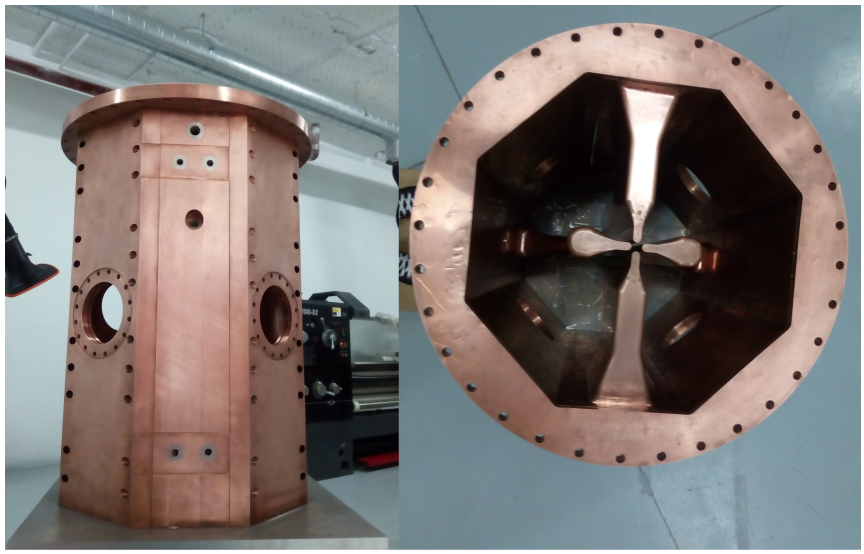

Figure 6.18: Longitudinal (left) and transversal (right) views of the copper prototype of the RFQ section.

Figure 6.19: Inside view of a copper prototype of the RFQ section.

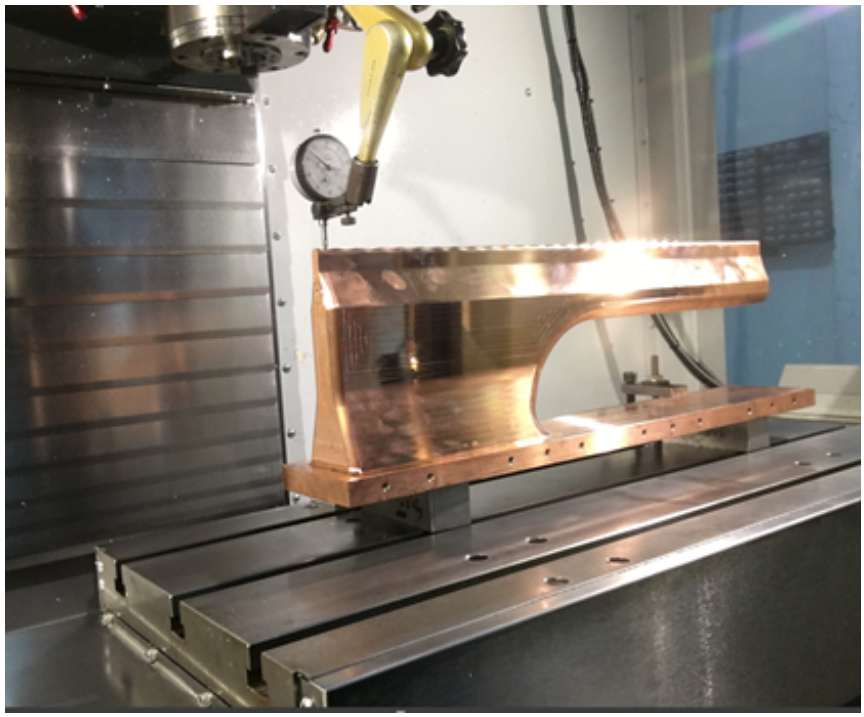

Figure 6.20: Metrology test of RFQ parts at the RF lab of the University of Huelva.

The geometry of the copper prototype was determined by the specific requirements of the LINCE project. The electromagnetic and technical viability studies were conducted by the University of Huelva (results shown in Appendix A of this document). The fabrication drawings were produced by AVS, which also contributed to the machining and production process with FAYSOL S.A.L. and MECA-TECA.

6.2.3 RF test

The frequency response of the cavity was performed with an Agilent N90000A CXA spectrum analyzer. The experimental setup is shown in Figure 6.21.

The transmission curve P (in dBm) as a function of the frequency is depicted in Figure 6.22, which shows a narrow resonance at 73 MHz in close agreement with the result of the simulation. The difference between the spectrum and simulations is due to the fabrication process. The tuners system can solve a frequency shift of 2 MHz, but in this case the RFQ should be re-machined, as the resonance is higher that the design frequency goal of 72 MHz.

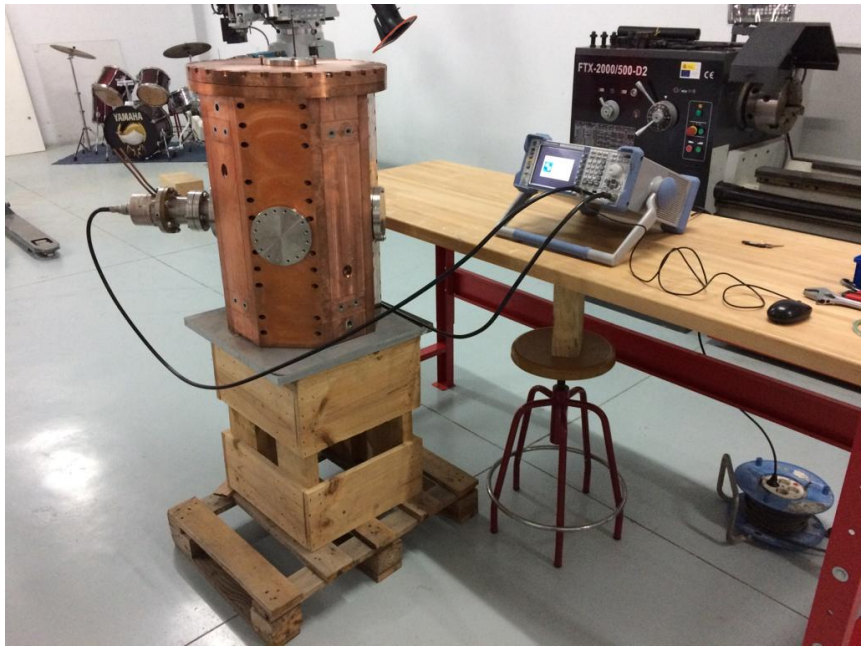

Figure 6.21: Set up for RF test of the copper prototype.

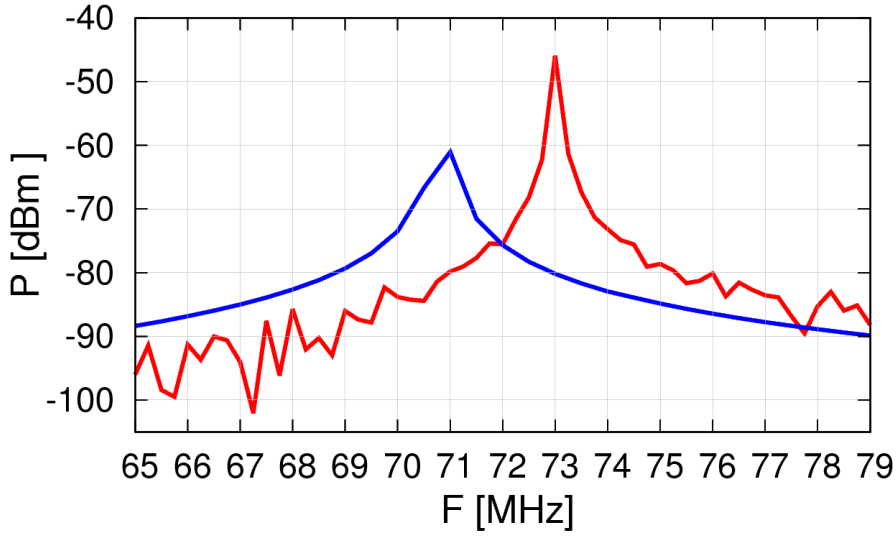

Figure 6.22: Experimental (red) and simulated (blue) frequency response of the copper prototype.

7

Summary and Conclusions

In this chapter I present a summary of the research work carried out, together with the main conclusions that can be drawn from the simulations and the data analysis.

The LINCE project was born from a previous project, the Linac Research Facility (LRF), for installing a low-energy heavy-ion facility at the University of Huelva. LINCE is a initiative for the installation of a new high-intensity, light- and heavy-Ion accelerator in Europe: the LINCE facility. It could gather the European nuclear physics community which needs a dedicated facility of stable ion beams at energies around 10 MeV/u.

The construction of this type of infrastructure was recommended by Committee for European collaboration in Nuclear Sciences (NuPECC), and the ECOS working group considered it as one of the most important priorities. This facility would be extremely useful for experiments requiring long beam times, often limited by beam and intensity availability of present facilities. Moreover, high-intensity ion accelerators are not only used in basic research, but also in industrial applications and societal benefits.

The research of this thesis have been focused on the beam dynamics of the LINCE superconducting linac and in the design of the RFQ system. To achieve this objective different design tools have been used: INVENTOR, COMSOL MULTIPHYSICS, TRACK and DESRFQ. The design study includes the beam dynamics, geometric, electromagnetic, and technical tests of the RFQ cavity. On the experimental side, the metrology and radiofrequency tests were carry-out at the RF laboratory of the University of Huelva.

Beam dynamics simulations have been performed using TRACK and DESRFQ codes. The whole study for the beam transport along LINCE comprises all elements in the beam line from the ion source until to the last cryostat at the exit, considering the target values of the beam energy, emittance and transmission. The beam dynamics used realistic field maps obtained from real measurements and electromagnetic simulations.

The sinusoidal modulation of the RFQ was obtained using DERSFQ and verified by simulations with TRACK. A procedure was developed to include the modulation into COMSOL MULTIPHYSICS. For the nearest future, still remains to be studied the trapezoidal design of the modulation and its subsequent implementation in the simulations and prototyping.

Simulations to study heat transfer and structural deformations were conducted using a 3D model of the RFQ using COMSOL. A method was developed, to carried out a complete response study of the cavity by coupling electromagnetic, thermal and mechanical effects in COMSOL. This method consisted of the following steps. The first step was the coupling of the electromagnetic simulation, in particular the power loss, with the thermal study. The following step was connecting the temperature simulations, the cooling using liquids, and the mechanical analysis. Finally, in the last step the field of displacements were connected with the meshing and the electromagnetic study, allowing to evaluate the total frequency shift of the cavity. The main goal was to obtain a minimum frequency shift in the RFQ. More detailed simulations shall be carried out to optimize parameters and operational conditions.

Four adjustable moving tuners per cavity were used to tune the resonant frequency of the RFQ to 72.75 MHz. The dissipation of the heat due to the power losses was obtained by applying different inlet temperatures and velocities of the coolant. The final frequency shift is 384 kHz with a flux of 8 l/min, and a temperature inlet of 20 °C was set up for the minimum cooling requirements for continuous operation. We are still working to verify the accuracy of beam dynamics, RF simulations and the behavior of the longitudinal emittance.

As a result of this study, an aluminum model for a RFQ section was built between the University of Huelva and Spanish companies. Frequency measurements were carried out using a Network Analyzer in the laboratory of the University of Huelva. In a future study, the windows on the vanes will be cut, and the frequency results will be compared with simulations.

It is important to say that the design strategy developed in this work to design the RFQ was extended to the design of the other resonant cavities of LINCE, and even to other R&D projects such as the rods- RFQ described in Appendix B.

On the other hand, the other important result of this study is the copper model of the RFQ section, which was built between the University of Huelva, Spanish companies and the Laboratori Nazionali di Legnaro (LNL). Frequency measurements were carried out using a Network Analyser in the laboratory of the University of Huelva. In a future study, the cavity needs to be re-machined and re-tested with the goal to obtain the needed resonant frequency.

Finally, if the project gains enough momentum, the construction of LINCE will largely impulse the science and technology in Europe, and in Spain in particular. As the Chinese proverb says: “All things are difficult before they are easy.”, and this work has been a first step.

Resumen y conclusiones

En este capítulo se presenta un resumen de la investigación realizada, junto con las principales conclusiones que se pueden extraer de las simulaciones y el análisis de datos.

El proyecto LINCE surgió a partir de un proyecto anterior, Linac Research Facility (LRF), el cual tenia como objetivo instalar un acelerador de iones pesados de bajo consumo de energía en la Universidad de Huelva. LINCE es una iniciativa para la instalación de un nuevo acelerador de alta intensidad, para iones ligeros y pesados en Europa: la instalación de LINCE. Podría agrupar a la comunidad europea de física nuclear que necesita una instalación dedicada de haces de iones estables en energías alrededor de 10 MeV/u.

El Comité de colaboración europea en ciencias nucleares (NuPECC) recomendó la construcción de este tipo de infraestructura, y el grupo de trabajo ECOS lo consideró una de las prioridades más importantes. Esta instalación sería extremadamente útil para experimentos que requieren largos tiempos de haz, a menudo limitados por la disponibilidad de haz y de intensidad de las instalaciones actuales. Además, los aceleradores de iones de alta intensidad no solo se utilizan en investigación básica, sino también en aplicaciones industriales de beneficios sociales.

La investigación de esta tesis se ha centrado en la dinámica del haz del linac superconductor LINCE y en el diseño del sistema de RFQ. Para lograr este objetivo se han utilizado diferentes herramientas de diseño: INVENTOR, COMSOL MULTIPHYSICS, TRACK y DESRFQ. El estudio de diseño incluye las pruebas de dinámica de haz, los diseños geométrico, electromagnético y técnico de la cavidad de RFQ. En el aspecto experimental, las pruebas de metrología y radiofrecuencia se llevaron a cabo en el laboratorio de radiofrecuencia de la Universidad de Huelva.

Se han realizado simulaciones de dinámica de haz utilizando los códigos TRACK y DESRFQ. Todo el estudio para el haz de transporte a lo largo de LINCE comprende todos los elementos en la línea del haz desde la fuente de iones hasta el último criostato obtenido en la salida, considerando los valores objetivo de la energía, la emisión y la transmisión del haz. La dinámica del haz utilizó mapas de campo reales obtenidos de mediciones reales y simulaciones electromagnéticas.

La modulación sinusoidal para la RFQ se reaizó con DERSFQ y se verificó mediante simulaciones con TRACK. Se llevó a cabo un procedimiento para

incluir la modulación en COMSOL MULTIPHYSICS. Para trabajos posteriores, aún queda por estudiar el diseño trapezoidal de la modulación y su posterior implementación en las simulaciones y prototipos.

Las simulaciones para estudiar los procesos de transferencia de calor, CFD y mecánica estructural se realizaron utilizando un modelo 3D de la RFQ utilizando COMSOL. Se desarrolló un método para llevar a cabo un estudio completo de la cavidad mediante el acoplamiento de efectos electromagnéticos, térmicos y mecánicos en COMSOL. Este método consistió en el acoplamiento de la simulación electromagnética, en particular la pérdida de potencia, con el estudio térmico. El siguiente paso fue conectar las simulaciones de temperatura, el enfriamiento con líquidos y el análisis mecánico. Finalmente, con el mallado resultado de los desplazamientos se realizó un nuevo estudio electromagnético, lo que permitió evaluar el cambio de frecuencia total de la cavidad. El objetivo principal era obtener un cambio de frecuencia mínimo en la RFQ. Se realizarán simulaciones más detalladas para refinar la optimización de los parámetros y las condiciones operativas.

Se usaron cuatro sintonizadores móviles ajustables por cavidad para sintonizar la frecuencia de resonancia a 72.75 MHz y para ajustar la estructura de cobre. La disipación del calor debido a las pérdidas de potencia se obtuvo aplicando diferentes temperaturas de entrada y velocidades del refrigerante. El cambio de frecuencia final es 384 kHz con un flujo de 8 l/min, y se estableció una entrada de temperatura de 20 °C como requisitos mínimos de enfriamiento para la operación continua de la RFQ. Seguiremos trabajando para verificar la precisión de los estudios de dinámica de haz, las simulaciones de RF y el comportamiento de la emitancia longitudinal.

Como resultado de este estudio, se construyó un modelo de aluminio para una sección de la RFQ entre la Universidad de Huelva y empresas españolas. Las mediciones de frecuencia se realizaron con un analizador de red en el laboratorio de la Universidad de Huelva. En un estudio futuro, las ventanas de las paletas se cortarán y los resultados de frecuencia se compararán con las simulaciones.

Es importante decir que la estrategia de diseño desarrollada en este trabajo para diseñar la RFQ se extendió al diseño de las otras cavidades resonantes de LINCE, e incluso a otros proyectos de R&D, como la RFQ de barras descrita en el apéndice B.

Por otro lado, el otro resultado importante de este estudio es el modelo de cobre para una sección de la RFQ, que se construyó entre la Universidad de Huelva, las empresas españolas y el Laboratori Nazionali di Legnaro (LNL). Las mediciones de frecuencia se realizaron con un analizador de red en el laboratorio de la Universidad de Huelva. Como parte de los trabajos posteriores, la cavidad

debe volver a mecanizarse y medirse con el objetivo de obtener la frecuencia de resonancia necesaria.

Finalmente, si el proyecto gana suficiente impulso, la construcción de LINCE impulsará en gran medida la ciencia y la tecnología en Europa, y en España en particular. Como dice el proverbio chino: "Todas las cosas son difíciles antes de ser fáciles".

Bibliography

[1] European Collaboration on Stable ion beams - ECOS. http://www.ensarfp7.eu/what-is-ensar/projects/ecos, 2017. Online; accessed 22 July 2017.

[2] The Nuclear Physics European Collaboration Committee is an Expert Committee of the European Science Foundation - NuPECC. http://www.nupecc.org/, 2017. Online; accessed 15 July 2017.

[3] Martel, I. and Bontoiu, C. and Ordúz, A. K. and Acosta, L. and Barrios, E. and Carrasco, R. and Dueñas Diaz, J.A. and Gordo Yáñez, D. and Peregrín, A. and Pinto Gómez, A. R. and Prieto Thomas, J. A. and Ruiz Pomares, M. J. and Junquera, T. and Sanchez-Segovia, J. and Ostroumov, P.N. and Villari, A.C.C. and Harakeh, M.N. ECOS-LINCE : a high-intensity heavy-ion facility for nuclear structure and reactions. 2016 - DOI:10.5506/APhysPolB.47.607.

[4] Aseev, V. and et al. *TRACK: The New Beam Dynamics Code*, 2005.

[5] Kolomiets, A. A. and et al. *DESRFQ Code*, 2005 - ISBN:0-7803-8859-3.

[6] CERN. MAD-X Methodical Accelerator Design. http://mad.web.cern.ch/mad/, 2016. Online; accessed 13 December 2016.

[7] Comsol Multiphysics Version 4.4. http://www.comsol.com/products/multiphysics/, 2016. Online; accessed 13 December 2016.

[8] Autodesk. Inventor. https://www.autodesk.es/products/inventor/overview, 2016. Online; accessed 13 December 2016.

[9] European COllaboration on Stable ion beams - ECOS. http://www.nupecc.org/pub/ECOS-Final.pdf, 2017. Online; accessed 22 July 2017.

[10] Fusion For Energy. International Fusion Materials Irradiation Facility - IFMIF. http://www.ifmif.org/, 2018. Online; accessed 29 January 2018.

[11] An International Facility for Antiproton and Ion Research - FAIR. https://fair-center.eu/, 2017. Online; accessed 15 November 2017.

[12] SPIRAL2: "Systéme de Production d

Ions Radioactifs en Ligne. http://pro.ganil-spiral2.eu/spiral2, 2017. Online; accessed 15 Augustt 2017.

[13] SPES Project. https://web.infn.it/spes/, 2017. Online; accessed 06 September 2017.

[14] I. Martel, C. Bontoiu, A.C.C. Villari, and A. Garbayo. Development of a 14.5 18 GHz ECR Ion Source at University of Huelva. In *Proceedings, 5th International Particle Accelerator Conference (IPAC 2014): Dresden, Germany, June 15-20, 2014*, 2014 - DOI:10.18429/JACoW-IPAC2014-MOPRI013.

[15] J. Labrador, C. Bontoiu, J. Dueñas, I. Martel, M. Carrera, A. Garbayo, and A. C.C. Villari. Design of a Multi-harmonic Buncher for LINCE. In *Proceedings, 5th International Particle Accelerator Conference (IPAC 2014): Dresden, Germany, June 15-20, 2014*, 2014 - DOI:10.18429/JACoW-IPAC2014-MOPME059.

[16] I. Martel, L. Acosta, R. Carrasco, T. Dueñas, J.A. Junquera, A.K. Ordúz, A. Peregrin, J.A. Prieto-Thomas, J. Sanches-Segovia, P.N. Ostroumov, A.C.C. Villari, F. Azaiez, G. de Angelis, M. Lewitowicz, and A. Maj. ECOS-LINCE: A High Intensity Multi-ion Superconducting Linac for Nuclear Structure and Reactions. In *Proceedings, 5th International Particle Accelerator Conference (IPAC 2014): Dresden, Germany, June 15-20, 2014*, 2014 - DOI:10.18429/JACoW-IPAC2014-THPME036.

[17] V. I. Zagrebaev. Fusion-fission dynamics of super-heavy element formation and decay. *Nuclear Physics A*, 734:164–167, April 2004 - 10.1016/j.nuclphysa.2004.01.025.

[18] RIKEN. `http://www.riken.jp/en/about/`, 2018. Online; accessed 05 May 2018.

[19] Lawrence Berkeley National Laboratory (Berkeley Lab). `http://www.lbl.gov/about//`, 2017. Online; accessed 24 September 2017.

[20] Flerov Laboratory of Nuclear Reactions. `http://flerovlab.jinr.ru/flnr/index.html/`, 2018. Online; accessed 15 June 2018.

[21] GSI Helmholtzzentrum fr Schwerionenforschung. `https://www.gsi.de/start/aktuelles.htm`, 2017. Online; accessed 22 July 2017.

[22] S. Hofmann, D. Ackermann, S. Antalic, H. G. Burkhard, V. F. Comas, R. Dressler, Z. Gan, S. Heinz, J. A. Heredia, F. P. He?berger, J. Khuyagbaatar, B. Kindler, I. Kojouharov, P. Kuusiniemi, M. Leino, B. Lommel, R. Mann, G. Mnzenberg, K. Nishio, A. G. Popeko, S. Saro, H. J. Schtt, B. Streicher, B. Sulignano, J. Uusitalo, M. Venhart, A. V. Yeremin, R. Eichler, N. V. Aksenov, A. V. Belozerov, G. A. Bozhikov, V. I. Chepigin, S. N. Dmitriev, R. Dressler, H. W. Gler, V. A. Gorshkov, F. Haenssler, M. G. Itkis, A. Laube, V. Ya. Lebedev, O. N. Malyshev, Yu. Ts. Oganessian, O. V. Petrushkin, D. Piguet, A. G. Popeko, P. Rasmussen, S. V. Shishkin, A. V. Shutov, A. I. Svirikhin, E. E. Tereshatov, G. K. Vostokin, M. Wegrzecki, and A. V. Yeremin. Confirmation Of Super Heavy Element Production In 48Ca Induced Fusion Reactions A Handshake Of Physics And Chemistry For Element 112. *AIP Conference Proceedings*, 1012(1):69–73, 2008 - DOI:10.1063/1.2939362.

[23] D. Seweryniak, T.L. Khoo, I. Ahmad, F.G. Kondev, A. Robinson, S.K. Tandel, M. Asai, B.B. Back, M.P. Carpenter, P. Chowdhury, C.N. Davids, S. Eeckhaudt, J.P. Greene, P.T. Greenlees, S. Gros, K. Hauschild, A. Heinz, R.-D. Herzberg, R.V.F. Janssens, D.G. Jenkins, G.D. Jones, S. Ketelhut, T. Lauritsen, C.J. Lister, A. Lopez-Martens, P. Marley, E.A. McCutchan, T. Nakatsukasa, P. Papadakis, D. Peterson, J. Qian, D. Rostron, I. Stefanescu, U.S. Tandel, X.F. Wang, and S.F. Zhu. Bridging the nuclear structure gap between stable and super heavy nuclei. *Nuclear Physics A*, 834(1):357c – 361c, 2010 - DOI:10.1016/j.nuclphysa.2010.01.039. The 10th International Conference on Nucleus-Nucleus Collisions (NN2009).

[24] Raj K. Gupta, Aurel S?ndulescu, and Walter Greiner. Interaction barriers, nuclear shapes and the optimum choice of a compound nucleus reaction for producing superheavy elements. *Physics Letters B*, 67(3), 1977 - DOI:10.1016/0370-2693(77)90364-1.

[25] The Advanced GAmma-Tracking Array AGATA. `https://web-docs.gsi.de/~gsgweb/proj/agata_project.html`, 2017. Online; accessed 17 November 2017.

[26] Clark, R. M. and Fallon, P. and Görgen, A. and Cromaz, M. and Deleplanque, M. A. and Diamond, R. M. and Lane, G. J. and Lee, I. Y. and Macchiavelli, A. O. and Ramos, R. G. and Stephens, F. S. and Svensson, C. E. and Vetter, K. and Ward, D. and Carpenter, M. P. and Janssens, R. V. F. and Wadsworth, R. Very Extended Shapes in the $A \sim 110$ Region. *Phys. Rev. Lett.*, 87:202502, Oct 2001 - DOI:10.1103/PhysRevLett.87.202502.

[27] Schunck, N. and Dudek, J. and Herskind, B. Nuclear hyperdeformation and the Jacobi shape transition. *Phys. Rev. C*, 75:054304, May 2007 - DOI:10.1103/PhysRevC.75.054304.

[28] Abusara, H. and Afanasjev, A. V. Hyperdeformation in the Cd isotopes: A microscopic analysis. *Phys. Rev. C*, 79:024317, Feb 2009 - DOI:10.1103/PhysRevC.79.024317.

[29] M. Veselsky and G.A. Souliotis. Production of exotic nuclei in peripheral nucleusnucleus collisions below 10 A?MeV. *Nuclear Physics A*, 872(1):DOI:10.1016/j.nuclphysa.2011.09.016, 2011.

[30] G. A. Souliotis, M. Veselsky, S. Galanopoulos, M. Jandel, Z. Kohley, L. W. May, D. V. Shetty, B. C. Stein, and S. J. Yennello. Approaching neutron-rich nuclei toward the r-process path in peripheral heavy-ion collisions at 15 MeV/nucleon. *Phys. Rev.*, C84:064607, 2011 - DOI:10.1103/PhysRevC.84.064607.

[31] G Schonwasser and H Hubel and GB Hagemann and P Bednarczyk and G Benzoni and A Bracco and P Bringel and R Chapman and D Curien and J Domscheit and B Herskind and DR Jensen and S Leoni and Lo Bianco, G and WC Ma and A Maj and A Neusser and SW Odegard and CM Petrache and D Rossach and Hans Ryde and KH Spohr and AK Singh. One- and two-phonon wobbling excitations in triaxial Lu-165. *Physics Letters B*, 552(1-2):9–16, 2003 - 1653.

[32] R. R. Chasman. Very extended nuclear shapes near $A = 100$. *Phys. Rev. C*, 64:024311, Jul 2001 - DOI:10.1103/PhysRevC.64.024311.

[33] Fallon, P. Gamma-ray spectroscopy of nuclei with large deformations. *The European Physical Journal A - Hadrons and Nuclei*, 20(1):9–14, Apr 2003 - DOI:10.1140/epja/i2002-10312-5.

[34] Naz, Tabassum and Ahmad, Shakeb and Abusara, Hazem. Triple-shape Coexistence and Superdeformation in Pb Isotopes. *Acta Physica Polonica Series B*, 49:1653, 10 2018 - DOI:10.5506/APhysPolB.49.1653.

[35] N. Steer, A and G. Jenkins, D and Glover, R and S. Nara Singh, B and S. Pattabiraman, N and Wadsworth, Robert and Eeckhaudt, S and Grahn, Tuomas and T. Greenlees, P and Jones, P and Julin, R and Juutinen, S and Leino, M and Nyman, Markus and Pakarinen, Janne and Rahkila, P and Sar J and Scholey, C and Sorri, Juha and Blank, B. Recoil-beta tagging: A novel technique for studying proton-drip-line nuclei. *Nuclear Instruments and Methods in Physics Research Section A: Accelerators, Spectrometers, Detectors and Associated Equipment*, 565:630636, 09 2006 - DOI:10.1016/j.nima.2006.06.034.

[36] Oertzen, W. Dimers based on the $\alpha + \alpha$ potential and chain states of carbon isotopes. *European Physical Journal A - EUR PHYS J A*, 357:355–365, 05 1997 - DOI:10.1007/s002180050255.

[37] H. MESSEL and S.T. BUTLER, editor. *CHAPTER 2 - Nuclear Fission, Nuclear Fusion Geothermal Energy*. Pergamon International Library of Science, Technology, Engineering and Social Studies. Pergamon, 1975 - DOI:10.1016/B978-0-08-019817-0.50009-4.

[38] C Beck. Clusters in light stable and exotic nuclei. 09 2018 - DOI:10.13140/RG.2.2.27308.10889.

[39] Cerny, J. *Nuclear Spectroscopy and Reactions 40-B*. Number parte 2 in Pure and applied physics. Elsevier Science, 2012 - ISBN:9780323142885.

[40] Nunes, F and Lovell, A and Ross, A and Titus, L and J. Charity, R and Dickhoff, W and Mahzoon, Hossein and Sarich, J and Wild, Stefan. One-nucleon Transfer Reactions and the Optical Potential. 09 2015.

[41] Casten, R. and Casten, R.F. *Nuclear Structure from a Simple Perspective*. Oxford science publications. Oxford University Press, 2000 - ISBN:9780198507246.

[42] G Ademard, J.P. WIELECZKO, E Bonnet, Abdou Chbihi, and John Frankland. On the emission of heavy clusters from medium mass compound nucleus. *International Journal of Modern Physics E-nuclear Physics - IJMPE*, 20:1054–1057, 04 2011 - DOI:10.1142/S021830131101926X.

[43] Douglas Cline. Pairing correlations and two-nucleon transfer between heavy nuclei. *Nuclear Physics A*, 520:c493 – c507, 1990 - DOI:10.1016/0375-9474(90)91170-V. Nuclear Structure in the Nineties.

[44] Steadman, S G and Rhoades-Brown, M J. Sub-Barrier Fusion Reactions. *Annual Review of Nuclear and Particle Science*, 36(1):649–681, 1986 - DOI:10.1146/annurev.ns.36.120186.003245.

[45] Stock, R. *Encyclopedia of Nuclear Physics and its Applications*. Encyclopedia of Applied Physics. Wiley, 2013 - ISBN:9783527649266.

[46] Brune, Carl R. and Davids, Barry. Radiative Capture Reactions in Astrophysics. *Annual Review of Nuclear and Particle Science*, 65(1):87–112, 2015 - DOI:10.1146/annurev-nucl-102014-022027.

[47] Shapiro, M.M. and Silberberg, R. and Wefel, J.P. *Particle Astrophysics and Cosmology*. Nato Science Series C:. Springer Netherlands, 2012 - ISBN:9789401117074.

[48] Pascal Garin and Masayoshi Sugimoto. Status of IFMIF Design and RD. *Fusion Engineering and Design*, 83(7):971–975, 2008 - DOI:10.1016/j.fusengdes.2008.05.028. Proceedings of the Eight International Symposium of Fusion Nuclear Technology.

[49] Ciattaglia, Sergio and Federici, Gianfranco and Barucca, Luciana and Lampasi, Alessandro and Minucci, Simone and Moscato, Ivo. The European DEMO fusion reactor: Design status and challenges from balance of plant point of view. pages 1–6, 06 2017 - DOI:10.1109/EEEIC.2017.7977853.

[50] P.-H Rebut. ITER: The First Experimental Fusion Reactor. *Fusion Engineering and Design*, 27:3–16, 1995 - DOI:10.1016/0920-3796(95)90113-2. Proceedings of the Third International Symposium on Fusion Nuclear Technology.

[51] John C. Slater. The Effects of Radiation on Materials. 22(3):237–256, March 1951 - DOI:10.1063/1.1699937.

[52] S. Was, Gary. *Simulation of Neutron Irradiation Effects with Ions*. 01 2007 - DOI:10.1007/978-3-540-49472-$0_1$1.

[53] Sophie Duzellier. Radiation effects on electronic devices in space. *Aerospace Science and Technology*, 9(1):93–99, 2005 - DOI:10.1016/j.ast.2004.08.006.

[54] RADiation Effects Facility - RADEF. `https://www.jyu.fi/science/en/physics/research/infrastructures/accelerator-laboratory/radiation-effects-facility`, 2018. Online; accessed 10 May 2018.

[55] Mettler, Fred A. and Bhargavan, Mythreyi and Faulkner, Keith and Gilley, Debbie B. and Gray, Joel E. and Ibbott, Geoffrey S. and Lipoti, Jill A. and Mahesh, Mahadevappa and McCrohan, John L. and Stabin, Michael G. and Thomadsen, Bruce R. and Yoshizumi, Terry T. Radiologic and Nuclear Medicine Studies in the United States and Worldwide: Frequency, Radiation Dose, and Comparison with Other Radiation Sources19502007. *Radiology*, 253(2):520–531, note =PMID: 19789227, 2009 - DOI:10.1148/radiol.2532082010.

[56] Future of low specific activity molybdenum-99/technetium-99m generator. *Current Radiopharmaceuticals*, 5(4), 2012.

[57] Valeriia N. Starovoitova, Lali Tchelidze, and Douglas P. Wells. Production of Medical Radioisotopes with Linear Accelerators. *Applied Radiation and Isotopes*, 85:39 – 44, 2014 - DOI:10.1016/j.apradiso.2013.11.122.

[58] Devlin, P.M. *Brachytherapy: Applications and Techniques*. Lippincott Williams & Wilkins, 2007 - ISBN:9780781762779.

[59] Mingqian, T. and Aiguo, W. *Nanomaterials For Tumor Targeting Theranostics: A Proactive Clinical Perspective*. World Scientific Publishing Company, 2016 - ISBN:9789814635431.

[60] Edlinger, C. and Hôpitaux de Paris. Comité d'Evaluation et de Diffusion des Innovations Technologiques. *Protontherapie*. Assistance Publique, Hôpiteaux de Paris, 2002.

[61] Ebrahimi Warkiani, Majid and Bhagat, Ali Asgar and Khoo, Bee Luan and Han, Jongyoon and Lim, C.T. and Qing Gong, Hai and Fane, A.G. Isoporous micro/Nanoengineered membranes. *ACS nano*, 7:1882–1904, 02 2013 - DOI:10.1021/nn305616k.

[62] Fleischer, R. L. and Price, P. B. and Walker, R. M. and Hubbard, E. L. Track Registration in Various Solid-State Nuclear Track Detectors. *Phys. Rev.*, 133:A1443–A1449, Mar 1964 - DOI:10.1103/PhysRev.133.A1443.

[63] Flerov, G. N. and Apel', P. Yu. and Didyk, A. Yu. and Kuznetsov, V. I. and Oganesyan, R. Ts. Use of Heavy-Ion Accelerators to Produce Nuclear Membranes. *Soviet Atomic Energy*, 67(4):763–770, Oct 1989 - DOI:10.1007/BF01123341.

[64] D. Gordo-Yáñez, R. Carrasco, I. Martel, A. Pinto Gómez, and C. Gómez. High-performance Accelerating Cryomodule for the LINCE Project. In *Proceedings, 5th International Particle Accelerator Conference (IPAC 2014): Dresden, Germany, June 15-20, 2014*, 2014 - DOI:10.18429/JACoW-IPAC2014-THPME035.

[65] Acosta, L. and Bontoiu, C. and Martel, I. and Pinto Gómez, A. and Villari, A.C.C and Lucas, J. Beam Transfer Studies for LINCE Experimental Areas. In *Proceedings, 5th International Particle Accelerator Conference (IPAC 2014): Dresden, Germany, June 15-20, 2014*, 2014 - DOI:10.18429/JACoW-IPAC2014-THPME032.

[66] C. Bontoiu, I. Martel, A. Falone, and C. Gómez. Particle Tracking Studies for the LINCE SC Linac. In *Proceedings, 5th International Particle Accelerator Conference (IPAC 2014): Dresden, Germany, June 15-20, 2014*, 2014 - DOI:10.18429/JACoW-IPAC2014-THPME033.

[67] Ordúz, A. K. and Bontoiu, C and Dueñas, J.A. and Martel, I. and Garbayo, A. Proposal for a 72.75 MHz RFQ for the Lince Accelerator Complex. In *IPAC 2015: Proceedings of the 6th International Particle Accelerator Conference*. Joint Accelerator Conferences Website (JACoW), 7 2015 - DOI:10.18429/JACoW-IPAC2015-THPF077.

[68] A. K. Ordúz, C. Bontoiu, J.A. Dueñas, I. Martel, and A. Garbayo. Thermal and Structural Analysis of the 72.75 MHz Lince RFQ. In *IPAC 2015: Proceedings of the 6th International Particle Accelerator Conference*. Joint Accelerator Conferences Website (JACoW), 7 2015 - DOI:10.18429/JACoW-IPAC2015-THPF076.

[69] I. Martel, C. Bontoiu, J.A. Dueñas, D. Gordo-Yáñez, A.K. Ordúz, and J. Sanchez-Segovia. A New RF Laboratory for Developing Accelerator Cavities at the University of Huelva. In *Proceedings, 6th International Particle Accelerator Conference (IPAC 2015): Richmond, Virginia, USA, May 3-8, 2015*, 2015 - DOI: 10.18429/JACoW-IPAC2015-WEPMN052.

[70] A. K. Ordúz, C. Bontoiu, I. Martel, Alberto Garbayo, and A. C. C. Villari. Studies for a 72.75 MHz Four Vanes CW-RFQ for ECOS-LINCE Project. pages 215–216, 2016 - DOI:10.5506/APhysPolB.47.619.

[71] A. K. Ordúz, C. Bontoiu, J. Dueñas, I. Martel, A. Garbayo, A. C. C. Villari, and P. N. Ostroumov. A Proposal for a 72.75 MHz RFQ for ECOS-LINCE Project. *Springer Proc. Phys.*, 182:215–216, 2016 - DOI:10.1007/978-3-319-21191-6$_2$0.

[72] Argonne Tandem Linac Accelerator System - ATLAS. `https://www.phy.anl.gov/atlas//`, 2017. Online; accessed 15 July 2017.

[73] Orduz, A. K. and C. Bontoiu and I. Martel and A. Garbayo and Villari, A. C C and Ostroumov, P. N. Development of a 72.75 MHz RFQ for the LINCE Accelerator Complex. In *IPAC 2014: Proceedings of the 5th International Particle Accelerator Conference*, pages 3304–3307. Joint Accelerator Conferences Website (JACoW), 7 2014 - DOI:10.18429/JACoW-IPAC2014-THPME037.

[74] Acceleratore Lineare Per Ioni - ALPI. `https://www.lnl.infn.it/index.php/en/accelerators-3/alpi`, 2017. Online; accessed 12 September 2017.

[75] Facility for Rare Isotope Beams - FRIB. `http:///www.a-v-s.es/`, 2017. Online; accessed 12 July 2017.

[76] Wangler, T.P. *RF Linear Accelerators*. Wiley Series in Beam Physics and Accelerator Technology. Wiley, 1998 - ISBN:9780471168140.

[77] A. W. Chao and M. Tigner, editors. *Handbook of Accelerator Physics and Engineering*. 1999 - ISBN:9789810235000.

[78] Arun Saini, Shekhar Mishra, Kirti Ranjan, Nikolay Solyak, and Vyacheslav Yakovlev. Designing of 9 Cell Reduced Beta Elliptical Cavity for High Intensity Proton Linac. *Conf. Proc.*, C100523:WEPEC009, 2010.

[79] P. Forck. *Lecture Notes on Beam Instrumentation and Diagnostics*. CreateSpace Independent Publishing Platform, 2015 - ISBN:9781506171487.

[80] Fritz Caspers. RF Engineering Basic Concepts: S-parameters. 01 2012 - arXiv:1201.2346v1.

[81] Wiedemann, Helmut. *Particle Accelerators Physics*. Springer-Verlag Berlin Heidelberg, 2007 - ISBN:978-3-540-49045-6.

[82] Kapchinskii, I. M. and Teplyakov, V. A. A Linear Ion Accelerator with Spatially Uniform Hard Focusing. *Prib. Tekh. Eksp.*, 1970(2):SLAC–TRANS–0099, 1970.

[83] Ostroumov, P.N. and Kolomiets, A.A. and Kashinky, D.A. and Minaev, S.A. and Peshinn, V.I. and Tretyakova, T.E. and Yaramishev, S.G. Design of 57.5 MHz CW RFQ for Medium Energy Heavy Ion Superconducting Linac. *Phisical Review Special Topics*, 5:060101–9, 2002 - DOI: 10.1103/PhysRevSTAB.5.060101.

[84] Schutt, Maximilian and Ratzinger, Ulrich and Zhang, Chuan. Development of a 325 MHz Ladder-RFQ of the 4-Rod-Type. In *Proceedings, 7th International Particle Accelerator Conference (IPAC 2016): Busan, Korea, May 8-13, 2016*, 2016 - DOI:10.18429/JACoW-IPAC2016-MOPOY024.

[85] Ferdinand, R and Congretel, G. and Curtoni, A. and Delferri, O. and France, A. and Leboeuf, D. and Thinel, J. and Toussaint, Jc. and Di Giacomo, M. SPIRAL2 RFQ Design. 07 2004 - http://accelconf.web.cern.ch/AccelConf/e04/PAPERS/WEPLT076.PDF.

[86] J. Drees and W. Paul. Beschleunigung von Elektronen in einem Plasmabetatron. *Zeitschrift für Physik*, 180(4):340–361, Aug 1964 - DOI:10.1007/BF01380519.

[87] G. Savard. Ion trap technology at accelerator facilities", journal = "Nuclear Instruments and Methods in Physics Research Section B: Beam Interactions with Materials and Atoms. 126(1):361 – 369, 1997 - DOI:10.1016/S0168-583X(97)01030-6. International Conference on Electromagnetic Isotope Separators and Techniques Related to Their Applications.

[88] Mustapha, B. and Kolomiets, A. A. and Ostroumov, P. N. Full three-dimensional Approach to the Design and Simulation of a Radio-frequency Quadrupole. *Phys. Rev. ST Accel. Beams*, 16:120101, Dec 2013 - DOI:10.1103/PhysRevSTAB.16.120101.

[89] Arnaudon, L. and Baudrenghien, P. and Baylac, M. and Bellodi, Giulia. and Body, Y. and Borburgh, Jan and Bourquin, Pierre. and Broere, J. and Brunner, Othmar. and Bruno, Luca. and Carli, C. and Caspers, Fritz. and M Cousineau, S. and Cuvet, Y. and Martins, Carlos. and Dobers, T. and Fowler, T. and Garoby, Roland. and Gerigk, Frank. and Zickler, T. Linac4 Technical Design Report. 01 2006 - CERN-AB-2006-084, 141.

[90] MD. Leitner, C. Benatti, S. W. Krause, J. Ottarson, D. Morris, S. Nash, G. Perdikakis, M. Portillo, R. J. Rencsok, T. Ropponen, L. Tobos, N. Usher, D. Wang, F. Marti, E. Tanke, X. Wu, Q. Zhao, O. K. Kester, A. Schempp, J. Schmidt, H. Zimmermann, and J. Haeuser. Commissioning Results of the RIA RFQ at MSU. In *Proceedings of 2011 Particle Accelerator Conference: New York, NY, USA, Mach 28- April 18, 2011*, page WEP226, 2011.

[91] Van der Geer, S. and de Loos, M. General Particle Tracer. User manual Version 2.83. `http://www.pulsar.nl/gpt`, 2016. Online; accessed 15 February 2017.

[92] Plastun, A. S. and Ostroumov, P. N. Practical Design Approach for Trapezoidal Modulation of a Radio-Frequency Quadrupole. *Physical Review Accelerators and Beams*, 21(3), March 2018 - DOI:10.1103/PhysRevAccelBeams.21.030102.

[93] JAVA SE. `http://www.oracle.com/technetwork/java/javase/downloads/index.html`, 2017. Online; accessed 17 September 2017.

[94] Martel, I. and Bontoiu, C. and Dueñas, J. and Gordo-Yáñez, D. and Ordúz, A. K. and Sanchez-Segovia, J. A New RF Laboratory for Developing Accelerator Cavities at the University of Huelva. In *Proceedings, 6th International Particle Accelerator Conference (IPAC 2015): Richmond, Virginia, USA, May 3-8, 2015*, page , 2015 - DOI:10.18429/JACoW-IPAC2015-WEPMN052.

[95] Argonne National Laboratoy - ANL. `http://www.anl.gov/`, 2017. Online; accessed 07 August July 2017.

[96] Kelly, M.P. and Conway, Z.A. and Gerbick, S.M. and Kedzie, M. and Reid, T.C. and Murphy, R.C. and Ostroumov, P.N. Superconducting 72 MHz, β=0.077 QUARTER-WAVE Cavity for ATLAS. In *Particle Accelerator Conference*, pages 892–894. Joint Accelerator Conferences Website (JACoW), 3 2011.

[97] Peter Ostroumov, Zachary Conway, Brahim Mustapha, and Alexander Plastun. Design and Beam Dynamics Studies of a Multi-Ion Linac Injector for the JLEIC Ion Complex. In *Proceedings, 57th ICFA Advanced Beam Dynamics Workshop on High-Intensity and High-Brightness Hadron Beams (HB2016): Malm, Sweden, July 3-8, 2016*, 2016 - Y010.18429/JACoW-HB2016-THPM51.

[98] Peter Ostroumov, Zachary Conway, Brahim Mustapha, and Alexander Plastun. Design and Beam Dynamics Studies of a Multi-Ion Linac Injector for the JLEIC Ion Complex. In *Proceedings, 57th ICFA Advanced Beam Dynamics Workshop on High-Intensity and High-Brightness Hadron Beams (HB2016): Malm, Sweden, July 3-8, 2016*, page , 2016 - DOI:10.18429/JACoW-HB2016-THPM5Y01.

[99] Laboratori Nationali di Legnaro. `http://www.lnl.infn.it/index.php/en/`, 2017. Online; accessed 25 June 2017.

[100] P.N. Ostroumov, A. Barcikowski, Z. Conway, S. Gerbick, M. Kedzie, M.P. Kelly, S. Kim, S. Kutsaev, R. Murphy, B. Mustapha, R. Pardo, D. Paskvan, T. Rei, S. Sharamentov, and G. Zinkann. Upgrade of Argonnes CW SC Heavy Ion Accelerator. In *Proceedings of PAC2013*, pages 737–739. Joint Accelerator Conferences Website (JACoW), 9 2013 - ISBN:978-3-95450-138-0.

[101] N. Saito, K.nand Bultman, E. Burkhardt, F. Casagrande, S. Chandrasekaran, S. Chouhan, C. Compton, J. Crisp, K. Elliott, A. Facco, A. Fox, P. Gibson, M. Johnson, G. Kiupel, B. Laxdal, M. Leitner, S. Lidia, D. Morris, I. Malloch, D. Millera, S. Miller, D. Norton, R. Oweiss, J. Ozelis, J. Popielarski, L. Popielarski, A. Rauch, T. Rose, R.and Russo, S. Shanab, M. Shuptar, S. Stark, N. Usher, G. Velianoff, D. Victory, J. Wei, G. Wu, X. Wu, T. X, Y. Xu, Y Yamazaki, Q. Zhao, and Zheng. W. Superconducting RF Development for FRIB at MSU. In *Proceedings of LINAC2014*, pages 790–794. Joint Accelerator Conferences Website (JACoW), 8 2014 - ISBN:978-3-95450-142-7.

[102] Ostroumov, P.N. and Mustapha, B. and Barcikowski, A. and Dickerson, C. and Kolomiets, A. A. and Kondrashev, S. A. and Luo, Y. and Paskvan, D. and Perry, A. and Schrage, D. and Sharamentov, S. I. and Sommer, R. and Toter, W. and Zinkann, G. Development and Beam Test of a Continuous Wave Radio Frequency Quadrupole Accelerator. *Phisical Review Special Topics*, 2012 - DOI:10.1103/PhysRevSTAB.15.110101.

[103] T. J. Schultheiss, J. W. Rathke, P. N. Ostroumov, and A. A. Kolomiets. RF, Thermal and Structural Analysis of the 57.5 MHz CW RFQ for the RIA Driver Linac. *Conference: 21st International Linear Accelerator Conference (LINAC 2002)*, 9 2002 - https://www.phy.anl.gov/accelerator$_rd/frib/publications/RFQ_LINAC02.pdf$.

[104] T. J. Schultheiss, J. W. Rathke, P. N. Ostroumov, A Barcikowski, and D. Schrage. RF Thermal and Structural Analysis of the 60.625 MHz RFQ for the ATLAS Upgrade. *Proceedings of 2011 Particle Accelerator Conference, New York, NY, USA*.

[105] Fabricación, Montaje y Mantenimiento Industrial - Faysol S.A.L. `http://faysol.com/index.php/es/`, 2016. Online; accessed 13 December 2016.

[106] Mecanizados y Rectificados Industriales - Meca-teca S.l. http://www.mecateca.es/, 2016. Online; accessed 13 December 2016.

[107] Added Value Solutions - AVS. http:///www.a-v-s.es/, 2016. Online; accessed 13 December 2016.

[108] M. Scholz. *Effects of Ion Radiation on Cells and Tissues*, pages 95–155. Springer Berlin Heidelberg, Berlin, Heidelberg, 2003 - DOI:10.1007/3-540-45668-6$_4$.

A

Appendix

Contents:

Part 1 Lince lattice. **Part 2** Publications and Proceedings.

Lattice LINCE

Distance [m]		*Harmonic*	*Voltage [V]*	*Length [cm]*	**Maximum Field**	
0.44	**mhb**	1	4005	100	4005	
		2	-1335		4005	
		3	900		4005	
		4	552		4005	
		Voltage [V]	*Length [cm]*	*Aperture radius [cm]*	**Maximum Field**	
1.11145	**eqd**	1.06E-02	17.145	4	2.17E-02	
1.3845	**eqd**	-9.93E-03	27.305	4	2.17E-02	
1.55595	**eqd**	9.75E-03	17.145	4	2.17E-02	
3.4274	**eqd**	1.16E-02	17.145	4	2.17E-02	
3.70045	**eqd**	-9.10E-03	27.305	4	2.17E-02	
3.8719	**eqd**	6.70E-03	17.145	4	2.17E-02	
5.64335	**eqd**	1.46E-02	17.145	4	2.17E-02	
5.9164	**eqd**	-1.49E-02	27.305	4	2.17E-02	
6.08785	**eqd**	2.17E-02	17.145	4	2.17E-02	
		Cells	*Voltage [V]*	*Length [cm]*	*Average radius [cm]*	*Phase [deg]*
6.24469	**rfq**	126	82.06	530	0.6	-125
		Quadrupole component [G]	*length [cm]*	*Effective length [cm]*	*Aperture radius [cm]*	**Maximum Field**
11.74926	**quad**	-4500	20	20	2.7	5400
12.00426	**quad**	5400	20	20	2.7	5400
12.25926	**quad**	-3000	20	20	2.7	5400
		Length [cm]	*Harmonics*	*Field level*	**Maximum Field**	
12.85926	**cav**	20	4	1.1		
		Peak magnet field at center [Gs]	*Length [cm]*	*Aperture radius [cm]*		
13.57826	**sol**	50000	21.9	1.27	90000	
		Length [cm]	*Harmonics*	*Field level*		
13.87826	cav	20	4	4.4	5.3	
14.12826	**cav**	20	4	4.4	5.3	
		Peak magnet field at center [Gs]	*Length [cm]*	*Aperture radius [cm]*		
14.44726	**sol**	58000	21.9	1.27	90000	
		Length [cm]	*Harmonics*	*Field level*		
14.74726	cav	20	4	4.4	5.3	
14.99726	cav	20	4	4.4	5.3	
		Peak magnet field at center [Gs]	*Length [cm]*	*Aperture radius [cm]*		
15.31626	**sol**	62000	21.9	1.27	90000	
		Length [cm]	*Harmonics*	*Field level*		
15.61626	cav	20	4	4.4	5.3	
		Peak magnet field at center [Gs]	*Length [cm]*	*Aperture radius [cm]*		
16.43226	**sol**	65000	26.6	1.27	90000	
		Length [cm]	*Harmonics*	*Field level*		
16.78226	cav	30	4	5.3	5.3	
17.18226	cav	30	4	5.3	5.3	
		Peak magnet field at center [Gs]	*Length [cm]*	*Aperture radius [cm]*		
17.49826	**sol**	88000	26.6	1.27	90000	
		Length [cm]	*Harmonics*	*Field level*		
17.84826	cav	30	4	5.3	5.3	
18.24826	cav	30	4	5.3	5.3	
		Peak magnet field at center [Gs]	*Length [cm]*	*Aperture radius [cm]*		
18.56426	**sol**	87000	26.6	1.27	90000	
		Length [cm]	*Harmonics*	*Field level*		
18.91426	cav	30	4	5.3	5.3	
19.31426	cav	30	4	5.3	5.3	
		Peak magnet field at center [Gs]	*Length [cm]*	*Aperture radius [cm]*		
19.63026	**sol**	85000	26.6	1.27	90000	
		Length [cm]	*Harmonics*	*Field level*		
19.98026	cav	30	4	5.3	5.3	
		Peak magnet field at center [Gs]	*Length [cm]*	*Aperture radius [cm]*		
20.74626	**sol**	90000	26.6	1.27	90000	
		Length [cm]	*Harmonics*	*Field level*		
21.09626	cav	30	4	5.3	5.3	
21.49626	cav	30	4	5.3	5.3	
		Peak magnet field at center [Gs]	*Length [cm]*	*Aperture radius [cm]*		
21.81226	**sol**	90000	26.6	1.27	90000	

		Length [cm]	***Harmonics***	***Field level***	
22.16226	cav	30	4	5.3	5.3
22.56226	cav	30	4	5.3	5.3
		Peak magnet field at center [Gs]	***length[cm]***	***Aperture radius [cm]***	
22.87826	sol	90000	26.6	1.27	90000
		Length [cm]	***Harmonics***	***Field level***	
23.22826	cav	30	4	5.3	5.3
23.62826	cav	30	4	5.3	5.3
		Peak magnet field at center [Gs]	***length[cm]***	***Aperture radius [cm]***	
23.94426	sol	90000	27.5	1.27	90000
		Length [cm]	***Harmonics***	***Field level***	
24.29426	cav	30	4	5.3	5.3
		Peak magnet field at center [Gs]	***Length [cm]***	***Aperture radius [cm]***	
25.06926	sol	90000	27.5	1.27	90000
		Length [cm]	***Harmonics***	***Field level***	
25.62326	cav	40	6	4.2	5.3
26.12326	cav	40	6	4.2	5.3
		Peak magnet field at center [Gs]	***Length [cm]***	***Aperture radius [cm]***	
26.55226	sol	90000	26.6	1.27	90000
		Length [cm]	***Harmonics***	***Field level***	
27.10626	cav	40	6	4.2	5.3
27.60626	cav	40	6	4.2	5.3
		Peak magnet field at center [Gs]	***Length [cm]***	***Aperture radius [cm]***	
28.03526	sol	90000	26.6	1.27	90000
		Length [cm]	***Harmonics***	***Field level***	
28.58926	cav	40	6	4.2	5.3
29.08926	cav	40	6	4.2	5.3
		Peak magnet field at center [Gs]	***Length [cm]***	***Aperture radius [cm]***	
29.51826	sol	90000	26.6	1.27	90000
		Length [cm]	***Harmonics***	***Field level***	
30.07226	cav	40	6	4.2	5.3

mhb	Multi harmonic buncher
eqd	Electrostatic Quadrupole
rfq	Radiofrequency quadrupole
quad	Magnetic quadrupole with fringe fields
cav	Accelerating cavity
sol	Dipole corrector combined with solenoid

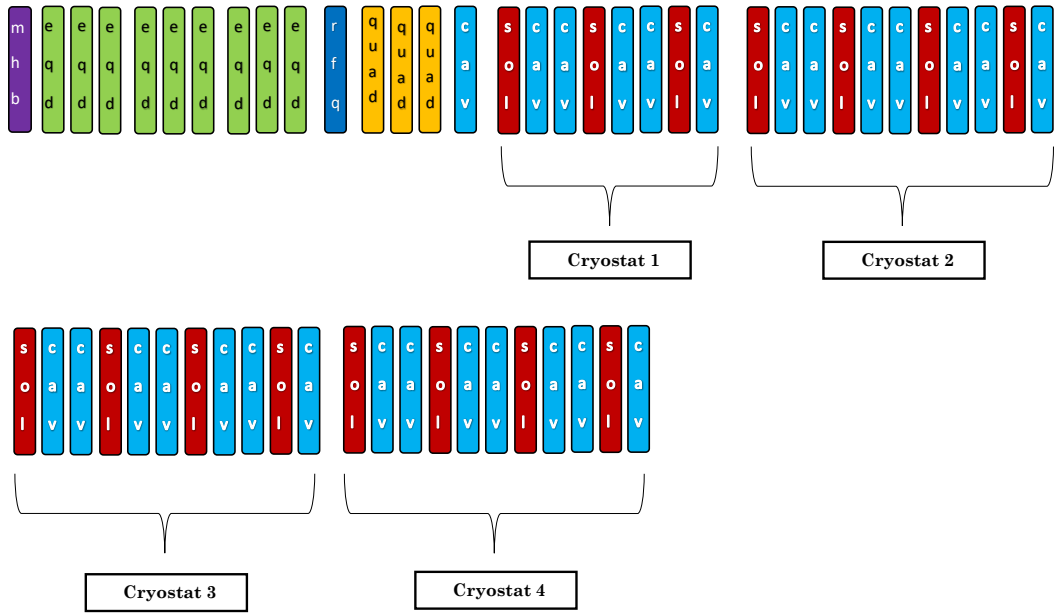

A Appendix

El artículo "A Proposal for a 72.75 MHz RFQ for ECOS-LINCE Project", que forma parte del apartado A Appendix, ha sido retirado de la tesis debido a restricciones relativas a derechos de autor. En sustitución del mismo ofrecemos la siguiente información: referencia bibliográfica, enlace a la revista y resumen.

- Ordúz, A.K., Bontoiu, C., Dueñas, J., Martel, I., Garbayo, A., Villari, A.C.C., Ostroumov, P.N.: "A Proposal for a 72.75 MHz RFQ for ECOS-LINCE Project". En: García-Ramos JE., Alonso C., Andrés M., Pérez-Bernal F. (eds) Basic Concepts in Nuclear Physics: Theory, Experiments and Applications. Springer Proceedings in Physics, vol 182. Springer, Cham. DOI: 10.1007/978-3-319-21191-6_20

Enlace al texto completo: https://doi.org/10.1007/978-3-319-21191-6_20

RESUMEN:
ECOS-LINCE (Martel I et al., Proceedings IPAC'14, 2014) is a proposal for a new European First Class high intensity heavy-ions accelerator for stable ions, with energies at and above the coulomb barrier. The low energy section will be achieved using a 72.75 MHz normal conducting four vanes RFQ designed to give a 460 keV/u boost for A/Q = 7 ions in about 5 m (Orduz AK et al., IPAC'14, 2014). The geometry vanes are modeled to accommodate windows in order to obtain a clear separation of the RFQ modes (Ostroumov P et al., Rev ST Accel Beams 15:110101, 2012). This article presents the experimental results of the RF test carried out on a aluminum prototype.

DEVELOPMENT OF A 72.75 MHZ RFQ FOR THE LINCE ACCELERATOR COMPLEX*

A.K. Orduz†, C. Bontoiu, I. Martel, Univ. of Huelva, Spain
A. Garbayo, AVS, Elgoibar, Gipuzkoa, Spain
A.C.C. Villari, FRIB, East Lansing, Michigan, USA
P.N. Ostroumov, ANL, 9700 S. Cass Av. Argonne, IL, USA

Abstract

Low-energy acceleration for the LINCE project [1] will be achieved using a 72.75 MHz normal conducting four vanes RFQ designed to give a 460 keV/u boost for A/Q = 7 ions in about 5 m. The vanes are modeled to accommodate windows for a clear separation of the RFQ modes and easy fitting to an octagonal resonance chamber. This article presents the main numerical results of the radio-frequency modeling and computational fluid dynamics (CFD). Particle tracking studies optimized for bunching and acceleration are shown as well.

INTRODUCTION

Development work has been carried for the highest mass-to-charge ratio considered i.e. A/Q = 7. The machine layout and performance must handle 2 ns long bunches of 40 keV/u kinetic energy. With the aim of raising the kinetic energy up to 500 keV/u a simulation was carried using the DESRFQ code [2] at 82 kV inter-vane potential on a vane tip geometry tested at ANL [3]. Thus, a 5.04 m long sinusoidal modulation was generated with the structure being split in 8 sections of 630 mm nominal length.

Complete beam dynamics simulations using ideal electric fields generated by DESRFQ and Track 3D [4] codes are reported in **BEAM DYNAMICS** proving that the target energy is reachable with 2 % energy spread and bunch duration within 1 ns. Resistive power losses obtained from an initial *RF study* in **RF ANALYSIS** are scaled and then coupled in **Heat transfer study** to a *heat transfer module* in order to obtain a temperature map at the vanes surface. Further in **CFD and structural analysis**, cooling is simulated in *fluid flow study* using water circulating through pipes drilled inside the vanes and thus a stable temperature distribution can be achieved for a given water flux. The remaining heat flux is coupled to a *solid mechanics study* which provides estimates for the displacement due to thermal expansion. Eventually, an evaluation of the RF frequency shift is obtained through a new *RF study* of the deformed structure. A complete loop of coupled numerical studies is achieved as shown in Fig. 1.

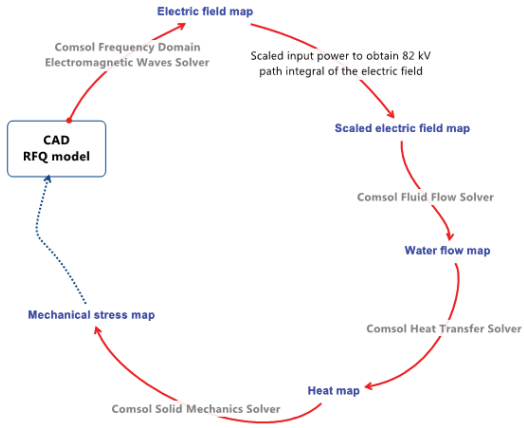

Figure 1: RFQ design work flow.

RF ANALYSIS

Eigenfrequency studies have been carried out using the Comsol software [6] for several development stages of the RFQ structure. Resonance frequencies and degeneracies for the quadrupole and dipole modes are shown in Table 1.

Table 1: Resonance Modes at Different Geometry Stages

Geometry Stage	Modes & Degeneracy	Frequency [MHz]
Cavity	TE_{111} (dip., 2)	451.83
	TE_{112} (dip., 2)	460.06
Cavity with vanes	TE_{211} (quad., 1)	183.30
	TE_{111} (dip., 2)	189.89
Cavity with vanes and windows	TE_{211} (quad., 1)	70.47
	TE_{212} (quad., 1)	75.34
Cavity with modulated vanes and windows	TE_{211} (quad., 1)	71.77
	TE_{212} (quad., 1)	76.98

Introducing the four vanes in the resonator enables the appearance of a quadrupole mode TE_{211} resonating around 183 MHz and one doubly degenerated dipole mode very close. The quadrupole electric field pattern in a transverse cross-section is shown in Fig. 2. The figure also shows that the magnetic field is directed longitudinally along the structure with its sign alternating from one quadrant to another.

Cutting RF windows through the vanes makes the magnetic field lines loop around the windows corners resulting in a reduction of the quadrupole mode frequency and a clear

* Work partially supported by the Spanish Government (MINECO-CDTI) under program FEDER INTERCONNECTA
† angie.orduz@dfa.uhu.es

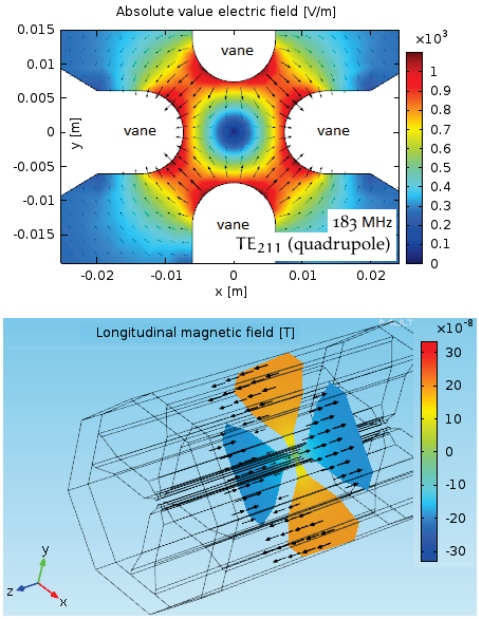

Figure 2: Quadrupole electric (top) and magnetic (bottom) field patterns for the vanes without windows.

separation from the dipole modes. This also brings the next order quadrupole mode into the range of the fundamental one. Adding the modulation raises the resonance frequency by about 1.3 MHz and using a system of fixed tuners it is possible to achieve the target frequency. Longitudinal and transverse electric fields in the input matcher region are shown in Fig 3.

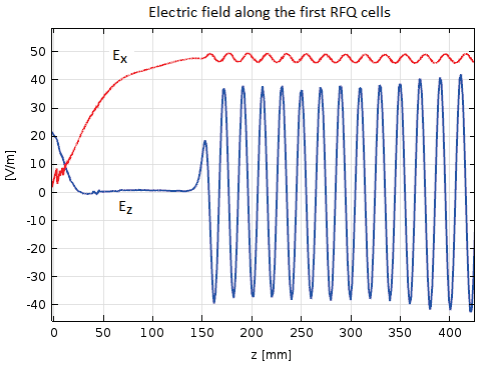

Figure 3: Longitudinal on-axis (blue) and horizontal off-axis (red) electric field for a few cells.

The quality factor of the current design is Q = 8670 and some of RF parameters for one RFQ section are listed in Table 2.

Table 2: RF Characteristics of One RFQ Section

Frequency [MHz]	Power Loss [kW]	Stored Energy [J]	Shunt Impedance [kΩ-m]
71.87	16.58	0.32	279.39

BEAM DYNAMICS

Complete beam dynamics simulations have been carried using Track 3D in order to check that the energy target is achievable, while keeping the beam transverse size within the inter-vane region. The electric RFQ quadrupole fields are generated internally by the numerical code for an inter-vane potential of 82 kV and the sinusoidal modulation obtained previously. Snapshots of the transverse and longitudinal phase space are shown in Fig. 4 for the entrance and exit of the RFQ. The input beam consists of bunches of about 2 ns length and 4 % total energy spread. This is the result of a multi-harmonic buncher [5] which induces longitudinal energy modulation.

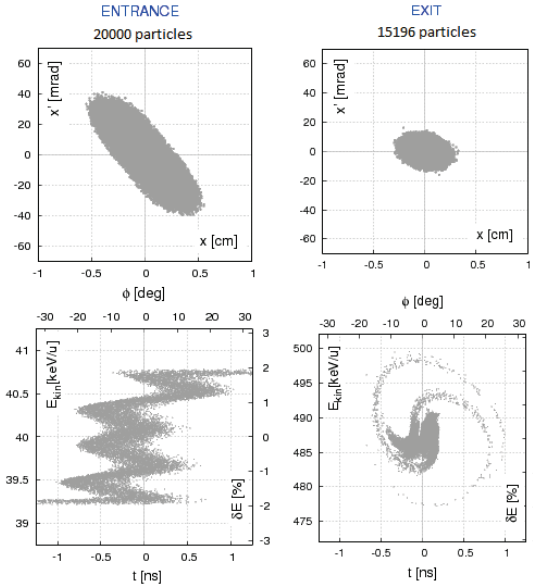

Figure 4: Beam distribution at the entrance (top) and exit (bottom) of the RFQ. The black circle represents the inter-vanes aperture. Particle transmission rate is around 76 % and we are currently working to improve it.

As shown in Fig. 5 the first part of the RFQ is used for bunching rather than acceleration. Starting with the 80th cell the aspect ratio remains constant and this enables a linear energy growth of about 6.5 keV/u.

ENGINEERING DESIGN

Results of a thermal study analysis study on the latest RFQ design is presented in the following sections.

ISBN 978-3-95450-132-8

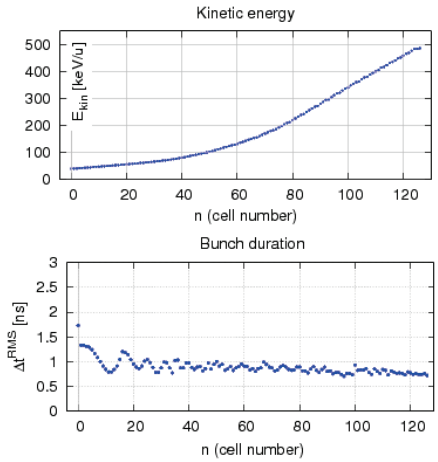

Figure 5: Kinetic energy along the whole RFQ structure.

Heat Transfer Study

Resistive power losses calculated in the **RF ANALYSIS** section are show in Fig. 6. This study is coupled with the CFD module for a non-isothermal turbulent flow in a quarter symmetry model (section) of the RFQ. Final mesh is optimized for each physics study (thermal, CFD and structural) with a total of 3.1×10^5 tetrahedral elements and minimum element size of 4 µm.The total resistive power dissipated by the RFQ working mode at mode at 71.87 MHz is 16.58 kW.

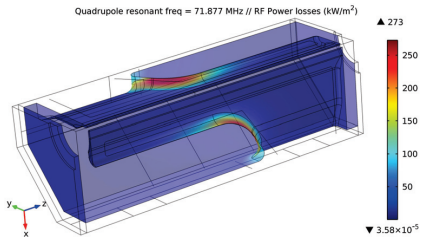

Figure 6: Heat map of the power resistive losses.

The heat is to be absorbed by the water cooling channels and the outer copper surfaces in convection to the ambient air with a heat transfer coefficient (HTC) of 10 W/m^2K [7]. An HTC on the cooling channels of 11.2 kW/m^2K was calculated by using turbulent flow 6×10^4 Reynolds number and an inlet temperature of 15 °C .

The aim was to obtain maximum deformation due to the thermal expansion ≤150 μm transversely and ≤100 μm longitudinally on the vane tip; which led to a maximum temperature of 35 °C. The design process showed that only cooling on the vanes were not acceptable and 3 more channels of 14 mm were added on the side plates for extra heat subtraction. Stationary studies of the copper structure without cooling and only convection flux with the surrounding air showed copper temperature to reach more than 1300 °C.

CFD and Structural Analysis

Fig. 7 shows the velocity field along the cooling channels of the vanes where a 0.53 bar pressure drop on the fluid is obtained. The cooling channels are to be implemented by holes drilled into solid copper parts with brazed lids and therefore maximum variation of these values occur mainly at the corners. The volume flow rate is optimized to obtain values below 5 m/s.

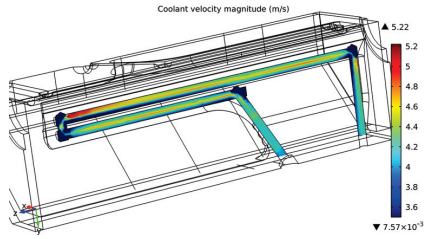

Figure 7: Flow rate along the cooling channels.

After 600 s the temperature of the copper on the cooling channels calculated by wall functions and surface roughness for drilled holes in copper of 0.61 mm reaches 20.7 °C at the window corner. The temperature increase of the coolant is 0.5 °C with a typical Reynolds number of 55×10^3. Latest calculations led to a final temperature of the copper ≤ 32.2 °C. Thermal expansion of the copper is implemented into a structural model to study the maximum stress and deformation along the structure. The deformation then is implemented back into a new RF study to analyze the variation of the resonant frequency. The von Mises stress on the copper has to be ≤7×108 N/m^2 as established by measured mechanical properties of brazing annealed OFE copper at INFN-LNL [8]. It can be observed that it causes the bottom part of the vane to expand and the top part to contract. This deformations which arise mostly on the levering part of the vanes create a frequency shift of a 0.20 % from 71.87 to 71.73 MHz.

CONCLUSIONS

Beam dynamics results are to be improved using realistic field maps obtained through RF simulations. This will include suitable input matcher and trapezoidal cells at the RFQ end, finished with an output matcher. Four adjustable moving tuners will be used to tune the resonant frequency to 71.75 MHz and fine tuning of the copper structure will be obtained by applying different inlet temperatures and velocities of the coolant. A variation of 3 °C in the inlet temperature showed a frequency shift of 50 kHz. A minimum velocity of 3 m/s and temperature inlet of 15 °C is set up for the minimum cooling requirements for continuous RFQ operation. We are still working for checking the accuracy of Beam Dynamics and RF simulations and to verify the behavior of the longitudinal emittance.

ISBN 978-3-95450-132-8

REFERENCES

[1] I. Martel et al., "LINCE: A High Intensity Multi-ion Superconducting Linac for Nuclear Structure and Reactions", IPAC'14, Dresden, Germany, June 2014, THPME036, These Proceedings.

[2] A. A. Kolomiets et al., *The RFQ Design Software DESRFQ*, (ITEP/ANL Technical Note, 2005).

[3] P. Ostroumov et al., Rev. ST Accel. Beams 15, 110101 (2012).

[4] V. Aseev et al., "TRACK: The new beam dynamics code", PAC'05, Knoxville, USA, TPAT028 (2005).

[5] C. Bontoiu et al., "Design of a Multi-harmonic Buncher for the LINCE Heavy-ion Accelerator Complex", IPAC'14, Dresden, Germany, June 2014, MOPME059, These Proceedings.

[6] Comsol website: `http://www.comsol.com/products/multiphysics/`

[7] Engineering Toolbox website: `http://www.engineeringtoolbox.com`

[8] INFN-Legnaro: `www.lnl.infn.it`

ISBN 978-3-95450-132-8

PROPOSAL FOR A 72.75 MHz RFQ FOR THE LINCE ACCELERATOR COMPLEX *

A.K. Orduz, C. Bontoiu, A. Berjillos, J.A. Dueñas, I. Martel, University of Huelva, Spain
A. Garbayo, AVS, Elgoibar, Gipuzkoa, Spain

Abstract

The low-energy part of the LINCE facility [1] can be based on a 72.75 MHz normal-conducting RFQ designed to give a 450 keV/u boost for A/Q=7 ions in about 5 m length. The vanes have been electromagnetically designed to accommodate dedicated RF windows producing effective separation of the RFQ modes in an octagonal-shaped resonance chamber [2]. This article outlines the optimization of the quality factor of the cavity by using numerical methods for electromagnetic calculations. Experimental results of RF test carried out on a prototype are also discussed.

INTRODUCTION

RFQ development, as a whole device is a very complex project which requires many iteration loops between physical concepts and engineering practices. Within the physical aspects, the development is carried out setting beam quality and specifications first. Considering a design mass-over-charge ratio A/Q=7 the RFQ must yield 460 keV/u energy gain working at a maximum inter-vane voltage of 82 kV. Results of the RF modelling process carried out in COMSOL [3], are outlined along the design stages from the shape of the resonator to the final modulated vanes including windows and tuners.

CAVITY OPTIMIZATION

Considering only two RFQ sections, the vanes and windows geometry can be optimized in order to produce the highest quality factor with a resonant frequency around 70 MHz such that adding modulation and tuners [2] would raise it in the 8 sections layout to about 72.75 MHz. This can be achieved in two stages:

- choice of the vane height and thickness in 2D with a predetermined cross-section in the beam region;
- optimization of the elliptical RF windows in 3D;

2D Optimization

The 2D optimization is achieved by doing a parametrization of the vane height which consists of several geometric pieces, namely a trapezoid, a rectangle, a stem and a half disk, all added on the top of the inter-vane radius R_0 = 6.16 mm. While the disk radius r_1 = 4.8 mm and stem height h_{stem} = 14 mm are kept constant, the rectangle and trapezoid height shown in Fig. 1 are taking values between 45 mm and 125 mm in steps of 2.5 mm.

* Work partially supported by the Spanish Government (MINECO-CDTI) under program FEDER INTERCONNECTA

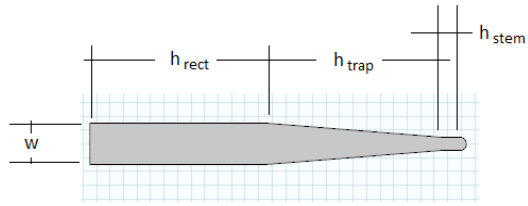

Figure 1: Transverse cross-section view of one vane.

Running the optimization process at three different values for the vane width w yields the quality factor and resonant frequency for the TM_{21} mode as shown in Fig. 2. For a given quality factor one must consider higher and thicker or shorter and thinner vanes. The trapezoid and rectangle heights are complementary in the sense that the same quality factor can be obtained decreasing any one of them and increasing the other one proportionally.

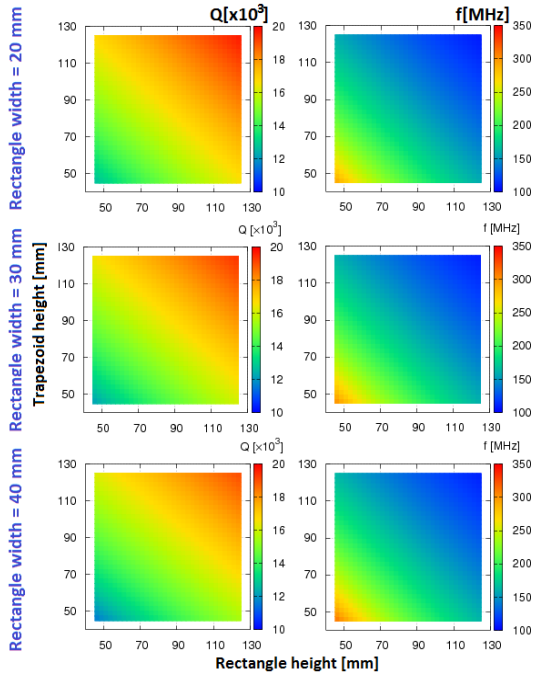

Figure 2: Evaluation of the quality factor and resonant frequency as function of rectangle and trapezoid height.

ISBN 978-3-95450-168-7

To proceed to the next stage, the parameters are set to w = 40 mm, $h_{rect} = h_{trap}$ = 130 mm and this yields Q = 19438 and f = 105.59 MHz.

3D Optimization

The vane transverse cross-section is extruded for the length of two RFQ sections that is L = 1 m. In a first approach an elliptical window with a_1 and b_1 as the minor and major semi-axes respectively is considered. Quality factor and frequency variation as a function of the two semi-axes can be seen in Fig. 3.

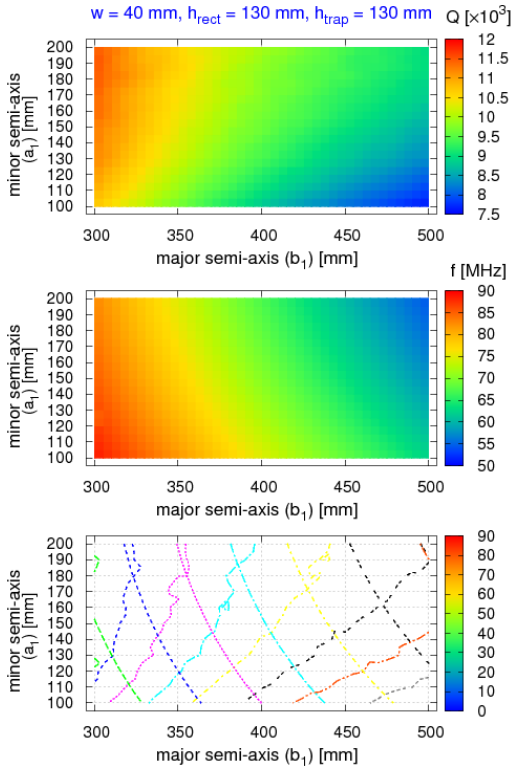

Figure 3: Evaluation of the quality factor and resonant frequency as function of the ellipse semi-axes.

Constant frequency lines are bent oppositely to constant quality factor lines and thus they intersect, though the curvatures are quite different. We choose b_1 = 375 mm and a_1 = 200 mm and the quality factor of 10221. The end caps volume is not used for calculations. Neither are the copper faces in the xy-plane at the two vane longitudinal limits. The RF analysis results for one RFQ section with these characteristics are show in Table 1.

Table 1: RF Characteristics of One RFQ Section

Parameter	Units	Simulation
Frequency	[MHz]	67.20
Quality factor		10221
Power loss per cavity	[kW]	17.73
Stored energy	[J]	0.40
Shunt impedance	[[kΩ−m]	237.59

RFQ PROTOTYPE

A section of aluminum cavity RFQ has been built in collaboration with Spanish companies and tested in the RF Laboratory at the University of Huelva as shown in Fig. 4. The test was performed at room temperature, using a coaxial coupler and a pickup loop antenna connected to a Agilent N9000A CXA spectrum analyzer, using the tracking generator mode to measure the frequency response of the cavity. The test procedures are explained in this section and results are compared with the simulations in COMSOL.

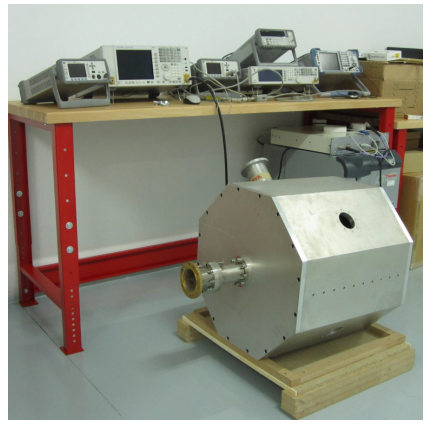

Figure 4: Aluminum RFQ section prototype.

Measurements

The main objective of the test is to obtain the frequency modes of the cavity, which can confirm the accuracy of the design. First cavity input and output signal generated by the computer connects, that is the entrance to pick up and the output is connected to the coupler.

The empty cavity resonates at 485 MHz in good agreement with COMSOL simulations as it can be seen from the two spectra shown in Fig. 5. The resonator (without vanes) is fed by a coupler installed on one of the end caps while the pickup antenna reads the frequency spectrum for a lateral wall.

CONCLUSIONS

The experimental results found are similar to those predicted by simulation, so it follows that the theoretical calculations were performed properly. Frequency measurements

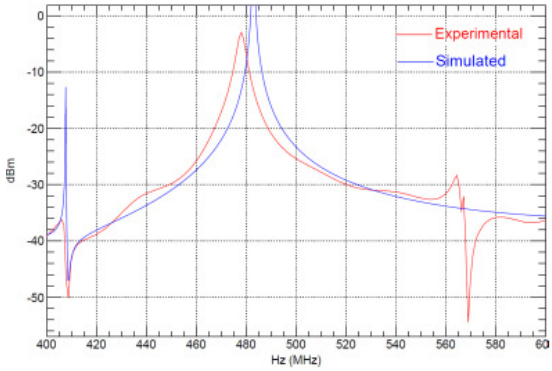

Figure 5: Experimental and simulated RFQ frequency mode.

will also carry out with the four vanes installed inside, followed by bed pull test bench. Future work will focus on improving the quality of the simulations and obtain better measurements of the whole RFQ.

The authors would like to express the highest appreciation and tanks for the useful guidance and help received from Peter N. Ostroumov (Argonne National Laboratory), Antonio C.C. Villari (Facility for Rare Isotope Beams) and Muhsin N. Harakeh.

REFERENCES

[1] I. Martel et al., "LINCE: A High Intensity Multi-ion Superconducting Linac for Nuclear Structure and Reactions", IPAC'14, Dresden, Germany, June 2014.

[2] A.K.Orduz et al., "Development of a 72.75 MHz RFQ for the LINCE Accelerator Complex", IPAC'14, Dresden, Germany, June 2014.

[3] Comsol website: `http://www.comsol.com`

ISBN 978-3-95450-168-7

THERMAL AND STRUCTURAL ANALYSIS OF THE 72.75 MHz LINCE RFQ*

A.K. Orduz, C. Bontoiu, A. Berjillos, J.A. Dueñas, I. Martel, University of Huelva, Spain
A. Garbayo, AVS, Elgoibar, Gipuzkoa, Spain

Abstract

The 72.75 MHz LINCE RFQ [1] is designed to function at room temperature. Effective operation of the RFQ cavity requires efficient water cooling in order to dissipate significant resistive power non-uniformly distributed on the copper walls and vanes. This amounts to about 10 kW for one 0.5 m long RFQ section. Cylindrical cooling channels have been designed and optimized by varying their diameter and position in order to minimize the frequency shift generated by thermal displacements. The article reports results of power loss simulations coupled with electromagnetic modelling studies and their consequences on the RFQ performance in terms of resonant frequency and thermal deformations.

INTRODUCTION

The four-vanes RFQ is designed for LINCE high intensity accelerator complex [2]. The structure provides a 72.75 MHz resonating mode with a 1.3 MHz margin controlled by the tuners [1]. The initial beam is made of 2 ns long bunches of 40 keV/u and the aim of the design is to achieve 500 keV/u. The modulation was simulated using the DESRFQ code [3] with 82 kV inter-vane potential on a vane tip tested in ANL [4].

A complete loop of coupled numerical studies is achieved as shown in Fig. 1. The **RF Analysis** has been carried with COMSOL [5] resulting in an estimate for the resistive power losses. These are scaled and coupled with **Heat Transfer** model in order to obtain a temperature map at the vanes surface. The next step is the optimization of the cooling system according to the heat map. Two optimization for channel position, channel diameter, fluid and velocity temperature are carried out. The final heat flux is coupled to a **Solid Mechanics** study to estimates the stress and displacements due to thermal expansion. The frequency shift is obtained through a new RF study of the deformed structure.

RF ANALYSIS

The first study has been done with DESRFQ and Track [6] codes. Eigenfrequency studies have been done using COMSOL software, as shown before [1]. For the last version of the study the whole structure with modulated vanes was simulated and a 73.25 MHz for the quadrupole mode TE_{211} resonance is obtained.

Heat Map

Resistive power losses are calculated and that show the maximum loses are in the window corners as it is show in

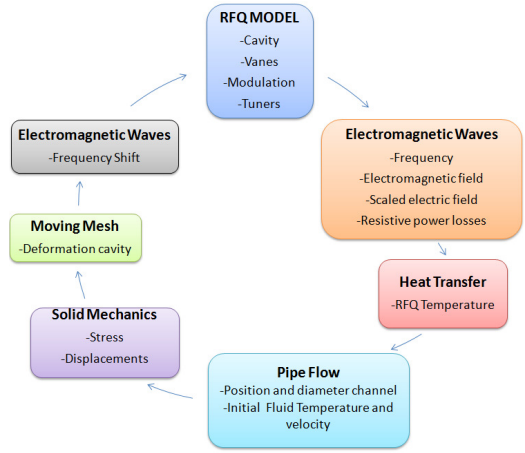

Figure 1: Study steps.

Fig. 2. This study is coupled with a non-isothermal pipe flow simulation in a quarter symmetry model (section) of the RFQ. The total resistive power dissipated by the RFQ working mode at 67.35 MHz is 10.67 kW. A cooling system must be design to control the heat dissipation in the RFQ.

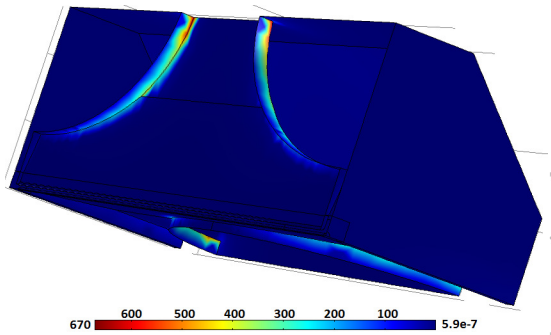

Figure 2: Resistive power losses [kW/m].

COOLING SYSTEM

According with the resistive power losses two models have been proposed as shown in Fig. 3. An initial cooling channel of rectangular profile has been considered due to its mechanical simplify as shown in Fig. 3(top) but proved unsatisfactory in the tip vanes. Therefore the second model Fig. 3(bottom) was studied whit better results.

* Work supported partially supported by the Spanish Government (MINECO-CDTI)under program FEDER INTERCONNECTA

ISBN 978-3-95450-168-7

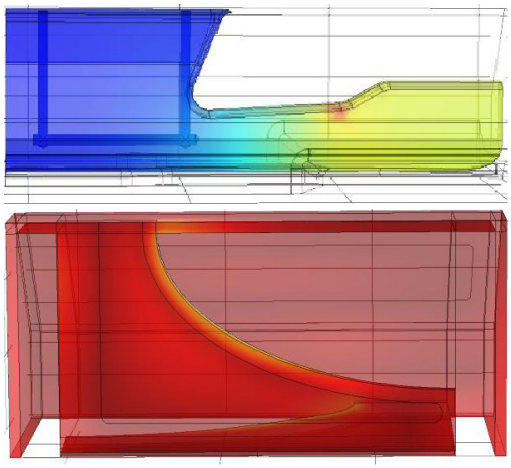

Figure 3: System cooling models.

Position and Diameter Optimization

Thermal simulations have been done with the variation of the position and diameter using sweep parametrization. The ranges for the simulation were 10 mm to 17 mm and 7 mm to 14 mm for the position and diameter respectively. While the geometry of the channels is constant its position relative to the vane changes as shown in Fig. 4.

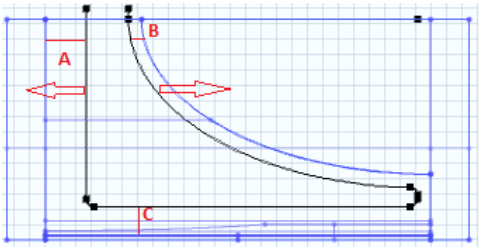

Figure 4: Flow rate along the cooling channels.

The aim of the study is to find temperature variations at different locations of the structure. Several geometric entities were selected to analyze the temperature during a time interval from 0 s to 8000 s. The selected entities were: 1. the RFQ volume, 2. the RFQ surface, 3. intermediate point on a side, 4. intermediate point on the vane tip, 5. line at the vane tip and 6. point near to the maximum power losses.

The data obtained for the volume and surface studies show that the initial temperature of 16.15 °C decrease to 16 °C. At the point located in the middle of the vane length, results show that the required diameter at the sides of the cavity may be lower than in the vanes, which is expected, considering that on the side walls the power losses are lower. The results for the line in the tip vane shown in Fig. 5, finding minimum values of 14 mm and 10 mm for the position and diameter respectively. The point 6 remains constant temperature during the time analyzed.

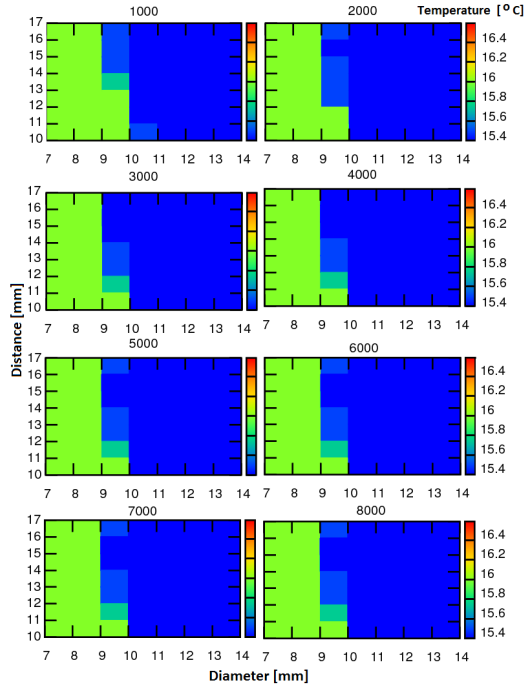

Figure 5: RFQ cavity temperatures as a function of the position and diameter of the cooling channel.

Temperature and Velocity Optimization

The aim of this section is to analyze the temperature dynamics in the structure temperature in function of the initial fluid conditions, temperature and velocity. The select ranges are 0 m/s to 5 m/s and 15 °C to 20 °C for the velocity and temperature, respectively. The same entities as before and time range are considered. All the results show that for higher temperatures of the fluid heat dissipation is smaller and by increasing the fluid velocity, the dissipation is greater as shown in Fig. 6. The maximum value for the fluid temperature is 20 °C and the minimum initial velocity is 3 m/s.

Selected values are shown in Table 1, the values may vary within the range shown in the same table, and this variation depends on the needs of future studies.

FREQUENCY SHIFT

The remaining heat flux is coupled to a solid mechanics study which estimates displacements. The last step is to run

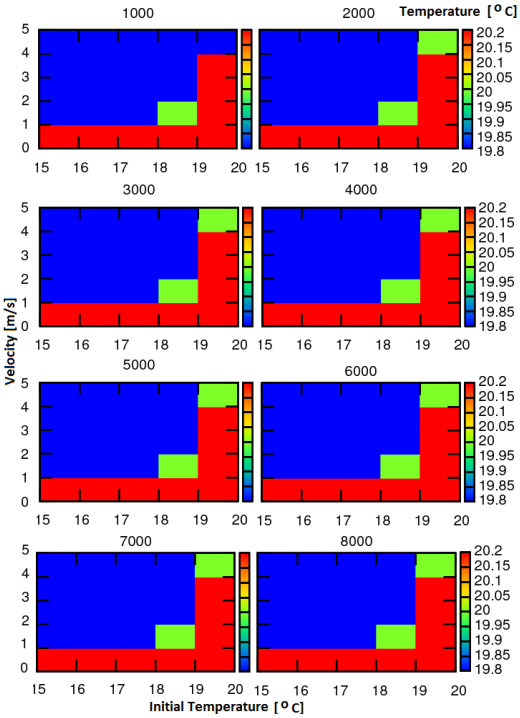

Figure 6: RFQ cavity temperatures as a function of the initial temperature and velocity of the fluid.

Table 1: Parameters

Parameter	Value	Interval	Units
Diameter	14	10-14	mm
Position	16	14-17	mm
Initial Temperature	18	15-19	°C
Initial Velocity	4	3-5	m/s

all the coupled modules with the selected parameters and obtain the frequency shift due to the thermal expansion.

Mechanical Stress

As shown in Fig. 7 the maximum values of the mechanical stress are in the corners of the RFQ ends and in the the elliptical windows. A maximum value of 22.6 MPa at the corners of the support surface of the structure is recorder. The surface which exhibits the most pressure is the support side. Given the above, the importance of a detailed analysis of the effect on support sides becomes obvious.

Displacement

Results for the displacements show maximum values at the ends of the vanes of 64.7 µm for the x axis and 98 µm as shown in Fig. 8 for y axis both in the direction of the beam,

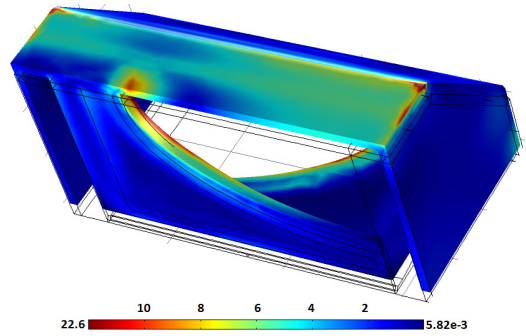

Figure 7: Mechanical stress map for the RFQ cavity [MPa].

and 2.04 µm on sides of the cavity. The difference between the displacements in the x and y axis are due to the RFQ support area considered fixed constraint.

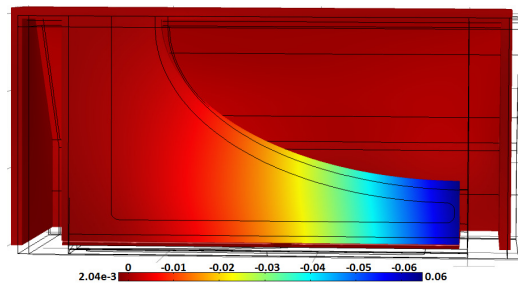

Figure 8: Displacement in x axis [mm] on the vanes.

With the parameters from the table 1 the frequency shift is 7.37 MHz. More details studies are considered in order to improve frequency shift estimates.

CONCLUSIONS

A method has been developed to study electromagnetic, thermal and mechanical effects as coupled studies implemented in COMSOL. With the main goal of minimizing the frequency shift of the RFQ, more detailed simulations shall be carried out refining optimization parameters and initial conditions.

The authors would like to express the highest appreciation and tanks for the useful guidance and help received from Peter N. Ostroumov (Argonne National Laboratory), Antonio C.C. Villari (Facility for Rare Isotope Beams) and Muhsin N. Harakeh.

ISBN 978-3-95450-168-7

REFERENCES

[1] A.K.Orduz et al., "Development of a 72.75 MHz RFQ for the LINCE Accelerator Complex", IPAC'14, Dresden, Germany, June 2014.

[2] I. Martel et al., "LINCE: A High Intensity Multi-ion Superconducting Linac for Nuclear Structure and Reactions", IPAC'14, Dresden, Germany, June 2014.

[3] A. A. Kolomiets et al., *The RFQ Design Software DESRFQ*, (ITEP/ANL Technical Note, 2005).

[4] P. Ostroumov et al., Rev. ST Accel. Beams 15, 110101 (2012).

[5] COMSOL website: `http://www.comsol.com`

[6] V. Aseev et al., "TRACK: The new beam dynamics code", PAC'05, Knoxville, USA, TPAT028 (2005).

STUDIES FOR A 72.75 MHz FOUR VANES CW-RFQ FOR ECOS-LINCE PROJECT*

A.K. Ordúz, C. Bontoiu, I. Martel

Department of Applied Physics, University of Huelva, Huelva, Spain

A. Garbayo, A.C.C. Villari

Added Value Solutions, Elgobiar, Gipuzkoa, Spain
and
Facility for Rare Isotope Beams, East Lansing, Michigan, USA

(Received January 18, 2016)

The ECOS is considering the construction of a new facility for accelerating high intensity stable beams with energies at and above the Coulomb barrier, the LINCE light and heavy ion accelerator. This facility could be based on a normal conducting CW-RFQ and a superconducting linac, working at 72.75 MHz. This paper presents a design study for the RFQ system which is able to achieve 500 keV/u output for $A/Q = 7$ ions in only 5 m length.

DOI:10.5506/APhysPolB.47.619

1. Introduction

The RFQ is one of the most important devices of the low-energy section of ECOS-LINCE [1]. A complete beam dynamics study was carried out with the codes DESRFQ [2] and TRACK [3], considering the highest mass-to-charge ratio to be $A/Q = 7$, and a maximum beam intensity of 1 mA. The initial acceleration of heavy ions delivered from an ECR (electron cyclotron resonance) ion source [4] which is similar to the system of INFN-Legnaro National Laboratories [5]. At the RFQ entrance, the beam is already bunched into 2 ns long pulses of 40 keV/u kinetic energy. At the exit, the beam should achieve 500 keV/u, maximum energy spread of 2%, and bunch length of 1 ns. This is the result of a multi-harmonic buncher [6] which induces longitudinal energy modulation. Optimum injection into the SC-linac imposes maximum normalized transverse and longitudinal emittances of 0.125 cm mrad and 25 ns keV/u, respectively [7]. The principal design characteristics are shown in Table I.

* Presented at the XXXIV Mazurian Lakes Conference on Physics, Piaski, Poland, September 6–13, 2015.

TABLE I

RFQ principal characteristics.

Characteristic	Value	Units
Frequency	72.75	MHz
Input kinetic energy	40	A keV
Output kinetic energy	500	A keV
Design mass-to-charge ratio	1–7	
Maximum vane voltage	82	keV
Maximum field strength	1.5	Kilpatric
Length	5	m
Average radius	6	mm

A combined electromagnetic, radiofrequency and thermo-mechanical design study has been carried out using COMSOL Multiphysics [8]. A particular RF-window system over the resonator vanes has been designed and optimized, in a similar manner to that realized in the ATLAS RFQ structure [9]. This has the advantage of greatly reducing the cavity volume for a given resonance frequency. The software allows varying the geometrical parameters to maximize the quality factor and accelerating fields, while reducing the resistive power losses.

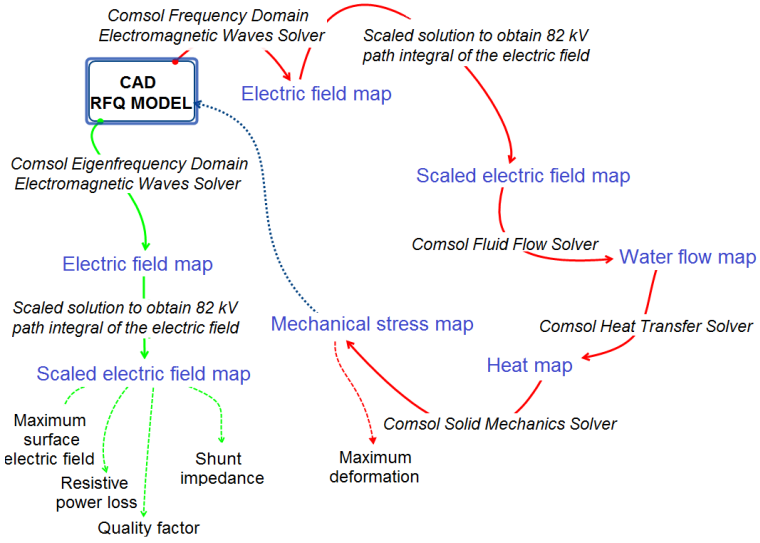

Fig. 1. RFQ design loop.

We used the Heat Transfer module coupled to the Mechanical Stress module to obtain the corresponding temperature map at the vanes [7] and the mechanical deformation, which may affect beam dynamics. To control the heating effects, we have studied a cooling system based on water circulating through pipes drilled inside the vanes [10]. The displacements and stress are obtained by coupling the heat-flux and solid-mechanics modules. Eventually, an evaluation of the RF frequency shift is obtained through a new RF study of the deformed structure. A simplified diagram of the design loop followed for performing the coupled numerical studies is shown in Fig. 1. In the final design, we achieved a total RFQ length of 5.04 m. It is proposed to construct the RFQ by coupling 10 sections of about 500 mm length each.

2. Optimization of the RFQ geometry

An optimization process of the quality factor, resistive power loss and resonant mode frequency TM_{21} has been carried out, following a loop of simulations in two stages. The first stage was dedicated to the optimization of the vane height and thickness using only the transverse shape of the vane without windows (2D), and the second one to the optimization of the RF window parameters (3D).

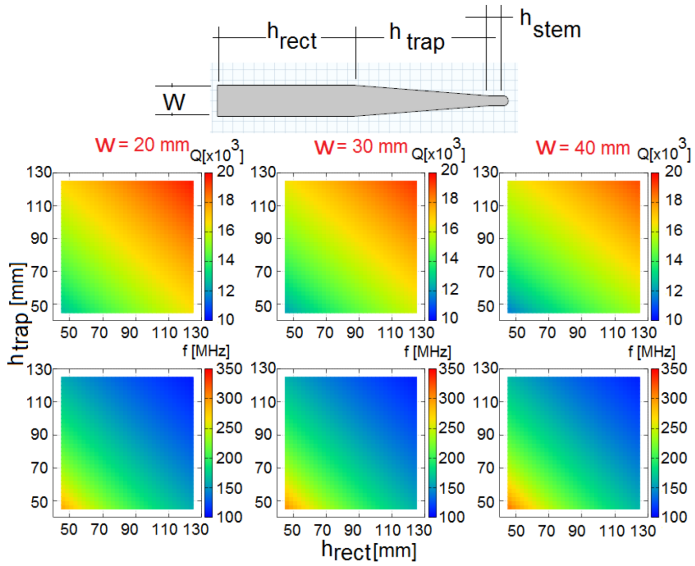

Fig. 2. Geometrical parameters of the vane. Bottom: Evaluation of the quality factor Q and resonance frequency as a function of vane geometry.

In Fig. 2 (top), we show the main parameters of the vane shape, which was divided in a rectangle, a trapezoid and a stem shape. As an example of the first stage optimization process, we plot in Fig. 2 (bottom) a scan of the parameters h_{rect} (height of the rectangular shape) and h_{trap} (height of the trapezoidal shape), for three values of the vane thickness W (rectangle width). In these calculations, the values for the tip radius $r_1 = 4.8$ mm, stem height $h_{\text{stem}} = 14$ mm and the inter-vane distance between electrodes $R_0 = 6$ mm keep constant. The selected values were $W = 40$ mm, $h_{\text{rect}} = 130$ mm and $h_{\text{trap}} = 130$ mm as there is the maximum quality factor.

In the second stage, we have studied different shapes of the RF windows varying (a_1) and (b_1) in order to obtain the maximum quality factor at the design frequency, and some results are shown in Fig. 3 (left). The best result is obtained by using elliptical window, with quality factor $Q \sim 10^4$ and shunt-impedance $r_s \sim 400$ kΩ-m. The process followed for the optimization of ellipse parameters is illustrated in Fig. 3 (right). The two plots in the upper part depict the variation of the value of the quality factor and resonant frequency, respectively, as a function of the major (b_1) and minor (a_1) semi-axis. The cavity Q value increases drastically by increasing a_1 and reducing b_1 but, at the same time, increasing the resonant frequency. For example, for $b_1 = 375$ mm, $a_1 = 200$ mm, it is obtained $Q \sim 10200$.

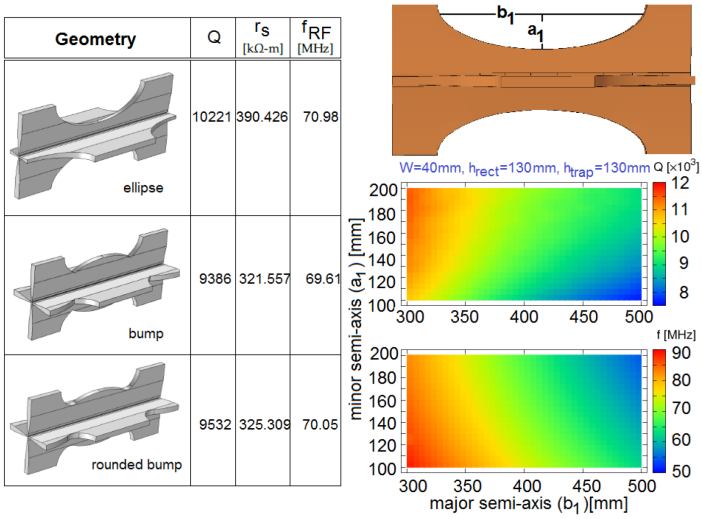

Fig. 3. Left: Three different shapes of the RF window considered in this study. Right: Evaluation of the quality factor Q and resonance frequency f as a function of semi-axes length a_1 and b_1 of the elliptical shapes.

3. RF analysis

The complete RFQ structure of 5 m length was simulated using the RF Module of COMSOL Multiphysics, and the main resonance modes are shown in Table II. Cutting RF windows through the vanes makes the magnetic field lines loop around window corners resulting in a reduction of the quadrupole mode frequency and a clear separation from the dipole modes. This also brings the next order quadrupole mode into the range of the fundamental one.

TABLE II

Resonance modes and degeneracies.

Geometry stage	Modes and Degeneracy	Frequency [MHz]
Cavity	TE_{111}	451.83
	TE_{112}	460.06
Cavity with vanes	TE_{211}	183.30
	TE_{111}	189.89
Cavity with vanes and windows	TE_{211}	70.47
	TE_{212}	75.34
Cavity with modulated vanes and windows	TE_{211}	71.77
	TE_{212}	76.98

Adding the modulation raises the resonance frequency by about 1.3 MHz, but with the aid of a dedicated RF-tuner system, it is possible to achieve the target frequency. A detailed study of the tuner geometry was also done by varying penetration depth, diameter and its position on the wall with respect to the beam entrance. The results of this study are shown in Fig. 4.

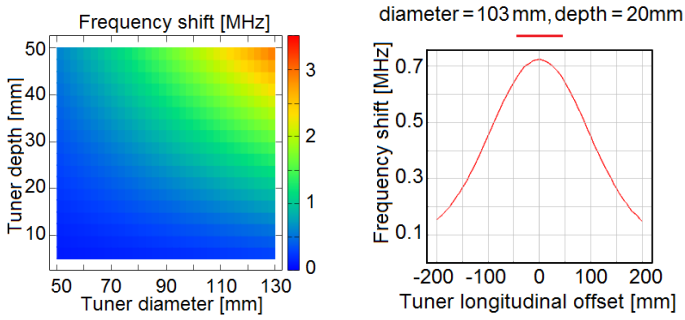

Fig. 4. Frequency shift of the whole RFQ as a function of tuner diameter and depth (left), and position offset (right).

The bandwidth of the tuner increases with diameter and penetration depth, and the maximum effect occurs when the tuner is on the center of the cavity wall, equidistant from both ends. A list of RF parameters for whole RFQ is given in Table III.

TABLE III

RF characteristics of the RFQ.

Frequency [MHz]	Power loss [kW]	Stored energy [J]	Shunt impedance [kΩ-m]	Quality factor
71.62	92.354	2.0478	390.43	9977

4. RFQ prototype

In order to test the quality and reliability of the calculations, a simple aluminium model of one RFQ section was built in collaboration with local Spanish companies. The system was assembled and tested in the RF Laboratory at the University of Huelva, as shown in Fig. 5 (left). The RF measurements were performed using an Agilent N90000A CKA spectrum analyzer. The cavity without vanes resonates at 485 MHz (dashed/red line), which is in agreement with COMSOL simulations (solid/blue line) with a difference of 5 MHz, the results are shown in Fig. 5 (above). Introducing the four vanes in the resonator leads to the appearance of a quadrupole mode TE_{211} and the system resonates at 157 MHz as shown in Fig. 5 (bottom) — it corresponds to the fundamental mode and it is very close to a doubly degenerated dipole mode.

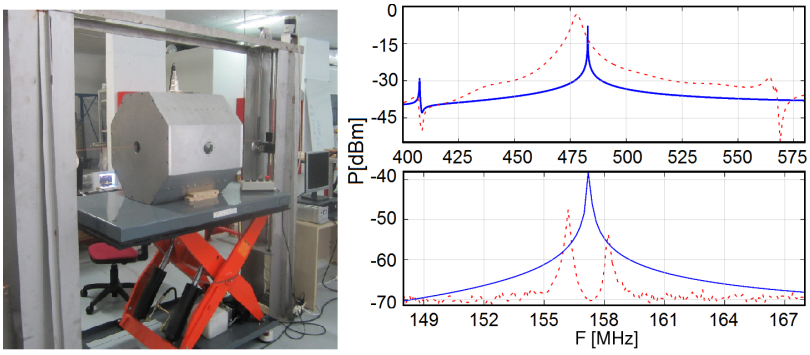

Fig. 5. Left: Aluminium RFQ section prototype. Right: Experimental and simulated RFQ frequency mode without vanes (above) and with vanes (bottom).

The differences between the spectrum and simulation are due to the construction characteristics of the structure like tolerance, precision, the size of the pick up antenna and the coupler. The prototype has 2 mm of precision, this variation can produce a maximum change of 20 MHz in the resonance frequency. The tuners system can solve a frequency shift of 2 MHz, therefore, we need to improve the measurement with the coupler in order to reduce the 5 MHz difference in the first test.

5. Conclusions

Beam dynamics simulations [7] have been carried out using TRACK and DESRFQ codes. The design has been obtained using realistic field maps and simulated in RF module, heat transfer, fluid flow and mechanical deformations of COMSOL. Future developments will include suitable input matcher and trapezoidal cells to shorten the length and improve the performance of the cavity.

REFERENCES

[1] I. Martel *et al.*, "ECOS-LINCE: A High Intensity Multi-ion Superconducting Linac for Nuclear Structure and Reactions", IPAC'14, Dresden, Germany, June 2014.

[2] A.A. Kolomiets *et al.*, "The RFQ Design Software DESRFQ", ITEP/ANL Technical Note, 2005.

[3] V. Aseev *et al.*, "TRACK: The New Beam Dynamics Code", PAC'05, Knoxville, USA, TPAT028, 2005.

[4] I. Martel *et al.*, "Development of a 14.5–18.0 GHz ECR Ion Source at the University of Huelva", IPAC'14, Dresden, Germany, June 2014.

[5] M. Cavenago *et al.*, "Operation of the LNL ECR Ion Source", EPAC14, Vienna, Austria, June 2000.

[6] C. Bontoiu *et al.*, "Design of Multi-harmonic Buncher for the LINCE Heavy-ion Accelerator Complex", IPAC'14, Dresden, Germany, June 2014.

[7] A.K. Orduz *et al.*, "Development of a 72.75 MHz RFQ for the LINCE Accelerator Complex", IPAC'14, Dresden, Germany, June 2014.

[8] `http://www.comsol.com`

[9] P. Ostroumov *et al.*, *Phys. Rev. ST Accel. Beams* **15**, 110101 (2012).

[10] A.K. Orduz *et al.*, "Thermal and Structural Analysis of the 72.75 MHZ LINCE RFQ", IPAC'15, Richmond, USA, May 2015.

B

Appendix

Contents:

This section is dedicated to the design of a **200 MHz four-rods RFQ** (proton and light-ion ($A/Q = 3$)) for Medical Applications.

B.1 A RFQ for Medical Applications

The project "Design of a proton accelerator using IH/CH structures for the production of radioisotopes and the treatment of uveal tumours – ICH15" has been financed by the Ministry of Economy and Competitiveness, through the Centre for Industrial Technological Development (CDTI), project code ITC-20151186.

This initiative is a development of the technological efforts carried out in the previous RD project GASP: Design of a superconducting Gantry for cancer treatment using proton therapy (ITC-20131073). More specifically, the ICH15 project proposes to carry out the design study of a proton accelerator system including the ion production source (protons in particular), the acceleration system, the beam distribution, and the connection/interface with the different accelerator beam lines in order to, simultaneously, perform treatments of uveal tumours and the production of radioactive isotopes. Based on the main characteristics of the facilities that use proton acceleration processes to treat cancer cells, the technology of cavities type IH/CH were selected.

Radiotherapy[108] plays an essential role in the treatment of cancer, either by the use of radiopharmaceuticals or by the direct irradiation of the tumour using energetic radiation. Radioisotopes are routinely used in medicine for both diagnostic and treatment purposes. An important new technique under development is the so-called theranostic approach, where two isotopes of the same chemical element are used for therapy and diagnosis. The irradiation technique using hadrons (protons, or other heavy ions) provides much more benefits as compared to photons. As the energy deposition density along the ion path is much higher, the dose to normal tissues during the treatment is smaller, and the maximum deposition occurs in a narrow region at the end of the path. The ICH15 project aims to design a heavy-ion facility for accelerating protons up to an energy of 70 MeV and about 5 MeV/u for heavy ions with $A/Q = 3$. The objective is to simultaneously produce radioisotopes and deliver

a low-energy proton beam for therapeutic purposes (e.g., to treat uveal tumours).

RFQ-rods design

This section approaches the design of the radio-frequency quadrupole (RFQ), which is one of the most important accelerator components in this project. Its purpose is to capture the input continuous beam and transform it in bunches which can be further accelerated and focused. Then, calculations on the energy requirements, and approaches for the beam modulation and its benefits are also outlined. Finally, the results of the transverse and longitudinal RFQ beam dynamics are presented.

The first question to be answered is: at which RFQ inter-vane potential V_0 can most of the beam be captured and transmitted along the structure? And then, what is the value of the transverse acceptance, i.e., the maximum value of the beam transverse phase space which passes through the whole RFQ? Such a value is related to the input energy and particle mass, but in practical simulations the initial phase angle ϕ is also of interest. Particles with mass-to-charge ratio $A/Q = 3$ and kinetic energy $E_kin = 10\,\mathrm{keV/u}$ are considered.

Assuming $A/Q = 3$ ions with $E_kin = 10\,\mathrm{keV/u}$ and $E_0 = 3\,\mathrm{MeV} \times 931.494\,\mathrm{MeV}$ the results found are shown in Table B.1.

Table B.1: Design values for ICH15 RFQ

Parameter	Value	Units
γ	1.0000107	
β	0.004633631	
Input velocity	1.388 x 10^6	m/s
Period	1454.3	ns

Finally, the parameters of the RFQ for ICH15 are described in Table B.2.

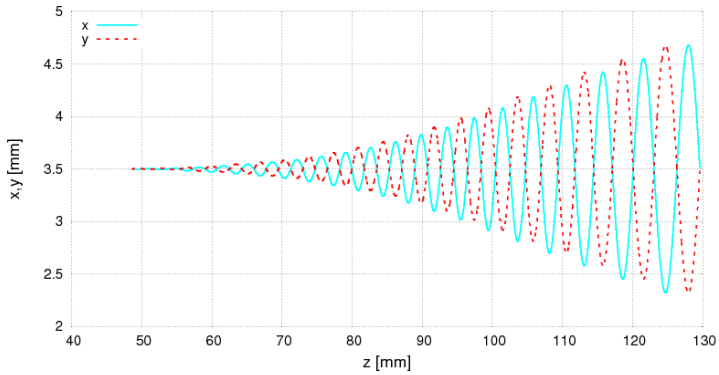

Figure B.1: Sinusoidal modulations computed for the horizontal (x) and vertical (y) vane pairs. The input matcher placed between $z = 0$ and $z = 48\,\text{mm}$ is not shown here.

Table B.2: Parameters for ICH15 RFQ

Parameter	Value	Units
Frequency	200	MHz
Period (290.56 RF periods)	5	ns
λ_0	1.498962290	m

Since the vane modulation has a fixed geometry and the RF wave comes in at a constant phase, the efficiency of the acceleration and bunching, as well as their interplay, rely on the careful choice of each cell length and amplitude. Therefore, the DESRFQ code was used to provide the distribution of these two parameters. The work resulted in specifications for a total of 97 RFQ cells which span about SI2 m between the RFQ entrance and exit. The axial profile of the first 20 cells is shown in Figure B.1.

It can be seen that they run in anti-phase, thus the axial field appears near the modulation surfaces due to the bending of the electric field lines. For the very first cells where the modulation depth (aspect ratio) is just above 1, the axial electric field components are very small.

As can be observed in Figure B.1, cell depth increases, as well as the modulation, following a z^4 function, thus enabling beam bunching

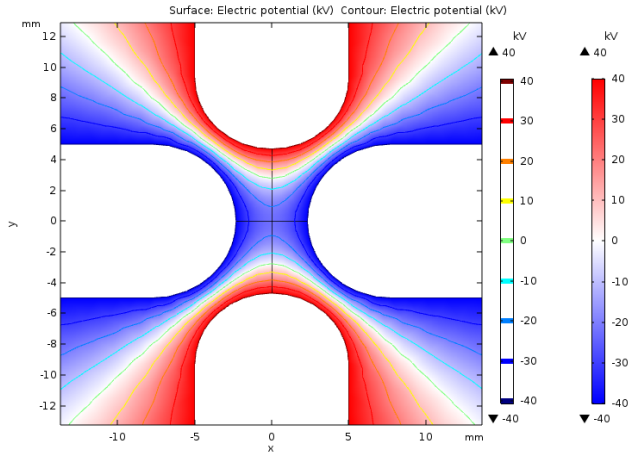

Figure B.2: Pattern of the electric potential between the vane tips for an inter-vane potential of 80 kV. The green lines represent the $V = 0$ interface between opposing vane polarities.

rather than acceleration. Then, as the modulation depth reaches its maximum (i.e., 2.2) the synchronism between cell length and the RF phase enables acceleration rather than bunching.

A few snapshots of the electric fields (potential and intensity) created by the modulated vanes in order to realize their effect

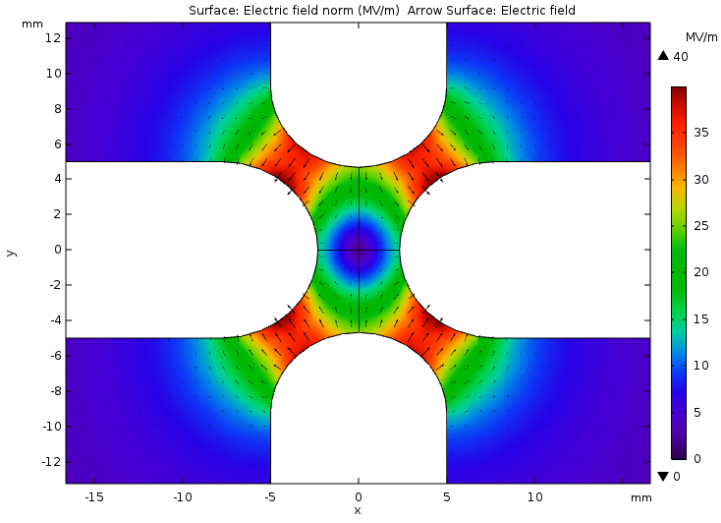

Figure B.3: Pattern of the field intensity for an inter-vane potential of 80 kV.

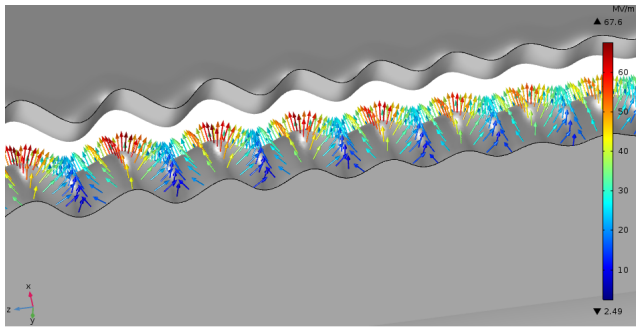

Figure B.4: Pattern of the electric field intensity vectors at the surface of one modulated vane tip for an inter-vane potential of 80 kV.

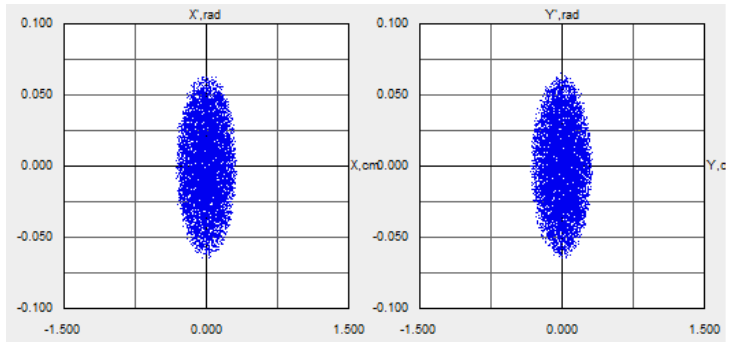

Figure B.5: Beam distribution at the injection into the RFQ as seen from its transverse horizontal (left) and vertical (right) phase space.

on particle beams are presented. Thus, Figure B.2 displays the electrostatic potential between the vanes as seen from a transverse cut. This provides the alternate focusing of the RFQ through the electric field lines shown in Figure B.3 below.

As the modulation is introduced, the electric field vectors distribute near the vanes, as shown in Figure B.4, and useful longitudinal field components appear.

The next step of the study was to obtain the results for transverse beam dynamics simulations and optimization for the RFQ. The main goal was to keep most of the beam focused within the region between the vanes, where bunching and acceleration take place. The transverse phase space of the injected beam is shown in Figure B.5.

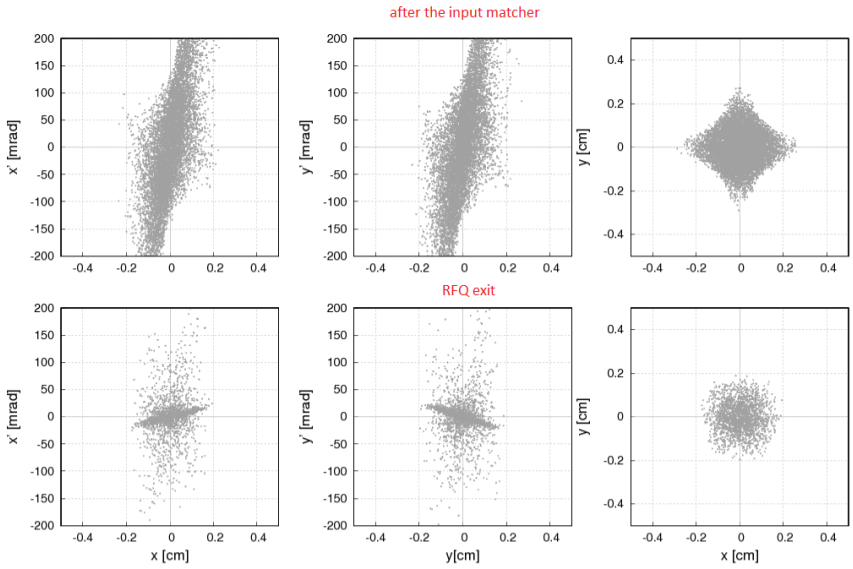

Figure B.6: Beam distribution at the injection into the RFQ as seen from its transverse horizontal (left) and vertical (right) phase space.

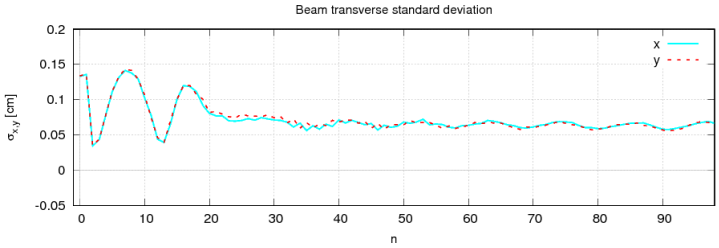

Figure B.7: Beam transverse standard deviation for the horizontal (solid-cyan) and vertical (dashed-red) plane.

The evolution of the beam transverse physical size and that of the transverse phase space can be observed in the snapshots of Figure B.6, as recorded at the entrance and exit of the RFQ. The total study was conducted every 10 RFQ cells. The beam is gradually focused toward the end of the RFQ, whereas the transverse phase space is reduced to a stable region which defines the acceptance.

Summarizing over all RFQ cells, the beam transverse standard deviation remains at about 0.65 mm, whereas the beam size remains at about 4 mm, as shown in Figures B.7 and B.8, respectively.

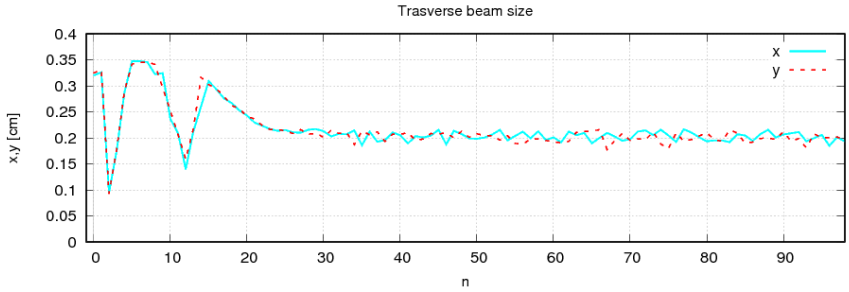

Figure B.8: Beam transverse width for the horizontal (solid-cyan) and vertical (dashed-red) plane.

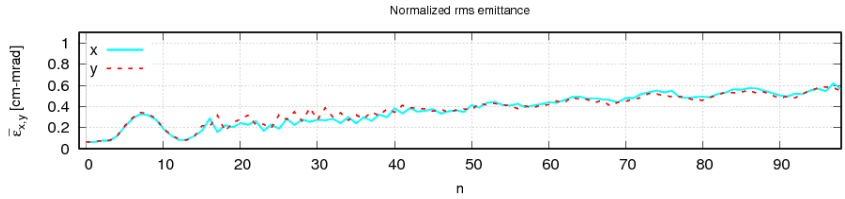

Figure B.9: Beam transverse normalized rms emittance for the horizontal (solid-cyan) and vertical (dashed-red) plane.

Similarly, the transverse emittance stabilizes around the value of SI0.6 cm-mrad, as shown in Figure B.9.

Beam bunching and acceleration was optimized using the DESRFQ and TRACK codes. The role of the modulation is to first bunch a continuous beam and then accelerate it to the design energy. In this project, the goal was to capture a 10 keV/u beam and produce a bunched beam at 500 keV/u for $A/Q = 3$ ions. For this reason, the first modulation cells must be smooth enough as described by the modulation aspect ratio (cell depth) and cell length. The choices for these two parameters are shown in Figures B.10 and B.11, respectively.

The modulation depth increases quartically (n^4) for the first 20 cells and remains locked at 2.2 thereafter.

On the contrary, the cell length remains constant for the first 10 cells, along which there is no acceleration, and then it increases along the RFQ to keep up with the beam velocity.

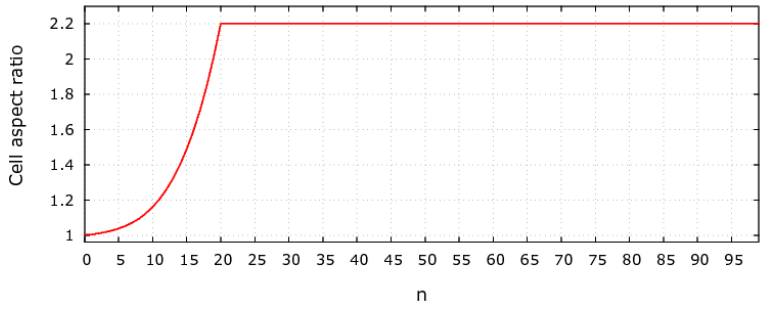

Figure B.10: Increase of the modulation aspect ratio (cell depth) along the RFQ.

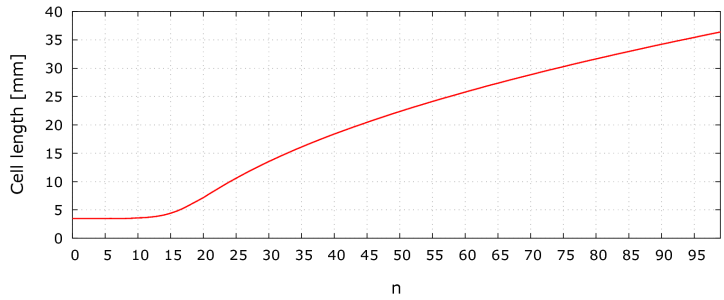

Figure B.11: Increase of the cell length along the RFQ, synchronized with the beam relativistic β factor.

Snapshots of the beam longitudinal phase space as it evolves along the RFQ structure are shown in Figure B.12. Bunching and acceleration are thus demonstrated along with the target energy (500 keV/u).

Snapshots of the beam longitudinal phase space as it evolves along the RFQ structure are shown in Figure B.12. Bunching and acceleration are thus demonstrated along with the target energy (500 keV/u).

The overall energy gain process is also summarized in Figure B.13.

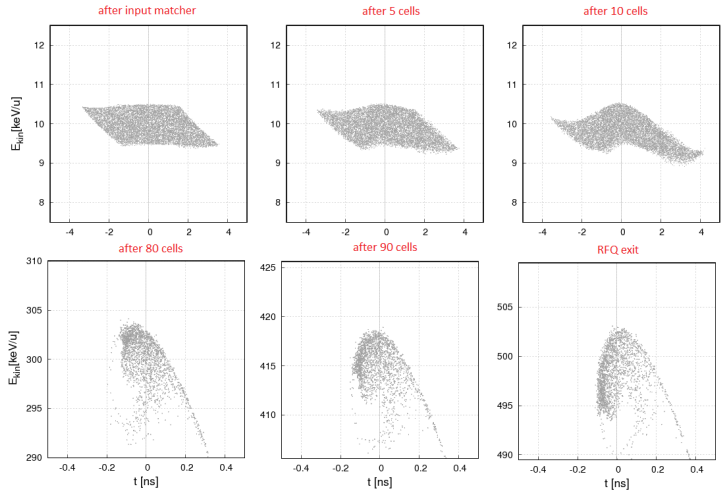

Figure B.12: Beam longitudinal phase spaces at various positions along the RFQ.

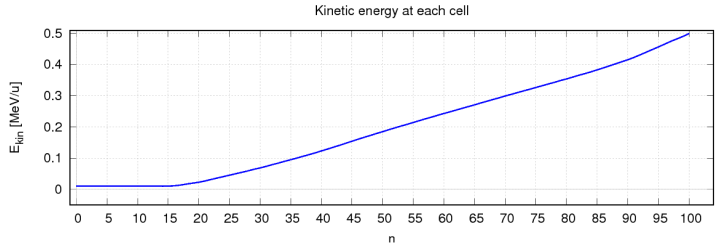

Figure B.13: Evolution of the beam kinetic energy along the RFQ cells.